

Report MDC-Q0778
Contract No. F49620-79-C-0039

AD A123166

MICROSTRUCTURE AND PROPERTIES OF POWDER-PROCESSED ALUMINUM-LITHIUM ALLOYS

S. M. L. Sastry
P. J. Meschter
J. E. O'Neal
K. K. Sankaran

McDonnell Douglas Research Laboratories
St. Louis, Missouri 63166

31 May 1982
Final Report for Period 1 April 1979 - 31 May 1982

Approved for public release; distribution unlimited

Prepared for:
UNITED STATES AIR FORCE
Air Force Office of Scientific Research
Bolling Air Force Base, DC 20332

DTIC
SELECTED
JAN 07 1983
E

MCDONNELL DOUGLAS RESEARCH LABORATORIES

MCDONNELL DOUGLAS

CORPORATION

83 01 07 049

DTIC FILE COPY

UNCLASSIFIED

SECURITY CLASSIFICATION OF THIS PAGE (When Data Entered)

REPORT DOCUMENTATION PAGE		READ INSTRUCTIONS BEFORE COMPLETING FORM	
1. REPORT NUMBER AOSR-TR- 82-1059 MDC 82-1059		2. GOVT ACCESSION NO. AD-A123166	
4. TITLE (and Subtitle) MICROSTRUCTURE AND PROPERTIES OF POWDER-PROCESSED ALUMINUM-LITHIUM ALLOYS		3. RECIPIENT'S CATALOG NUMBER	
		5. TYPE OF REPORT & PERIOD COVERED FINAL REPORT 1 APRIL 1979 - 31 MAY 1982	
		6. PERFORMING ORG. REPORT NUMBER	
7. AUTHOR(s) S. M. L. Sastry, P. J. Meschter, J. E. O'Neal, and K. K. Sankaran		8. CONTRACT OR GRANT NUMBER(s) F49260-79-C-0039	
9. PERFORMING ORGANIZATION NAME AND ADDRESS McDonnell Douglas Research Laboratories McDonnell Douglas Corporation P. O. Box 516 St. Louis, MO 63166		10. PROGRAM ELEMENT, PROJECT, TASK AREA & WORK UNIT NUMBERS 61102F 2306/A1	
11. CONTROLLING OFFICE NAME AND ADDRESS Air Force Office of Scientific Research Building 410 Bolling AFB, DC 20332		12. REPORT DATE 21 May 1982	
		13. NUMBER OF PAGES 76	
14. MONITORING AGENCY NAME & ADDRESS (if different from Controlling Office)		15. SECURITY CLASS. (of this report) UNCLASSIFIED	
		15a. DECLASSIFICATION/DOWNGRADING SCHEDULE	
16. DISTRIBUTION STATEMENT (of this Report) Approved for public release; distribution unlimited.			
17. DISTRIBUTION STATEMENT (of the abstract entered in Block 20, if different from Report)			
18. SUPPLEMENTARY NOTES			
19. KEY WORDS (Continue on reverse side if necessary and identify by block number)			
Aluminum alloys	Cobalt	Bismuth	Al-Li-Zn-Mg Strength
Lithium	Titanium	Cadmium	Rapid Solidification Ductility
Manganese	Zirconium	Al-Li	Roller Quenching Slip
Chromium	Tin	Al-Li-Cu	Powder-processing Dispersion-strengthening
Iron	Antimony	Al-Li-Cu-Mg	
20. ABSTRACT (Continue on reverse side if necessary and identify by block number) Al-Li alloys possess unique combinations of high specific strength and high specific modulus and can provide potential weight savings and life-cycle-cost reductions in aircraft structures. The low ductility and toughness of these alloys have thus far restricted their commercial use. Al-Li alloys are strengthened by the precipitation of a large volume-fraction of the incoherent, ordered δ' (Al₃Li) phase, which results in increased planarity of slip during deformation and thereby reduces the ductility, especially in ingot-processed alloys that generally possess large grain sizes.			

With the objective of improving the ductility of Al-Li alloys through grain refinement and the introduction of incoherent dispersoids, the microstructure and properties of rapidly solidified Al-3Li alloys containing nominal additions of 0.5 wt% each of Mn, Cr, Fe, Co, Ti, and Zr, and 0.1 wt% of Y were investigated. Additions of Sn, Sb, and Bi also were made to eliminate segregation of the tramp elements, particularly Na, to the grain boundaries and thus prevent intergranular embrittlement. Cd additions were made to lower the δ' /Al-matrix interfacial energy and thus cause a finer δ' distribution. Rapid solidification results in significant microstructural refinement by preventing segregation of alloying additives and suppressing the formation of coarse solidification constituents. The microstructure of the consolidated and heat-treated alloys consists of a bimodal distribution of 40-nm strengthening δ' precipitates and \approx 45-85 nm incoherent dispersoids. The alloys are essentially unrecrystallized and have a partially developed subgrain structure. In contrast to the binary Al-3Li alloy in which slip is highly planar, the deformation substructure of the alloys containing dispersoids is more homogeneous and conducive to improved ductility.

The measured yield stress of the alloys containing dispersoids is higher than that of the binary alloy in the solution-treated condition and comparable in the aged condition, but the measured values are generally lower than theoretical estimates. This discrepancy suggests that dispersion strengthening is partially offset by the presence of Li in the dispersoids, which reduces the amount of Li available for precipitation as δ' . In rapidly solidified Al-3Li-0.5Co, the modulus-normalized yield stress increases with increases in temperature, whereas in Al-3Li-0.2Zr the yield stress decreases drastically with increasing temperature above 75°C because of the ineffectiveness of subgrains acting as slip barriers.

To obtain guidelines for optimizing alloy compositions and processing methods for commercial, multicomponent, Al-Li alloys, three alloys based on the Al-Li-Cu, Al-Li-Cu-Mg, and Al-Li-Zn-Mg systems were rapidly solidified by inert-gas atomization. The powders were consolidated by extrusion at 400°C, solution-annealed at 520-570°C, and aged for 6-64 h at 165-238°C. Addition of dispersoid-forming elements to the multicomponent alloys did not result in the increased ductility observed in ternary Al-Li-X alloys. This difference may be the result of retained constituent particles or increased hydrogen levels in rapidly solidified powders.

PREFACE

This report was prepared by the McDonnell Douglas Research Laboratories (MDRL), St. Louis, MO, for the Air Force Office of Scientific Research (AFOSR), Bolling AFB, DC, under Contract F49620-79-C-0039. The AFOSR Program Manager was Dr. A. H. Rosenstein.

The work was performed in the Solid State Sciences Department of MDRL under the supervision of Dr. C. R. Whitsett. The principal investigator was Dr. S. M. L. Sastry; co-investigators were Dr. P. J. Meschter, Mr. J. E. O'Neal, and Dr. K. K. Sankaran.

This report has been reviewed and is approved.

C. R. Whitsett

C. R. Whitsett
 Director - Research
 McDonnell Douglas Research Laboratories

D. P. Ames

D. P. Ames
 Staff Vice President
 McDonnell Douglas Research Laboratories

Accession For	
NTIS GRA&I	<input checked="" type="checkbox"/>
DTIC TAB	<input type="checkbox"/>
Unannounced	<input type="checkbox"/>
Justification	
By _____	
Distribution/	
Availability Codes	
	Avail and/or
Dist	Special
A	



AIR FORCE OFFICE OF SCIENTIFIC RESEARCH (AFOSR)
 NOTICE OF CONTRACT F49620-79-C-0039
 This report is the property of AFOSR and is
 approved for distribution under AFOSR 100-12.
 MATTHEW S. [unclear]
 Chief, Technical Information Division

TABLE OF CONTENTS

<u>Section</u>	<u>Page</u>
1. INTRODUCTION.....	1
2. RESEARCH OBJECTIVES AND APPROACH.....	3
3. EXPERIMENTAL PROCEDURE.....	5
3.1 Alloy Compositions.....	5
3.2 Rapid Solidification Processing and Consolidation of Al-Li Alloys.....	6
3.3 Microstructures and Property Evaluation.....	10
4. RESULTS AND DISCUSSION.....	11
4.1 Microstructures and Deformation Behavior of Al-Li-X Alloys.....	11
4.1.1 Microstructures of Al-Li-X Alloy Flakes.....	11
4.1.2 Deformation Behavior of Al-Li-X Alloys.....	19
4.1.3 Mechanisms of Strengthening in Al-Li-X Alloys.....	22
4.1.4 High-Temperature Deformation of Al-Li-X Alloys.....	27
4.2 Microstructures of Multicomponent Al-Li Base Alloys.....	34
4.2.1 Microstructures of Solution-Treated Alloys.....	38
4.2.2 Microstructures of Solution-Treated-and-Aged Alloys...	41
4.2.3 Microstructures of Al-Li-Cu-Mg Alloy.....	44
4.2.4 Microstructures of Al-Li-Mg-Zn Alloy.....	46
4.3 Deformation and Mechanical Properties of Al-Li-Cu and Al-Li-Mg Alloys.....	48
4.3.1 Mechanical Properties.....	48
4.3.2 Fracture Morphology.....	52
4.3.3 Discussion of Structure-Properties Relations.....	55
4.4 Deformation and Mechanical Properties of Al-Li-Mg-Zr Alloy...	57
5. SUMMARY AND CONCLUSIONS.....	59
6. REFERENCES.....	62
7. PUBLICATIONS RESULTING FROM THIS CONTRACT.....	66
8. COUPLING ACTIVITIES WITH GROUPS DOING RELATED RESEARCH.....	68
DISTRIBUTION LIST.....	69

LIST OF ILLUSTRATIONS

<u>Figure</u>	<u>Page</u>
1. Cross-sectional drawing of roller-quenching apparatus for preparing rapidly solidified Al-Li alloys.....	7
2. Photograph of the roller-quenching apparatus showing the roller assembly.....	8
3. Photograph of roller-quenched flakes.....	8
4. Microstructures of as-roller-quenched Al-3Li alloys.....	12
5. Microstructures of cast Al-3Li and Al-3Li-0.16Ti.....	14
6. Microstructures of the Al-3Li alloys in the extruded condition....	15
7. Microstructures of solution-annealed alloys.....	16
8. Microstructures of solution-treated-and-aged Al-3Li alloys.....	18
9. Relation of yield strength and ductility for Al-3Li and Al-3Li-X alloys.....	20
10. Substructures of solution-treated-and-aged Al-3Li alloys deformed in tension.....	21
11. Variation of yield stress with Li-concentration for Al-Li solid solutions.....	23
12. δ' -precipitation strengthening as a function of the amount of Li available for δ' -precipitation.....	25
13. Temperature dependence of yield stress of solution-treated and solution-treated-and-aged Al-Li-X alloys.....	28
14. Deformation substructure at 25°C in solution-treated Al-Li-Zr alloy.....	31
15. Deformation substructure at 25°C of solution-treated and solution-treated-and-aged Al-Li-Co alloy.....	31
16. Dislocation substructures in Al-3Li-0.6Co deformed in compression at 25°C.....	32
17. Deformation substructure at 75°C in solution-treated Al-Li-Zr alloy.....	32
18. Deformation substructure at 200°C in Al-Li-Co alloy.....	33
19. Al_3Li morphology in solution-treated-and-aged Al-3Li-0.2Zr alloy deformed in tension.....	33
20. Solvus lines at 500°C and 550°C for the Al-rich region of the Al-Li-Cu ternary system.....	34
21. Phase relations at 500°C at the Al-corner of the Al-Cu-Li system.....	35

LIST OF ILLUSTRATIONS (Continued)

<u>Figure</u>	<u>Page</u>
22. Microstructures of Al-3Li-1.7Cu-0.23Mn alloy in the extruded condition.....	36
23. Microstructures of Al-3.7Li-1.6Cu-0.98Ti alloy in the extruded condition.....	37
24. Microstructures of Al-3Li-1.7Cu-0.42Co-0.24Zr alloy in the extruded condition.....	38
25. Transmission electron micrographs of Al-Li-Cu-Co-Zr as-extruded, Al-Li-Cu-Co-Zr solution-annealed 530°C/1 h, and Al-Li-Cu-Ti solution-annealed 530°C/1 h.....	39
26. Microstructures of Al-Li-Cu alloys solution-annealed 530°C/1 h and water-quenched.....	40
27. Transmission-electron micrographs of Al-2Li-1.7Cu-0.23Mn alloy....	42
28. Selected area diffraction analysis of δ' and T_1 phases in Al-4Cu-2Li alloy solution-treated at 500°C for 0.5 h, water quenched to 25°C, and annealed at 100°C for 96 h.....	42
29. Selected area diffraction analysis of δ' and T_1 phases in Al-4Cu-2Li alloy solution annealed at 500°C for 0.5 h, water quenched to 25°C, and annealed at 100°C for 96 h.....	43
30. Selected area diffraction analysis of δ' and T_1 phases in Al-4Cu-2Li alloy solution annealed at 500°C for 0.5 h, water quenched to 25°C, and annealed at 100°C for 96 h.....	43
31. Selected area diffraction analysis of δ' and T_1 phases in Al-4Cu-2Li alloy solution annealed at 500°C for 0.5 h, water quenched to 25°C, and annealed at 225°C for 192 h.....	44
32. Transmission electron micrographs of Al-Li-Cr-Co-Zr alloy solution-treated 530°C/1 h and aged.....	45
33. Microstructures of Al-Li-Cu-Mg-Fe-Ni alloy.....	46
34. Microstructures of Al-Li-Mg-Zn-Cu-Co alloy.....	47
35. Transmission electron micrographs of Al-Li-Mg-Zn-Cu-Co alloy.....	49
36. Aging curves for Al-Li-Cr and Al-Li-Cu-Mg alloys solution-annealed 530°C/1 h.....	50
37. Micrographs of tensile fracture surfaces of Al-3Li-1.7Cu-0.23Mn...	52
38. Tensile fracture surfaces of Al-Li-Cr-Co-Zr alloy.....	54
39. Aging curves for Al-Li-Mg-Zn alloy solution-annealed for 1 h at various temperatures and aged at 190°C.....	57

LIST OF TABLES

<u>Table</u>	<u>Page</u>
1. Chemical Compositions of Al-Li and Al-Li-X Ingots.....	5
2. Chemical Compositions of the Al-Li-X Alloy Extrusions.....	6
3. Nominal and Analyzed Chemical Compositions of Multicomponent Al-Li Alloys.....	9
4. Processing Histories of Multicomponent Al-Li Alloys.....	10
5. Characteristics of Dispersoid-Forming Additions to Aluminum Alloys.....	17
6. Room-Temperature Tensile Properties of Roller-Quenched, Extruded, and Heat-Treated Al-Li-X Alloys.....	19
7. Dispersoid Parameters in Al-Li-X Alloys.....	26
8. Comparison of Estimated and Measured Yield Stresses of Al-Li-X Alloys.....	26
9. Microstructures of Al-Li, Al-Li-Co, and Al-Li-Zr.....	28
10. Mechanical Properties of Al-Li-Cu and Al-Li-Cu-Mg Alloys.....	51
11. Hydrogen Contents of Aluminum Alloy Powders and Consolidated Forms.....	56
12. Mechanical Properties of Al-Li-Mg-Zn Alloy, Commercial 7091 and 7075.....	58

1. INTRODUCTION

Al-Li alloys combine high specific strength with high specific modulus and thus potentially can reduce the weight and life-cycle-cost of aircraft structures (References 1 and 2). However, these alloys are difficult to cast and fabricate and possess low values of ductility and toughness, factors which have thus far restricted commercial development of these alloys. Recent investigations have focused on optimizing the compositions of higher-strength, multicomponent alloys such as those based on the Al-Li-Mg (References 3-6), Al-Li-Cu (References 2, 7-15), and Al-Li-Cu-Mg (References 12, 15-18) systems.

Binary Al-Li alloys are hardened by precipitation of the metastable, coherent δ' (Al_3Li) phase (References 19 and 20). This phase is a superlattice with a structure similar to that of face-centered-cubic (f.c.c.) Cu_3Au and Ni_3Al (L1_2 structure), and the lattice misfit with respect to the Al matrix is about 0.9%. The δ' precipitates vary in size from about 10 nm after aging for 24 h at 100°C to about 30 nm after aging for a similar time at 200°C . Above 200°C , the δ' precipitates coarsen rapidly, obeying Lifshitz-Wagner kinetics. Although no hardening is observed upon annealing at room temperature, there is a considerable increase in alloy hardness upon aging at elevated temperatures. The high-temperature aging also results in a significant decrease in ductility.

The low ductility of Al-Li alloys is due primarily to precipitation of a high volume-fraction of δ' , which results in severe planar slip during plastic deformation. The severity of planar slip is intensified by the large grain sizes usually found in ingot-processed Al-Li alloys. The alloys fail intergranularly at low strain because of the localization of deformation in the grain boundary region resulting from the nucleation of voids at the coarse grain-boundary precipitates and their propagation by coalescence within the precipitate-free zones adjacent to the grain boundaries (Reference 21). Poor toughness of Al-Li alloys may be caused by the presence of the impurity elements, Na and K, at the grain boundaries. Na concentrations in excess of 0.004 wt% have been shown to cause sub-grain boundary embrittlement and toughness loss in Al-Mg-Li alloys (Reference 22).

In the present investigation, a systematic study was conducted to identify beneficial alloying elements and microstructures in aluminum-lithium alloys

and to provide guidelines for the systematic development of rapid solidification and powder metallurgical methods for producing Al-Li alloys. Improved ductility and toughness of Al-Li alloys should result from the slip homogenization that can be effected by grain refinement and by ancillary element additions to provide a controlled distribution of incoherent dispersoids. A significant degree of microstructural refinement and corresponding property enhancement can be obtained in Al-Li alloys through processing by the rapid solidification technique followed by consolidation and hot deformation. The high freezing rates obtained during such processing, in addition to minimizing or even eliminating the segregation of impurity and solute elements, result in significant grain refinement. In addition to improving the toughness and fatigue properties of Al-Li alloys that deform by planar slip, the fine grain sizes can be expected to improve the elevated-temperature formability of these alloys and possibly render the alloys superplastic. The solubilities of potential dispersoid-forming elements in Al should be increased by rapid quenching, thus permitting the development of more highly alloyed materials than can be obtained by conventional ingot-casting techniques with improved strength and toughness.

2. RESEARCH OBJECTIVES AND APPROACH

→ The overall objectives of this research program were to determine the source of brittleness in Al-Li alloys, determine ductility enhancement through slip homogenization effected by grain refinement and incoherent dispersoids, compare the properties of Al-Li alloys prepared from different types of rapidly solidified powders with the properties of cast Al-Li alloys and other commercial high-strength Al alloys, and identify and recommend for further development promising Al-Li alloy compositions for use in aircraft structures. The approach followed was that of rapid solidification and powder-processing, which result in significant microstructural refinement and make possible the processing of novel Al-Li alloy compositions not amenable to ingot-casting methods. ←

The specific objectives of the research program were to systematically investigate:

- a) the effectiveness of fine, incoherent dispersoids resulting from minor additions of the dispersoid-forming elements, Co, Ti, Zr, Y, Fe, Mn, and Cr and the effectiveness of grain refinement resulting from the rapid solidification by roller quenching for homogenizing slip and enhancing ductility in Al-3Li.
- b) the effectiveness of the addition of Sn, Bi, and Sb to Al-3Li for suppressing the grain-boundary segregation of the tramp elements, Na and K, through the precipitation of the latter elements as intermetallic compounds,
- c) the effectiveness of Cd addition in retarding δ' coarsening by reducing the energy of the δ' /Al-matrix interface,
- d) the influence of the major alloying elements Cu, Mg, and Zn, added separately or in combination, on the properties of rapidly solidified Al-Li alloys,
- e) the precipitation behavior and structure-property relations in multicomponent Al-Li alloys,
- f) the influence of various powder-processing techniques on the properties of multicomponent Al-Li alloys, and
- g) guidelines for the selection of Al-Li alloy compositions that possess optimum combinations of specific strength, specific modulus, toughness, fatigue, and corrosion properties.

The research described in this report was conducted in three phases:

Phase I - An investigation was conducted of the strength and ductility enhancement effected by (1) microstructural refinement resulting from rapid solidification, (2) modification of slip behavior by stable, incoherent, second-phase dispersoids, (3) grain refinement, (4) suppression of segregation of tramp Na to grain boundaries, and (5) modification of δ' precipitate morphology.

Phase II - The microstructural development in Al-Cu-Li, Al-Cu-Mg-Li, and Al-Zn-Mg-Li alloys as a function of cooling rate, particulate morphology, and heat treatment was studied. The synergistic effects of powder-processing and alloy chemistry on microstructures were evaluated.

Phase III - The effects of peak-aged, overaged, and underaged microstructures on the deformation behavior of multicomponent alloys were determined, and guidelines for the optimization of Al-Li alloy compositions and processing methods were recommended.

3. EXPERIMENTAL PROCEDURE

3.1 Alloy Compositions

The nominal compositions of the Al-Li alloys used in this investigation are listed in Tables 1 and 2. All alloys, except the high-purity Al-3Li-0.1Y alloy and the commercial-purity Al-3Li alloy designated CP3, were prepared from 99.99% pure Al and an Al-10Li master alloy. Additions of Mn, Cr, Fe, Co, Ti, and Zr were made in the form of commercially available Al-25Mn, Al-20Cr, Al-25Fe, Al-20Co, Al-10Ti, and Al-6Zr master alloys. Additions of Cd, Sn, Sb, and Bi were made in elemental form. The Al-10Li master alloy used for preparing the high-purity alloys was made from 99.999% pure Al with < 2 parts per million (p.p.m.) Na and high-purity Li with < 70 p.p.m. Na. The Al-10Li master alloy used for preparing the commercial-purity alloys was made from commercially pure Al and Li containing 100 p.p.m. Na. The Al-3Li-0.1Y and Al-3Li(CP3) alloys were procured from Reynolds Metals Co. and Cabot Berylco Co., respectively. 2.5-kg ingots of each of the alloys were prepared by melting and casting in an inert atmosphere. Master alloy additions were made to molten Al at 775°C in a carbon-bonded silicon carbide crucible. After vigorous stirring to disperse and dissolve the additives, the alloys were cast into a steel mold.

The alloys for the phase II and phase III studies were procured from Reynolds Metals Co. and Homogeneous Metals Company, respectively. The phase II and phase III alloys were prepared by comelting appropriate amounts of 99.99% Al, Al-10Li alloys with a Na content < 0.001 wt%, and Al-Cu or Al-Zr master alloys under vacuum. The alloys were melted and cast as book-mold ingots in an argon atmosphere.

TABLE 1. CHEMICAL COMPOSITIONS OF Al-Li AND Al-Li-X INGOTS.

Alloy and nominal composition	Chemical composition wt% (at.%)	
	Li	X
Al-3Li (high purity)	3.05(10.90)	—
Al-3Li-Zr	3.34(11.85)	0.08(0.022)Zr
Al-3Li-Ti	3.23(11.50)	0.16(0.082)Ti
Al-3Li-Co	3.17(11.31)	0.23(0.097)Co
Al-3Li-Y	3.30(11.72)	0.04(0.011)Y

QP21-0768-24

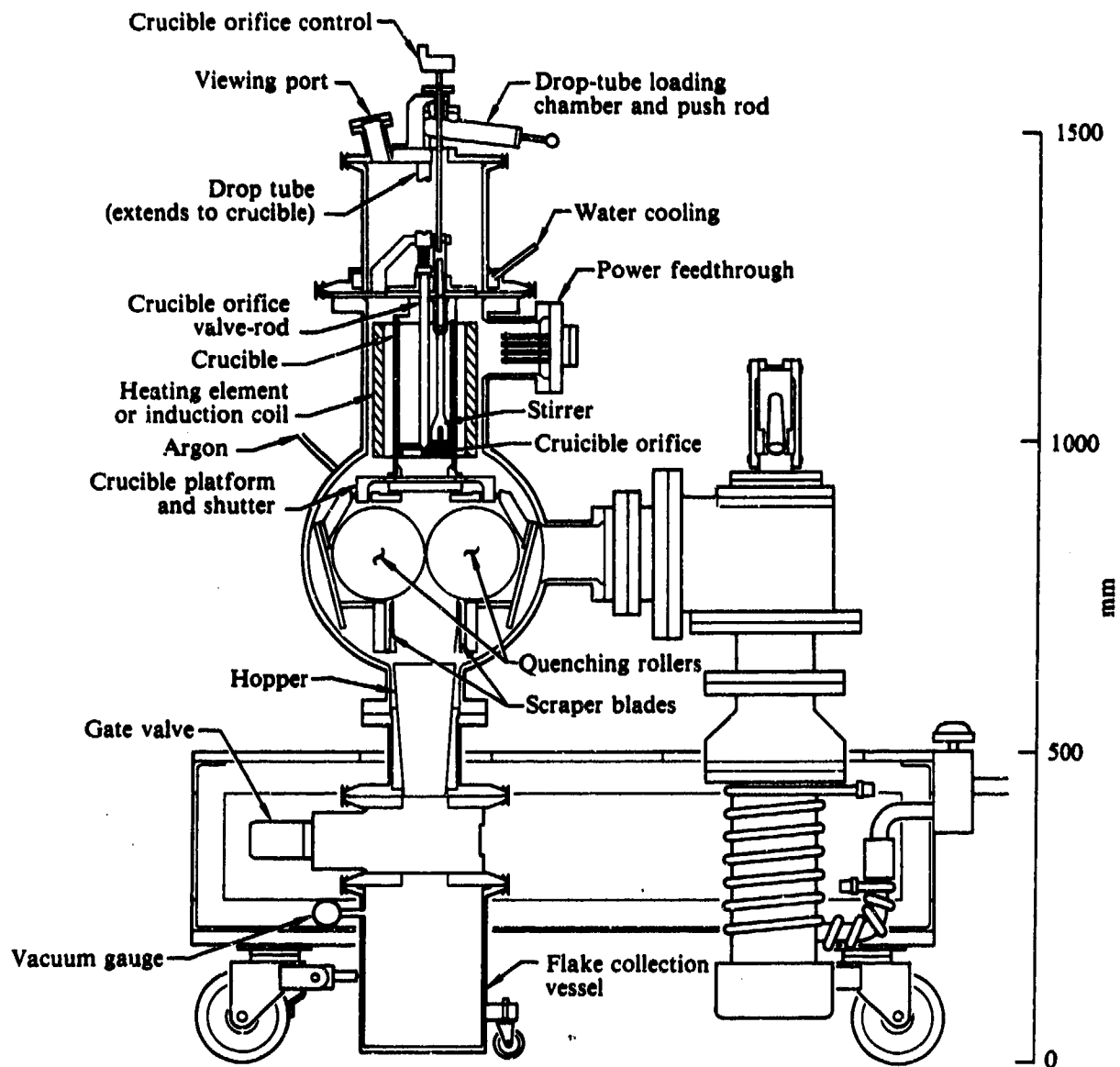
**TABLE 2. CHEMICAL COMPOSITIONS OF THE
Al-Li-X ALLOY EXTRUSIONS.**

Alloy number	Alloy and nominal composition	Chemical composition wt% (at.%)		
		Li	X	Fe
High-purity alloys				
1	Al-3Li(HP)	2.70(9.74)	—	< 0.01
2	Al-3Li-0.5Mn	2.81(10.12)	0.24(0.11)Mn	0.02(0.01)
3	Al-3Li-0.5Cr	2.18(7.99)	0.38(0.19)Cr	0.05(0.02)
4	Al-3Li-0.5Fe	2.78(10.03)	0.49(0.22)Fe	0.49(0.22)
5	Al-3Li-0.5Co	2.95(10.60)	0.64(0.27)Co	0.05(0.02)
6	Al-3Li-0.5Ti	3.01(10.78)	0.18(0.09)Ti	0.03(0.01)
7	Al-3Li-0.5Zr	2.95(10.59)	0.27(0.07)Zr	0.05(0.02)
8	Al-3Li-0.2Cd	2.76(9.97)	0.40(0.09)Cd	0.05(0.02)
9	Al-3Li-0.1Y	2.37(8.63)	< 0.01Y	0.05(0.02)
Commercial-purity alloys				
10	Al-3Li(CP1)	2.36(8.59)	—	0.05(0.02)
11	Al-3Li(CP2)	2.67(9.64)	—	0.03(0.01)
12	Al-3Li(CP3)	2.54(9.20)	—	0.11(0.05)
13	Al-3Li-0.1Sn	2.73(9.87)	0.35(0.07)Sn	0.05(0.02)
14	Al-3Li-0.1Sb	2.17(9.77)	< 0.05Sb	0.05(0.02)
15	Al-3Li-0.1Bi	2.75(9.91)	< 0.05Bi	0.05(0.02)

QP21-0786-25

3.2 Rapid Solidification Processing and Consolidation of Al-Li Alloys

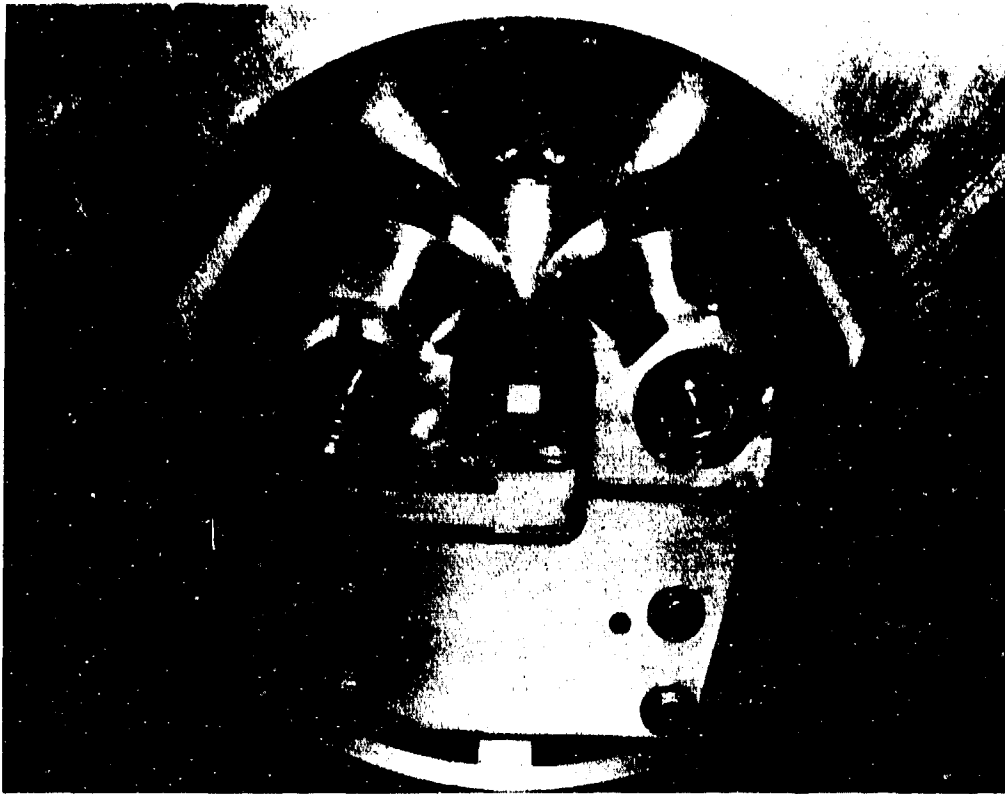
The phase I Al-Li and Al-Li-X alloys were rapidly solidified at rates $> 10^4$ °C/s into flakes by roller-quenching in the apparatus shown schematically in Figure 1. The roller-quenching apparatus consists of a furnace assembly, roller assembly, and flake collection assembly, all of which are enclosed in a vacuum chamber. The roller assembly consists of two parallel stainless-steel rollers, each 15 cm long and 15 cm in diameter, with provision for adjusting the roller separation from 25 μ m to 2 mm. The rollers are rotated in opposite directions at 1725 rpm by a motor and gear assembly through a set of high-speed rotary vacuum-feedthroughs. Figure 2 is a photograph of a part of the apparatus showing the roller assembly. About 2 kg of the alloy are melted under an inert atmosphere in a graphite crucible by induction heating. A graphite valve controls the rate of molten-alloy drop formation from a 1.5-2 mm diam orifice in the bottom of the crucible. The drops are splat-cooled by the rotating rollers, which typically have 50-200 μ m clearance. The rolled droplets are ejected as flakes, which are collected and



GP21-0766-1

Figure 1. Cross-sectional drawing of roller-quenching apparatus for preparing rapidly solidified Al-Li alloys.

stored in an inert atmosphere pending further processing. Typical flakes as shown in Figure 3 are about 2.5 cm long, 0.5 cm wide, and 50 μm thick. The splats are particularly suited for transmission electron microscopical examination of the as-solidified microstructure and the microstructural response to different heat treatments.



GP21-0766-2

Figure 2. Photograph of the roller-quenching apparatus showing the roller assembly.



1 cm

GP21-0766-3

Figure 3. Photograph of roller-quenched flakes.

Roller-quenched flakes of the Al-3Li, Al-3Li-0.16Ti, and Al-3Li-0.23Co alloys listed in Table 1 and alloys listed in Table 2 were consolidated by compacting the flakes into 75% dense billets in aluminum cans, degassing the billets while progressively heating to the extrusion temperatures, and extruding the billets at a reduction-of-area ratio of 20:1. The Table 1 alloys were extruded at 300°C into 6.3 mm diam rods, and the Table 2 alloys were extruded at 400°C into 11.5 mm diam rods.

The Al-2.5Li-1.5Cu-0.5Mn alloy for phase II and phase III studies was processed by argon-gas atomization into powder by Kawecki-Berylco. The powder was compacted at room temperature to ~ 70% density into an Al-alloy can and extruded at 400°C into a fully-dense 37 x 12 mm bar using an extrusion ratio of 30:1. The other multicomponent alloys listed in Table 3 were processed by vacuum atomization into powder by Homogeneous Metals, Herkimer, NY. The powder was preconsolidated at room temperature to 70% density and extruded at 400°C into bar stock at a reduction ratio of 30:1. The processing histories of the multicomponent Al-Li based alloys are summarized in Table 4.

TABLE 3. NOMINAL AND ANALYZED CHEMICAL COMPOSITIONS OF MULTICOMPONENT Al-Li ALLOYS.

Nominal composition (wt%)	Analyzed composition (wt%)					
	Li	Cu	Mg	Zn	Fe	Others
Al-2.5Li-1.5Cu-0.5Mn Extrusion	3.00	1.68	—	—	< 0.05	0.23Mn
Al-3Li-1.5Cu-0.5Ti Ingot	2.96	2.12	0.01	0.004	0.16	0.53Ti, 0.05Si
Extrusion	3.72	1.58	0.45	1.14	0.88	0.98Ti, 0.11Si
Al-3Li-1.5Cu-1.5Mg-1Fe-1Ni Ingot	2.76	1.79	0.98	0.002	0.93	0.92Ni, 0.05Si
Extrusion	3.44	1.91	1.43	0.56	0.87	0.77Ni, 0.12Si
Al-1.5Li-1.5Cu-2Mg-6Zn-0.5Co Ingot	1.54	1.98	1.28	0.54	0.31	< 0.05Co, 0.04Si
Extrusion	2.12	1.64	1.83	8.26	0.32	0.36Co, 0.08Si
Al-3Li-1.5Cu-0.5Co-0.2Zr Ingot	3.06	1.69	< 0.01	—	0.02	0.42Co, 0.24Zr
Extrusion	3.14	1.58	< 0.01	—	0.039	0.44Co, 0.21Zr

GP21-0766-26

TABLE 4. PROCESSING HISTORIES OF MULTICOMPONENT Al-Li ALLOYS.

Nominal composition	Rapid-solidification method	Dendrite arm spacing (μm); approximate solidification rate (K/s)	Powder vendor	Extrusion conditions	Extrusion vendor
Al-2.5Li-1.5Cu-0.23Mn	Inert gas atomization	$\sim 2.5, (10^4)$	Cabot Berylco	Compacted at room temperature to 70% density, extruded at 400°C at an extrusion ratio of 30:1 to 37 × 13 mm bar (no can)	Kawecki Berylco
Al-3Li-1.5Cr-0.5Ti Al-3Li-1.5Cr-1.5Mg-1Fe-1Ni Al-1.5Li-1.5Cr-2Mg-6Zn-0.5Co	Vacuum atomization	2 - 5, ($10^3 - 10^4$)	Homogeneous Metals, Inc.	Compacted in 6061-Al can at room temperature to 70% density; extruded at 400°C at an extrusion ratio of 30:1 to 37 × 13 mm bar	Nuclear Metals, Inc.
Al-3Li-1.5Cr-0.5Co-0.2Zr	Vacuum atomization	2 - 5, ($10^3 - 10^4$)	Homogeneous Metals, Inc.	As above, except extruded at an extrusion ratio of 16:1	Nuclear Metals, Inc.

GP21-0766-27

3.3 Microstructures and Property Evaluation

The microstructures of the alloys were studied by both optical and transmission electron microscopy, and selected area-diffraction and dark-field imaging techniques were employed to identify the strengthening phases in differently heat-treated alloys. Tensile properties of the alloys were determined as functions of heat treatment and orientation relative to the extrusion direction. Fracture surface morphologies were characterized by scanning electron microscopy, and the tensile properties and fracture morphologies were correlated with microstructure.

4. RESULTS AND DISCUSSION

4.1 Microstructures and Deformation Behavior of Al-Li-X Alloys

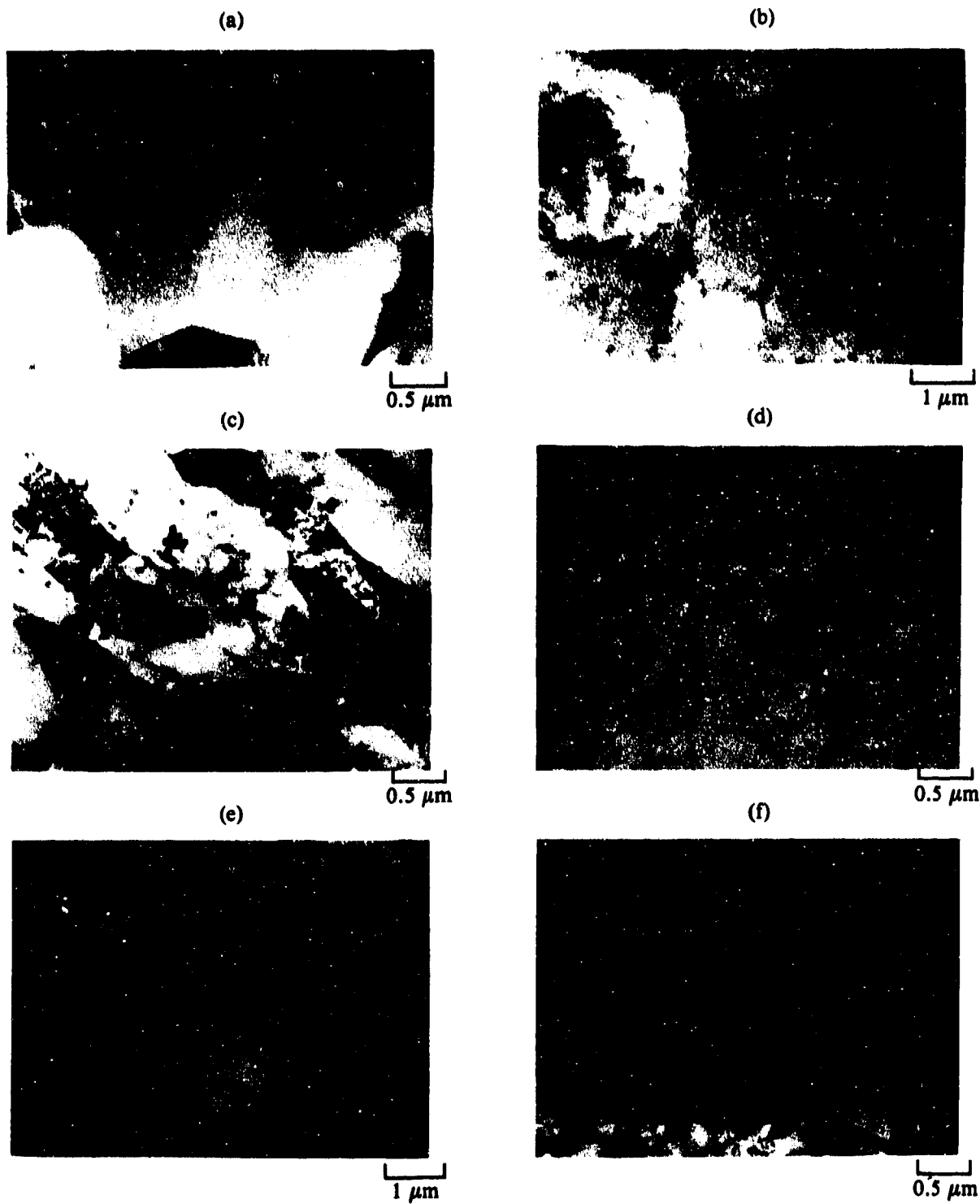
4.1.1 Microstructures of Al-Li-X Alloy Flakes

Microstructures of the Al-3Li and Al-3Li-X alloys in the as-roller-quenched condition are shown in Figure 4. For comparison, the microstructures of ingot-cast, high-purity Al-3Li and Al-3Li-0.16Ti are shown in Figure 5. Rapid solidification is seen to result in significant microstructural refinement by preventing the segregation of alloying additives and by suppressing the formation of coarse solidification constituents; both effects result from the slow solidification rates of ingot-casting processes. This refinement includes extended solubility of Li and other elements, uniform distribution of fine particles containing dispersoid-forming elements, and reduction in as-solidified grain size.

During ingot solidification of Al-3Li, the first solid to freeze has about 1.2 wt% Li (Reference 23). As freezing progresses, Li is rejected to the remaining liquid, until the last liquid to freeze may have 20 wt% or more Li. Thus Li is strongly segregated to the interdendritic regions (Figure 5a). Upon rapid solidification of Al-3Li, diffusion of Li and nucleation of Li-containing intermetallic compounds are suppressed, and a homogeneous, supersaturated, solid solution is produced (Figure 4a).

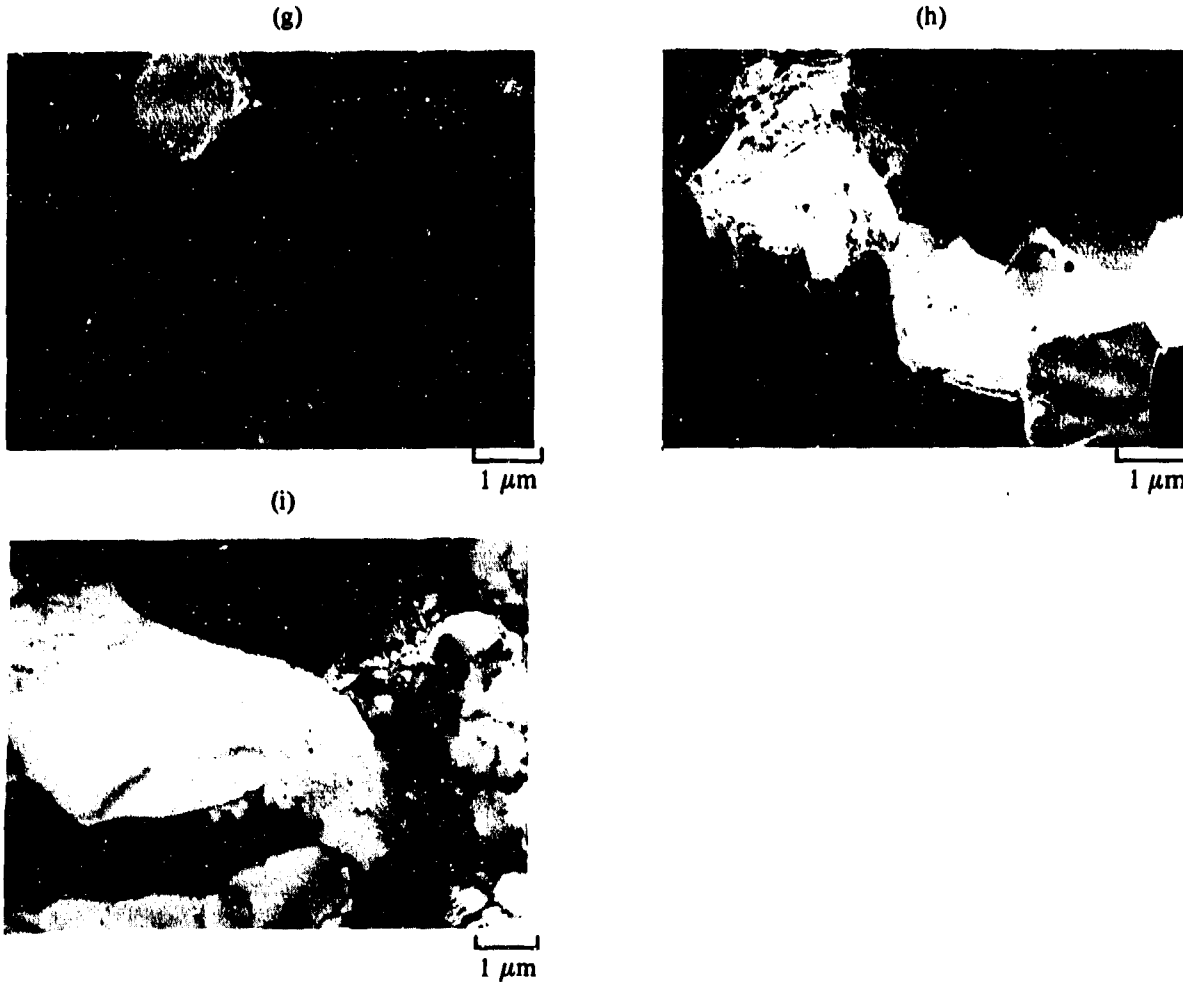
Dispersoid formation upon rapid solidification was observed in all Al-Li-X alloys except Al-3Li-Ti and Al-3Li-Y. Dispersoids were also observed in the commercial-purity Al-3Li alloy, which contains 0.1 wt% Fe as an impurity. In all cases, dispersoids were $< 1 \mu\text{m}$ in diameter and homogeneously distributed, in contrast to the nonuniform distribution of dispersoid-forming elements in cast alloys.

When Al alloys containing dispersoid-forming additives are cast, the slow solidification rates result in a dendritic microstructure and segregation of the additives, with the severity of segregation depending on the amount of the addition. Even in alloys that contain dispersoid-forming elements in amounts lower than their respective maximum solid solubilities, the segregated additives cannot be redissolved because of the sharp decrease of their solid solubilities with decreasing temperature. Elevated-temperature annealing of cast alloys results in intermetallic precipitates, which are nonuniformly



QP21-0766-4

Figure 4. Microstructures of as-roller-quenched Al-3Li alloys: (a) Al-3Li (high purity), (b) Al-3Li (commercial purity), (c) Al-3Li-0.16 Ti, (d) Al-3Li-0.23Co, (e) Al-3Li-0.24Mn, (f) Al-3Li-0.38Cr, (g) Al-3Li-0.49Fe, (h) Al-3Li-0.08Zr, and (i) Al-3Li-0.04Y.



GP21-0788-5

Figure 4. (Concluded).

distributed because of the segregation of the constituent elements in the as-cast structure (Reference 24). Rapid solidification suppresses segregation and results in a uniform dispersoid distribution in those cases where second-phase separation is not suppressed.

Rapid solidification in Al-3Li and Al-3Li-X alloys is observed to produce fine grain sizes on the order of 1-2 μm , in comparison with dendrite arm spacings of approximately 100 μm in cast ingots (Figure 5). The suppression of segregation by rapid solidification implies that crystallite nucleation rather than alloying-element diffusion in the liquid controls the grain size, resulting in a uniform distribution of fine, equiaxed grains.

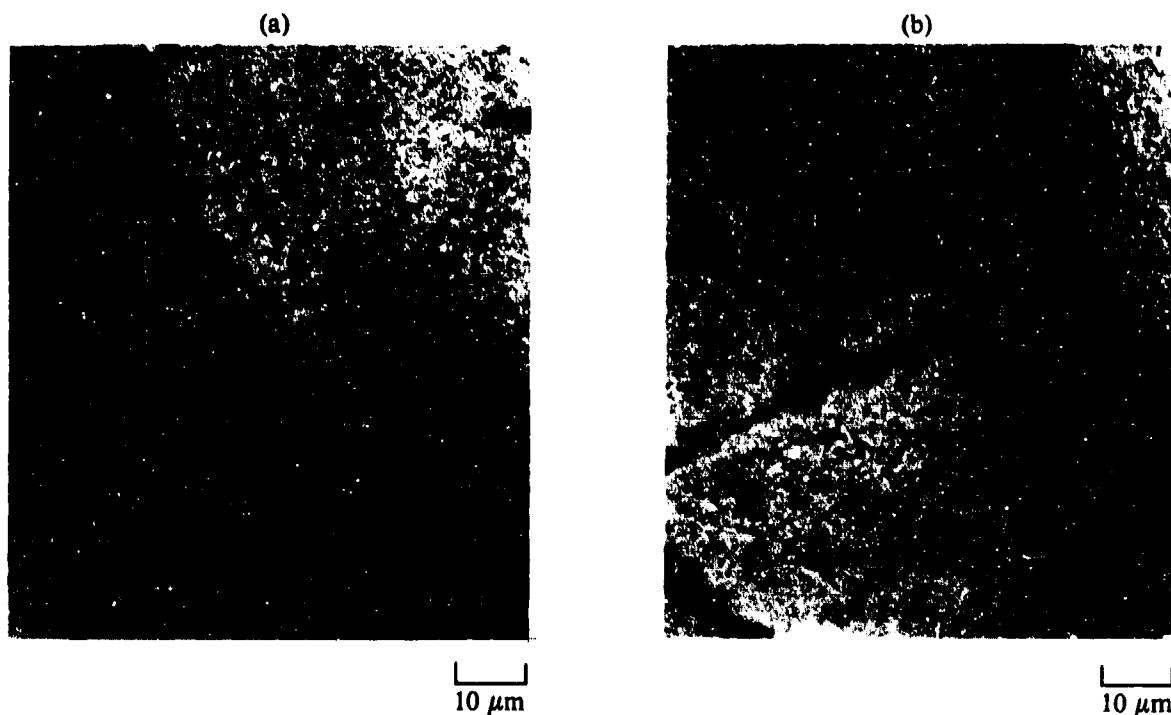


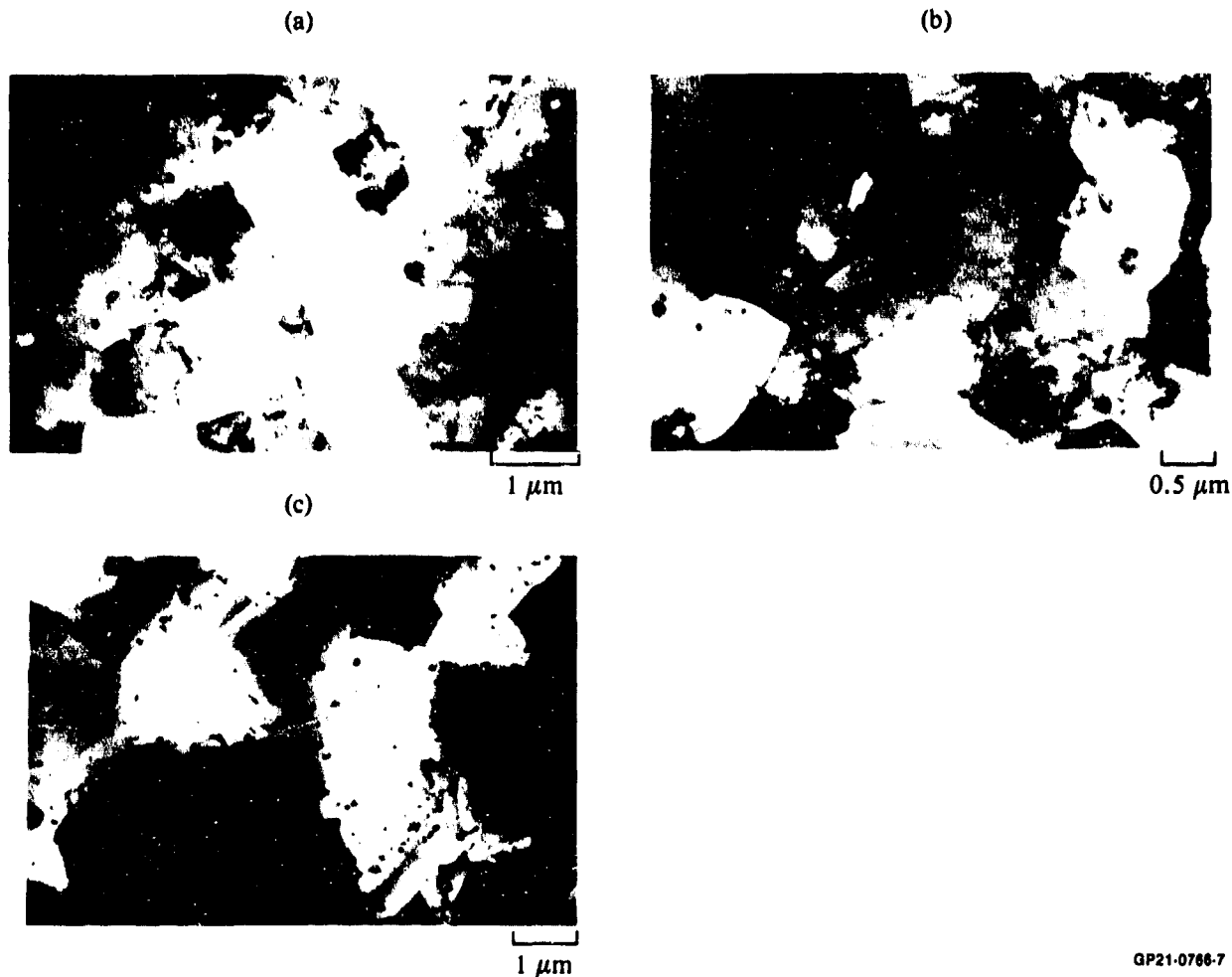
Figure 5. Microstructures of cast (a) Al-3Li and (b) Al-3Li-0.16Ti.

GP21-0768-6

The fine, homogeneous distribution of dispersoids formed in Al-3Li-X alloys during rapid solidification is favorable for effective dispersal of slip. To preserve this capability in the final processed forms of the alloys, the dispersoids should remain fine through thermomechanical processing, solution treatment, and aging steps. Likewise, uniformity of deformation is promoted by maintenance of a fine grain size through high-temperature processing.

Microstructures of Al-3Li, Al-3Li-0.16Ti, and Al-3Li-0.23Co alloys in the as-extruded condition are shown in Figure 6. A well-refined subgrain microstructure, 1-2 μm in size, is observed in each of the alloys. Second-phase separation of 0.1 μm-diam dispersoids is observed in the Al-3Li and Al-3Li-0.16 Ti alloys, but the size and distribution of the Co-containing dispersoids in the Al-3Li-0.23Co alloy are unaffected by the extrusion process.

Extrusions of the Al-3Li-X alloys listed in Table 2 were solution heat treated at 540°C for 0.5 h and quenched in water to room temperature. Transmission electron micrographs of several of these alloys in Figure 7 show retention of 0.1-0.25 μm diam, spherical, incoherent dispersoids during the solution treatment step. This high thermal stability of the dispersoids is



GP21-0766-7

Figure 6. Microstructures of the Al-3Li alloys in the extruded condition: (a) Al-3Li, (b) Al-3Li-0.16Ti, and (c) Al-3Li-0.23Co.

another advantage for the production by rapid solidification of alloys containing slip-dispersing elements.

Because of the relatively low volume-fraction of the dispersoids, selected area diffraction patterns could not be obtained to determine their identity. Since the alloys were held for fairly extended periods of time at 400-500°C during extrusion and solution treatment, it is reasonable to suppose that the dispersoids are phases of the Al-X systems that are in stable equilibrium with the binary Al-X solid solutions. These phases for the systems shown in Figures 7a-7e are Al_6Mn , Al_7Cr , Al_3Fe , Al_9Co_2 , and Al_3Ti , respectively.

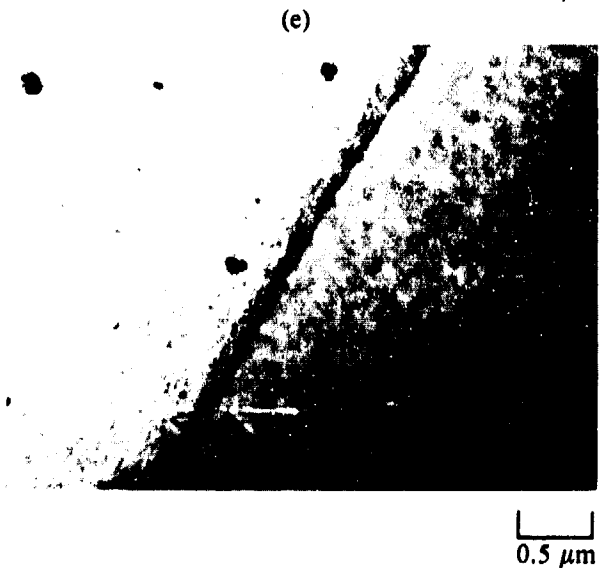
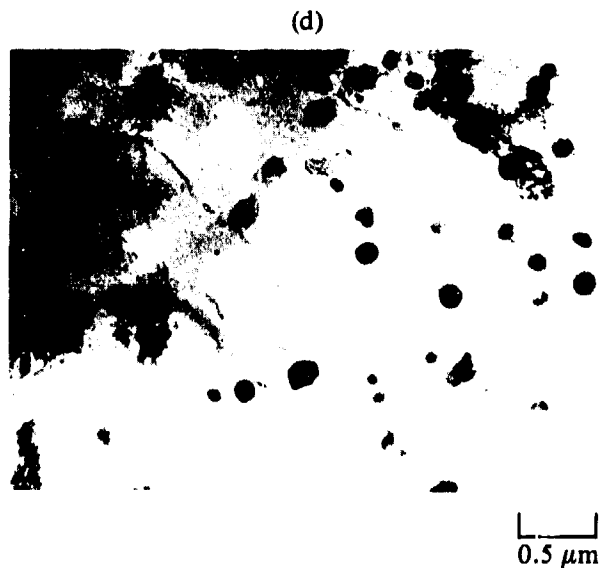
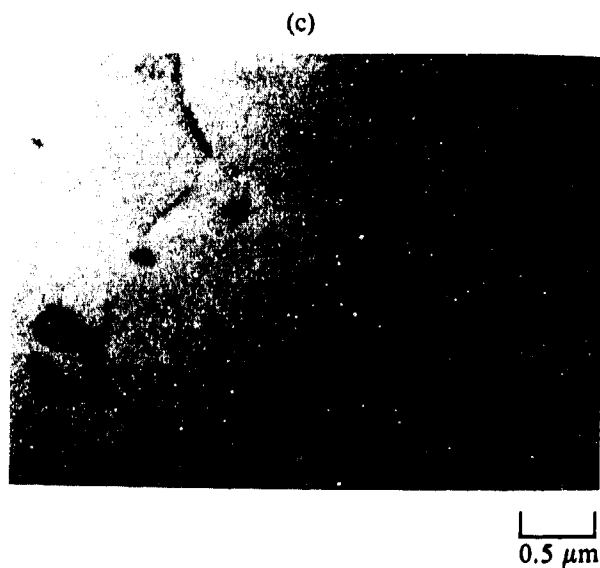
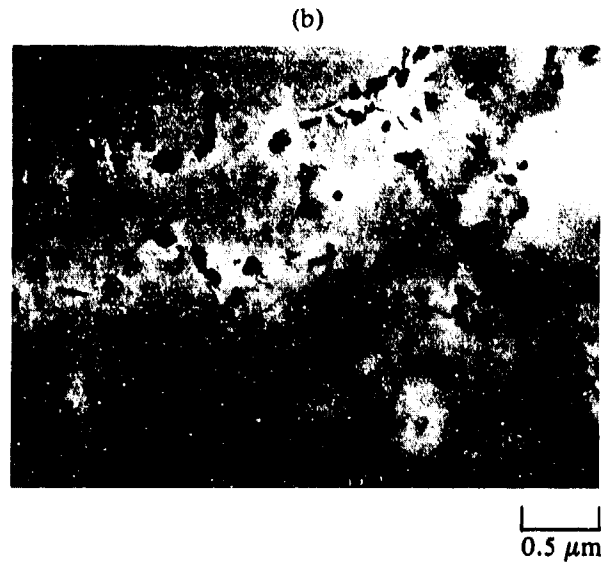
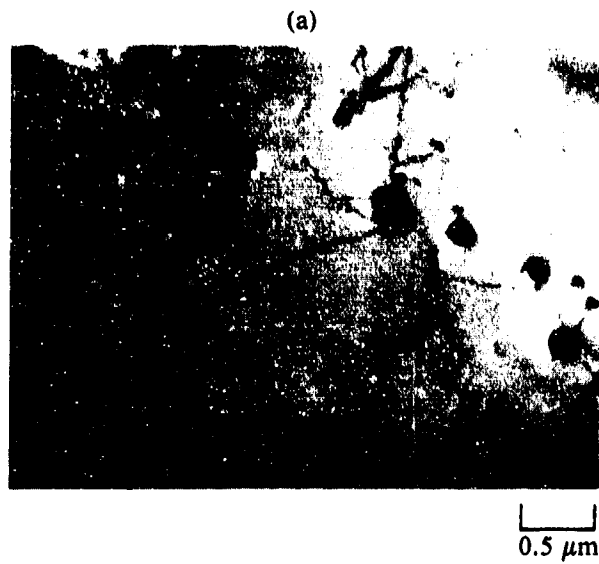


Figure 7. Microstructures of solution-annealed alloys:
(a) Al-Li-Mn, (b) Al-Li-Cr, (c) Al-Li-Fe,
(d) Al-Li-Co, and (e) Al-Li-Ti.

GP21-0766-6

Since all five of the ternary additions discussed above are effective in forming fine dispersoids which persist through the heat-treatment steps, assessment of which addition is most effective is made on the basis of the minimum density increase of the alloy per volume percent dispersoids added and the ease of producing the desired volume fraction of dispersoids in the as-solidified flakes. The most favorable dispersoid-forming element thus is one with fairly high solubility in liquid Al, low solubility in solid Al, low atomic mass, a large Al:X ratio in the dispersoids, and low reactivity with crucible materials and the atmosphere.

Of Ti, Cr, Mn, Fe, and Co, the data in Table 5 show that iron and cobalt are the best dispersoid-forming additions, primarily because of their low solubilities in the matrix and the good correspondence between nominal and analyzed compositions, which primarily reflects low losses by reaction with the crucible or the atmosphere during melting in the roller-quenching apparatus. This relatively low reactivity is expected based on the low stabilities of iron and cobalt oxides and carbides relative to the corresponding chromium, manganese, and titanium compounds.

Zirconium additions are a special case. The equilibrium body-centered-tetragonal Al_3Zr phase is readily bypassed during rapid solidification, and a face-centered-cubic Li_2 modification is formed on subsequent annealing. This phase is coherent with the matrix and remains coherent and metastable upon prolonged annealing at 500-600°C (Reference 25). The precipitation of metastable Al_3Zr in the Al-3Li-Zr system has a significant influence on the deformation behavior, which is discussed in the next section.

TABLE 5. CHARACTERISTICS OF DISPERSOID-FORMING ADDITIONS TO ALUMINUM ALLOYS.

Al-X system	Equilibrium solid solubility at 540°C (wt%)	Equilibrium dispersoid	Density of dispersoids (mg/m^3)	wt% X required for 1 vol% dispersoids	Calculated density of alloy (mg/m^3)	Actual wt% in Al-3Li for nominal 0.5 wt% added
Al-Ti	0.092	Al_3Ti	3.354	0.5477	2.732	0.18
Al-Cr	0.570	Al_7Cr	3.214	0.819	2.715	0.38
Al-Mn	0.517	Al_6Mn	3.308	0.819	2.717	0.24
Al-Fe	0.0136	Al_3Fe	3.816	0.587	2.713	0.49
Al-Co	~ 0.016	Al_9Co_2	3.594	0.449	2.711	0.64

QP21-0788-28

The Al-3Li and Al-3Li-X alloys do not recrystallize during extrusion, but rather show a fully recovered subgrain structure (Figure 6). These alloys do recrystallize in the absence of Zr upon solution heat treatment at 540°C (Figure 7).

After solution heat-treating at 540°C for 0.5 h, the Al-3Li and Al-3Li-X alloys were aged at 180-200°C for 16-24 h. Figure 8 shows typical microstructures resulting from this heat treatment. The microstructure of Al-3Li consists of a uniform distribution of 40-nm diam δ' (Al_3Li) precipitates, while the Al-3Li-0.16Ti and Al-3Li-0.64Co alloys have a bimodal distribution of δ' and dispersoids. The size of δ' following aging at 200°C for 24 h is about 40 nm, which is comparable to the value reported by Noble and Thompson (Reference 19) of 30 nm in similarly aged binary Al-Li alloys. For the heat-

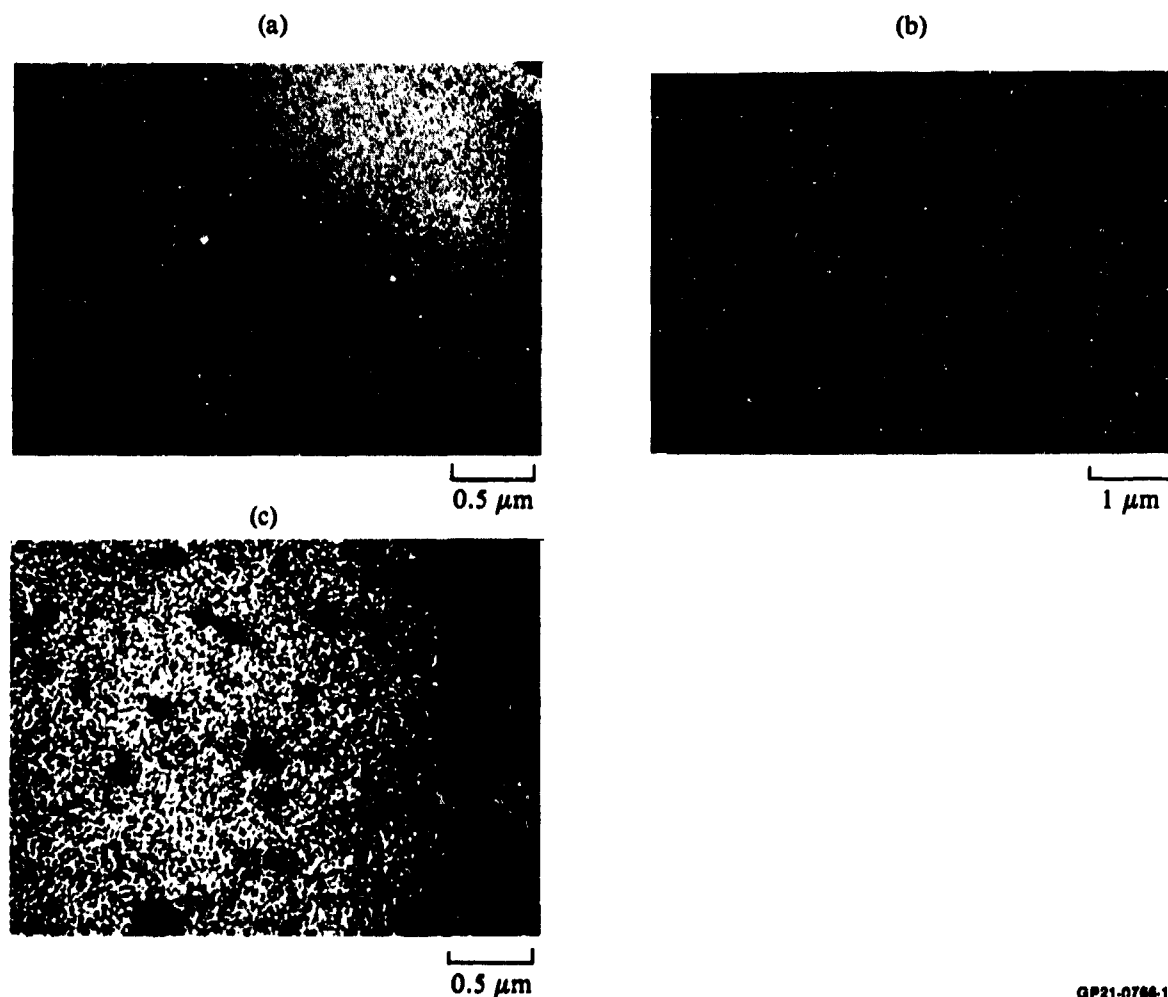


Figure 8. Microstructures of solution-treated-and-aged Al-3Li alloys: (a) Al-3Li aged 180°C/16 h, (b) Al-3Li-0.16Ti aged 180°C/16 h, and (c) Al-3Li-0.64Co aged 200°C/24 h.

treatment temperatures employed, grain boundary precipitation of the equilibrium δ (AlLi) phase and precipitate-free zones near the grain boundaries are not observed.

4.1.2 Deformation Behavior of Al-Li-X Alloys

The room-temperature tensile properties of the roller-quenched Al-3Li alloys are presented in Table 6, which includes the properties of Al-3Li-Mn and Al-3Li-Zr extrusions processed from cast ingots (Reference 5). The Al-Li-Y extrusion was defective and did not yield meaningful results. Many of the results for the different alloys cannot be directly compared because the actual lithium contents were not the same. Trends with compositional and

TABLE 6. ROOM-TEMPERATURE TENSILE PROPERTIES OF ROLLER-QUENCHED, EXTRUDED, AND HEAT-TREATED AL-LI-X ALLOYS.

Alloy number and composition	Solution annealed at 540°C for 0.5 h and cold-water quenched			Solution annealed at 540°C for 0.5 h, cold-water quenched, and aged at 200°C for 24 h		
	Yield stress at 0.2% offset (MPa)	Ultimate tensile strength (MPa)	Total elongation (%)	Yield stress at 0.2% offset (MPa)	Ultimate tensile strength (MPa)	Total elongation (%)
High-purity alloys						
1 Al-2.70Li	69	212	24.8	296	376	5.5
2 Al-2.8Li-0.24Mn	77	223	31.0	281	413	8.9
3 Al-2.18Li-0.038Cr	106	181	17.4	282	341	10.0
4 Al-2.78Li-0.49Fe	77	208	19.0	286	372	8.2
5 Al-2.95Li-0.64Co	104	256	19.9	296	409	8.3
6 Al-3.01Li-0.18Ti	97	266	22.3	319	387	4.5
7 Al-2.95Li-0.27Zr	223	347	14.2	483	519	7.8
8 Al-2.76Li-0.40Cd	64	205	26.9	309	403	8.8
Commercial-purity alloys						
10 Al-2.36Li(CP1)	60	185	24.9	265	370	6.1
11 Al-2.67Li(CP2)	77	197	21.6	296	393	7.6
12 Al-2.54Li(CP3)	68	193	27.2	276	363	7.0
13 Al-2.73Li-0.35Sn	71	210	24.5	285	385	8.2
14 Al-2.71Li- <0.05 Sb	68	210	28.0	304	405	7.6
15 Al-2.75Li- <0.05 Bi	64	161	27.6	312	416	8.0
Ingot-processed alloys (Reference 5)						
16 Al-3.58Li-0.13Zr	—	—	—	454	480	2.0
17 Al-2.78Li-0.32Mn	—	—	—	264	376	5.0

GP21-0796 29

process variations are clearer from plots of yield stress as a function of percent elongation to fracture (Figure 9). Intercomparison of the results yields the following conclusions:

a) Rapid solidification of binary Al-3Li alloys improves ductility in comparison with ingot-processed alloys (compare alloys 1 and 10 with 16 and 17). This improvement is a direct result of grain refinement and improved homogeneity in the rapidly solidified alloys. Lithium-rich regions in the ingot material are not entirely relieved by thermomechanical processing and act as pathways for crack propagation.

b) Addition of dispersoid-forming elements to rapidly solidified Al-3Li alloys results in a further 3-5% increase of ductility (compare alloys 2-5, 8, and 11-15 with alloys 1 and 10). The reason for this ductility increase is apparent from examination of the deformation substructures of Al-3Li and Al-3Li-0.64Co in Figure 10. The deformation substructure of the Al-3Li alloy reveals intense planar slip with arrays of dislocations in parallel

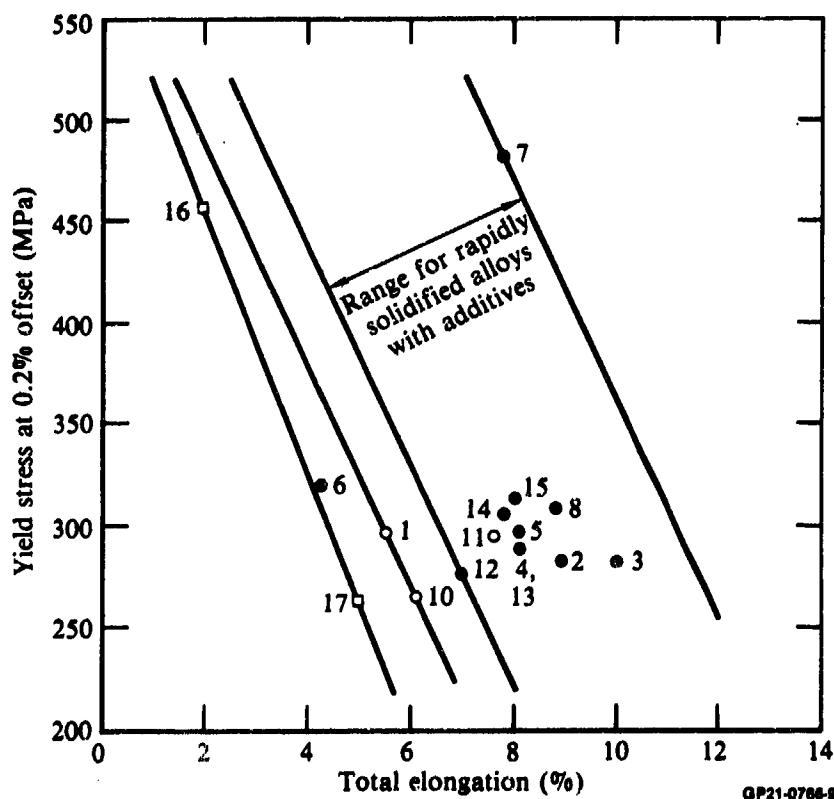


Figure 9. Relation of yield strength and ductility for Al-3Li and Al-3Li-X alloys. Numbers correspond to alloy numbers in Table 6. (□) Ingot-processed alloys, Reference 5, (◐) rapidly solidified Al-3Li alloys, and (●) rapidly solidified Al-3Li-X alloys.

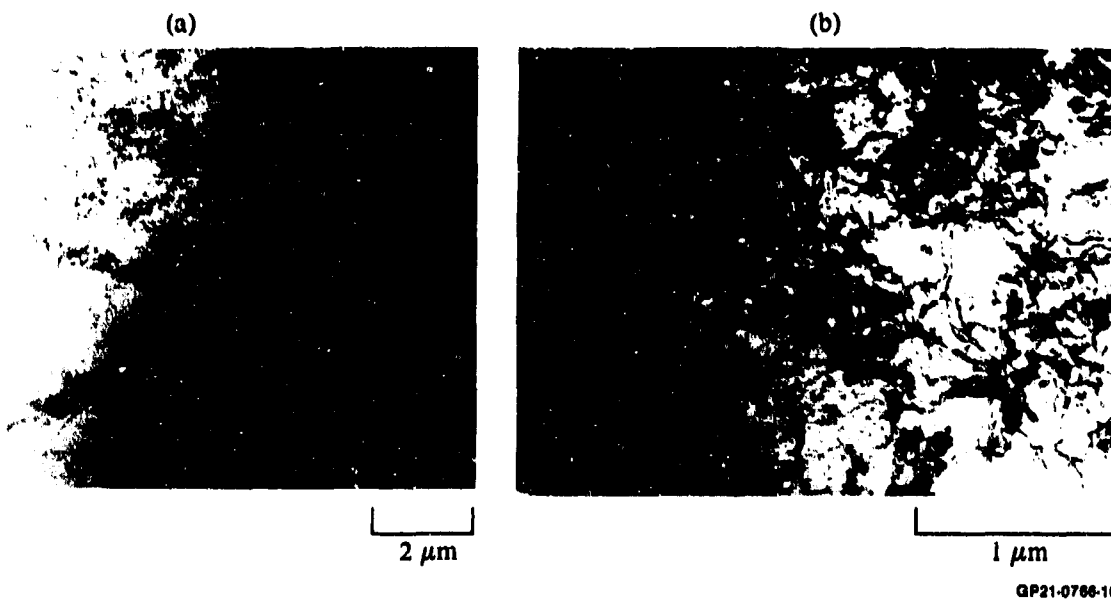


Figure 10. Substructures of solution-treated-and-aged Al-3Li alloys deformed in tension: (a) Al-3Li (high priority) and (b) Al-2.95Li-0.74Co.

bands (Figure 10a). In contrast, the deformation substructure of Al-3Li-0.64Co is essentially homogeneous and consists of dislocation debris at the dispersoid particles resulting from dispersoid-dislocation interactions. The dispersoid particles thus cause the spreading of slip bands, which results in smaller stress concentrations at the heads of the slip bands. The stress concentrations are further reduced by the fine grain size of the rapidly solidified alloys. The ability of the dispersoid particles and the fine grain size to disperse slip increases the ductility of Al-Li alloys.

c) All of the element additions that form incoherent dispersoids, except Ti, yield approximately the same amount of ductility increase. The size and spacing of dispersoids, rather than their chemical composition, determine the ductility increases resulting from slip dispersal. The tensile test data do not change the conclusion of the previous section that Fe and Co are the most effective dispersoid-forming additives.

d) Comparison of yield-stress data for the solution-annealed and solution-annealed and quenched conditions shows that most of the strength of the aged alloys is attributable to precipitation of δ' . The strengths of Al-3Li-X alloys containing incoherent dispersoids are not significantly greater than for binary Al-3Li alloys. Thus, dispersion strengthening is a relatively minor contribution to the room-temperature mechanical properties

of the alloys. A semiquantitative model for calculating yield stress contributions in Al-3Li-X alloys is discussed in the following section.

e) Small (0.2-0.3 wt%) additions of Zr cause 180-200 MPa increments in strength of Al-3Li alloys without significantly reducing the ductility (compare alloy 7 with alloys 2-5, 8, and 11-15). This strength increase is caused by precipitation of the coherent dispersoid Al_3Zr , which prevents recrystallization during thermomechanical treatment and provides substructure strengthening in the aged alloy. The coherent dispersoids also provide some direct dispersion strengthening.

4.1.3 Mechanisms of Strengthening in Al-Li-X Alloys

The observed macroscopic flow stress of the various Al-Li alloys is a superposition of the flow stress contributions from the δ' precipitates, dispersoids, and the Al-Li solid solution matrix. In Al-Li alloys, the δ' precipitates differ from the Al-matrix in composition and degree of order. These precipitates represent effective obstacles to dislocation motion and can interact with moving dislocations in the following possible ways (Reference 26):

- (a) par elastic interaction by virtue of their distortion,
- (b) dielastic interaction by virtue of their difference in shear modulus from that of the matrix,
- (c) since δ' is coherent with the matrix, shearing of δ' particles by dislocations and creation of an interface at the particle surface whose energy corresponds to a repulsive force on the dislocations,
- (d) since δ' is ordered, creation of an antiphase boundary when the particle is sheared by the first dislocation; although the energy of the antiphase boundary corresponds to a repulsive force, a second dislocation restores order and is attracted to the particle, and
- (e) interaction through differences in the stacking fault energy between δ' and the Al-matrix.

The lattice mismatch between the Al-matrix and δ' is small ($-0.8 \pm 0.02\%$, Reference 20), and thus distortion and interfacial energy are small. Since δ' is a superlattice, its shear modulus must be higher than that of the matrix, and only mechanisms (b) and (d) are expected to contribute to the flow stress of Al-Li alloys.

Strengthening resulting from the ordered nature of the precipitates varies directly with $f^{1/3}$ and $r^{1/2}$, where f and r are the volume fraction and radius of the ordered particles (Reference 27). Since the aging conditions for the various alloys are identical and the volume fraction of δ' in Al-Li alloys varies directly as the amount of Li available for precipitation as δ' , the increase in flow stress resulting from δ' precipitation in the various alloys is directly proportional to the cube root of the concentration of Li.

The solubility limit at 200°C of Li in Al with respect to metastable δ' has been determined to be 6.2 at.% (Reference 28). The yield stress of an Al-6.2 at.% Li solid solution was obtained by extrapolation of the plot of the yield stress of the binary alloys in the solution-annealed condition as a function of the square root of the Li concentration (Figure 11). A parabolic hardening law was used since the data of Jones and Das (Reference 29), which are the only data available on the flow stress of Al-Li solid solutions, fit

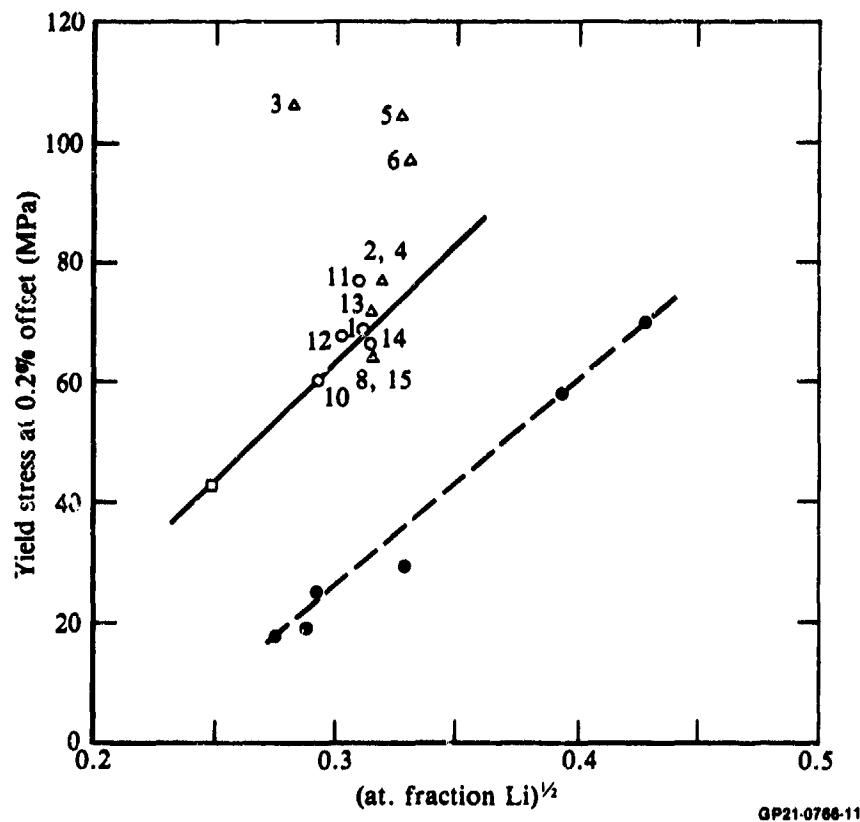


Figure 11. Variation of yield stress with Li-concentration for Al-Li solid solutions: (○) binary alloys, (△) alloys with dispersoid-forming elements, (— — —) data from Reference 34. Numbers correspond to those of the alloys in Tables 2 and 6; (□) Li concentration of 6.2 at.%.

this model rather well as shown by the dashed line in Figure 11. The higher strength levels of the rapidly solidified alloys compared with those of the ingot-processed alloys studied by Jones and Das (Reference 29) are due to the microstructural refinement and substructural strengthening resulting from rapid solidification processing. The contribution to flow stress from the Al-Li solid solution was assumed to be that of the yield stress of an Al-6.2 at.% Li solid solution which was obtained from the plot as 43 MPa.

The amount of Li available for precipitation as δ' is the total atomic fraction less 0.062. In aged, binary Al-Li alloys, the obstacles to dislocation motion are the Li atoms in solid solution and δ' precipitates. Since these two obstacles are fairly weak, the overall flow stress, σ , of the binary alloy is given by (Reference 30):

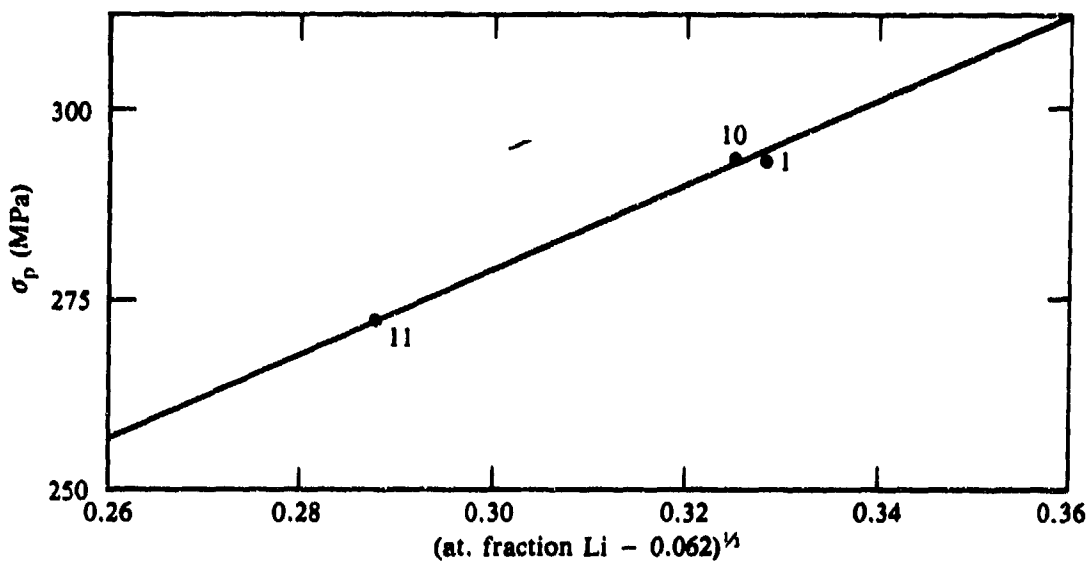
$$\sigma^2 = \sigma_m^2 + \sigma_p^2, \quad (1)$$

where σ_m and σ_p are the flow stress contributions from the solid solution and the precipitates, respectively. The δ' -precipitation strengthening contribution was obtained from a plot of $(\sigma^2 - \sigma_m^2)^{1/2}$ as a function of $(\text{Li concentration} - 0.062)^{1/3}$ (Figure 12). The dispersoid parameters in the Al-Li-Mn, Al-Li-Cr, Al-Li-Fe, Al-Li-Co, and Al-Li-Ti alloys were measured from transmission electron micrographs, and the dispersion-strengthening contribution was calculated from the modified Orowan relation (Reference 31):

$$\sigma_d = 1.03 \frac{G|\vec{b}|}{2\pi L} \ln \left(\frac{x}{r_0} \right), \quad (2)$$

where

- σ_d = particle by-passing stress,
- G = shear modulus of the matrix (≈ 29 GPa for Al-Li alloys),
- b = Burgers vector,
- L = mean planar interparticle spacing,
- x = mean particle size, and
- r_0 = inner cut-off radius = $4|\vec{b}|$.



QP21-6766-12

Figure 12. δ' -precipitation strengthening as a function of the amount of Li available for δ' -precipitation. Numbers correspond to those of the alloys in Tables 2 and 6.

A value of 0.32 for the Poisson's ratio of aluminum was used in deriving the above equation. The dispersoid parameters and the calculated values of the flow stress contributions from the dispersoids, σ_{md} , are presented in Table 7.

From the estimated strengthening contributions resulting from δ' precipitation (σ_p), dispersoids (σ_{md}), and the Al-Li solid solution matrix (σ_m), the overall flow stress was calculated. Since dispersoids are relatively stronger obstacles, the overall flow stress is given by (Reference 30):

$$\sigma = (\sigma_m^2 + \sigma_p^2)^{1/2} + \sigma_{md} \quad (3)$$

Table 8 compares the estimated yield-stress values with those of the measured values for the Al-Li-Mn, Al-Li-Cr, Al-Li-Fe, Al-Li-Co, and Al-Li-Ti alloys. Since in the solution-treated condition, the measured yield-stress values of the alloys containing dispersoid-forming elements are higher than those of the binary alloys, the lower values of the yield stress of the aged alloys compared with the estimated values suggest that the dispersion strengthening is offset to some extent by the presence of Li in the dispersoids. Overall strengthening of these alloys results predominantly from δ' precipitation, and any decrease in the volume fraction of this phase will cause substantial strength reductions.

TABLE 7. DISPERSOID PARAMETERS IN Al-Li-X ALLOYS.

Alloy	x (nm)	L _c (nm)	L (nm)	V _f	σ _{md} (MPa)
Al-Li-Mn	72	881	809	0.0002	21
Al-Li-Cr	60	417	357	0.0009	45
Al-Li-Fe	82	829	747	0.0003	21
Al-Li-Co	44	196	152	0.0034	98
Al-Li-Ti	46	507	461	0.0002	30

x = Mean particle size
 L_c = Mean planar center-to-center dispersoid spacing
 L = Mean planar inter-dispersoid spacing = L_c - x
 V_f = Volume fraction of dispersoids
 σ_{md} = Calculated dispersion strengthening

GP21-0766-30

TABLE 8. COMPARISON OF ESTIMATED AND MEASURED YIELD STRESSES OF Al-Li-X ALLOYS.

Alloy	σ _p (MPa)	σ _m (MPa)	σ _{md} (MPa)	Estimated yield stress $\sqrt{(\sigma_p^2 + \sigma_m^2)} + \sigma_{md}$ (MPa)	Measured yield stress (MPa)
Al-Li-Mn	301	43	21	325	281
Al-Li-Cr	258	43	45	307	282
Al-Li-Fe	299	43	21	323	282
Al-Li-Co	308	43	98	409	296
Al-Li-Ti	311	43	30	344	319

σ_p = Estimated strengthening from δ' precipitation
 σ_m = Estimated yield stress of Al-6.2 at.% Li solid solution
 σ_{md} = Estimated macroscopic dispersion strengthening

GP21-0766-31

Cadmium was added to Al-3Li with the objective of refining δ' by reducing the energy of the δ'-Al matrix interface. However, Cd additions do not result in additional precipitation strengthening (point 8 in Figure 9). As observed by Hardy (Reference 32), the effect of Cd is selective and depends entirely on the structural relation between the matrix and strengthening precipitates. The δ'/Al-matrix interfacial energy is small, and it appears that Cd does not

further reduce this energy to cause finer precipitate distribution and additional strengthening.

Tin, antimony, and bismuth were added to scavenge the tramp elements Na and K, prevent their segregation at grain boundaries, and thus suppress intergranular fractures. In the Al-Li-Sb and Al-Li-Bi alloys, the amounts of the additives were smaller than intended. The increased ductility of the Al-Li-Sn alloy may be due partly to the effect of Sn in neutralizing the deleterious influence of Na. The effects of these elements cannot be isolated, and the improved ductility of these alloys also may be due partly to the presence of 0.05 wt% of the dispersoid-forming element Fe, which is a residual impurity. However a comparison of the ductilities of identically heat-treated, high-purity Al-3Li alloys (containing < 20 p.p.m. Na) and commercial-purity Al-3Al alloys (containing ~ 30 p.p.m. Na) indicate that Na in concentrations < 30 p.p.m. has no deleterious effect on the ductility of Al-Li alloys.

4.1.4 High-Temperature Deformation of Al-Li-X Alloys

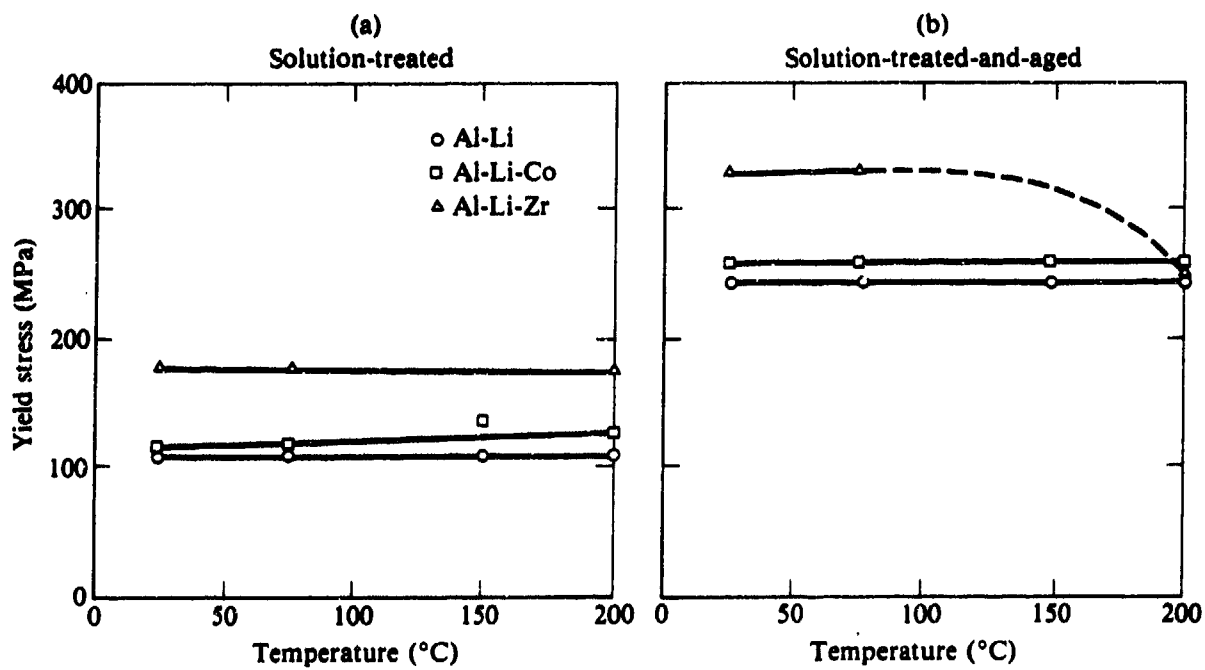
In the present investigation the deformation behavior as a function of strain and temperature was studied in Al-3Li, Al-3Li-0.5Co, and Al-3Li-0.5Zr alloys. The microstructures of the alloys in solution treated (ST) and solution treat-and-aged (STA) conditions are summarized in Table 9. These three alloys were chosen to study the superposition of solid-solution, precipitation, dispersion, and subgrain strengthening contributions. The impetus for the study of the temperature dependence of Al-3Li alloys arises from the similarity of this alloy system to the γ/γ' nickel-base superalloys which show remarkably superior high-temperature tensile and creep properties. The nature of the hardening precipitate is the same, i.e., an ordered, coherent precipitate having the $L1_2$ structure, and hence one should expect similar high-temperature behavior in Al-3Li alloys also.

The temperature dependence of the yield stress of the alloys in the ST and STA conditions is shown in Figure 13. The most striking feature of the results shown in Figure 13 is the absence of the strong temperature dependence of the flow stress typically found in f.c.c. metals and alloys. In Al-Li alloys, the modulus-normalized flow stress increases with an increase in temperature in a manner similar to that observed in γ' strengthened nickel-base superalloys (Reference 33) and $Ti_3Al(\alpha_2)$ precipitation-strengthened Ti-Al

TABLE 9. MICROSTRUCTURES OF Al-Li, Al-Li-Co, AND Al-Li-Zr.

Alloy	Microstructure in ST condition	Microstructure in STA condition
Al-3Li	Al-Li solid solution, some short-range order	Al-Li solid solution + Al ₃ Li (δ') precipitates
Al-3Li-0.64Co	Al-Li solid solution + Co ₂ Al ₉ dispersoids	Al-Li solid solution + Co ₂ Al ₉ dispersoids + Al ₃ Li precipitates
Al-3Li-0.27Zr	Partially recrystallized Al-Li solid solution + Al ₃ Zr precipitates + fine subgrains	Partially recrystallized Al-Li solid solution + Al ₃ Zr precipitates + Al ₃ Li precipitates + fine subgrains

QP21-0766-43



QP21-0766-38

Figure 13. Temperature dependence of yield stress of (a) solution-treated and (b) solution-treated-and-aged Al-Li-X alloys.

alloys (Reference 34). The mechanical behavior of the Al-Li alloy is largely determined by the size and volume fraction of δ' . The increase in flow stress with an increase in temperature in the solution-treated Al-3Li alloy is due to the in-situ precipitation during high-temperature testing of the strengthening δ' precipitate. Evidence for such precipitation was found by TEM examination

of the deformed specimens. The anomalous temperature dependence of the flow stress of the solution-treated-and-aged Al-3Li alloy arises from at least two factors:

- a) thermally activated formation of sessile cross slip barriers in the δ' (Al₃Li) phase and
- b) thermal restoration of order in Al₃Li phase.

The barriers in the first category include the formation of sessile dislocation segments resulting from cross slip of superdislocations from (111) planes to (100) planes (Reference 35) and the formation of antiphase tubes by the dragging of nonaligned jogs (Reference 36) within the Al₃Li particle. In view of the lower antiphase boundary energy on cube planes, screw-type superlattice dislocations cross slip onto {100} planes and become sessile. These sessile dislocations provide barriers to glide on the primary plane and cause work hardening in Al₃Li. Because cross slip becomes increasingly favorable with increasing temperature, the barrier strength of Al₃Li increases with increasing temperature. The concept of restoration of order as a possible cause of the temperature dependence of flow stress was proposed recently (Reference 34). When a leading dislocation shears an Al₃Li particle, disorder is created on the slip plane in the particle, and the movement of another dislocation is facilitated because it restores the order. If, however, after the movement of the first dislocation, order is restored within the sheared region of the particle by diffusion, then the next dislocation that encounters the particle has to overcome the same obstacle strength experienced by the first dislocation. This thermal restoration of order increases with temperature, causing the anomalous temperature dependence of the flow stress.

The yield stress of Al-Li-Co is a linear superposition of the flow stress contributions from the Al-Li matrix, δ' precipitates, and Co₂Al₉ dispersoids. The observed temperature dependence of the flow stress of Al-Li-Co alloys is as expected from the nonthermally activated strengthening by incoherent dispersoids. In contrast to Al-Li-Co alloy, the flow stress of STA Al-Li-Zr alloys decreases drastically with temperature above 75°C. In this alloy, the principal strengthening contributions are Al-Li solid-solution strengthening, δ' precipitation strengthening, a small amount of dispersion strengthening from Al₃Zr, and subgrain strengthening. The decrease in flow stress with temperature is caused by the inefficiency of subgrains acting as slip barriers at high temperatures.

The deformation substructures at 25°C of Al-3Li-Zr and Al-3Li-Co alloys are shown in Figures 14 and 15. In contrast to the extensive planar arrays of dislocations observed in binary Al-Li alloys, the Zr-containing alloy has dispersed tangled dislocation substructures. The small (< 3 μm) subgrains in the alloy effectively reduce the mean slip length and decrease the stress concentrations. This alloy in both the ST and STA conditions has higher ductility than the binary Al-Li alloy. In the Co₂Al₉ dispersoid-containing alloys, the dispersed phase markedly alters the deformation substructure by providing dislocation sources and barriers for dislocation motion. Dislocations overcome the dispersed-phase particles by Orowan bypass and Hirsch cross-slip mechanisms, which results in the dispersal of planar dislocation arrays and a significant reduction in stress concentrations at grain boundaries and slip-band intersections. The ductility of this alloy is about three times that of the binary Al-3Li alloy. The dislocation substructures of Al-3Li alloys containing incoherent dispersoids deformed in compression at 25°C at strains of ~ 5, 20, and 40% are shown in Figure 16. The slip-band/dispersoid interaction results in localized dislocation channels during the initial stages of deformation. With increasing deformation, dislocations are swept into the channels, resulting in well-defined dislocation mats whose spacing is determined by the spacing of the dispersoids. With increasing deformation temperature, dislocation cross slip and climb become dominant, planarity of slip is reduced significantly (Figure 17), and a dislocation cell structure begins to develop. In specimens deformed at 200°C, deformation seems to occur by the movement of unit dislocations (Figure 18) in contrast with the superdislocation motion at lower temperatures. The transition from unit dislocation motion to superdislocation motion manifests itself in the differences in morphology of δ' precipitates in specimens deformed at different temperatures (Figure 19). In the specimens deformed at 75°C, the δ' precipitates contain extensive defect structure (dislocations, antiphase boundaries); however, in the specimens deformed at 200°C, because of the thermal restoration of order and higher diffusion rates, the precipitates are relatively clean and defect free. Also at this temperature, deformation seems to proceed by the bypassing of δ' precipitates rather than by precipitate shearing.

The high-temperature mechanical properties of Al-3Li based alloys shown in Figure 13 indicate the potential use of Al-Li alloys for intermediate temperature applications requiring short-term tensile strengths.



Figure 14. Deformation substructure at 25°C in solution-treated Al-Li-Zr alloy.

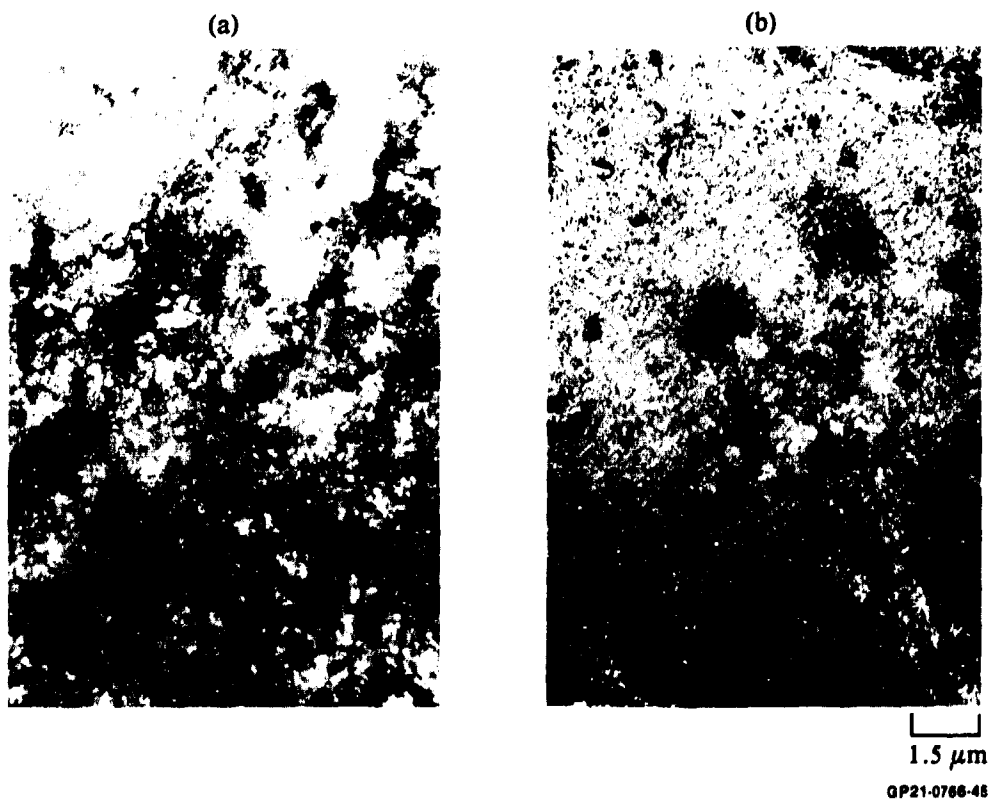
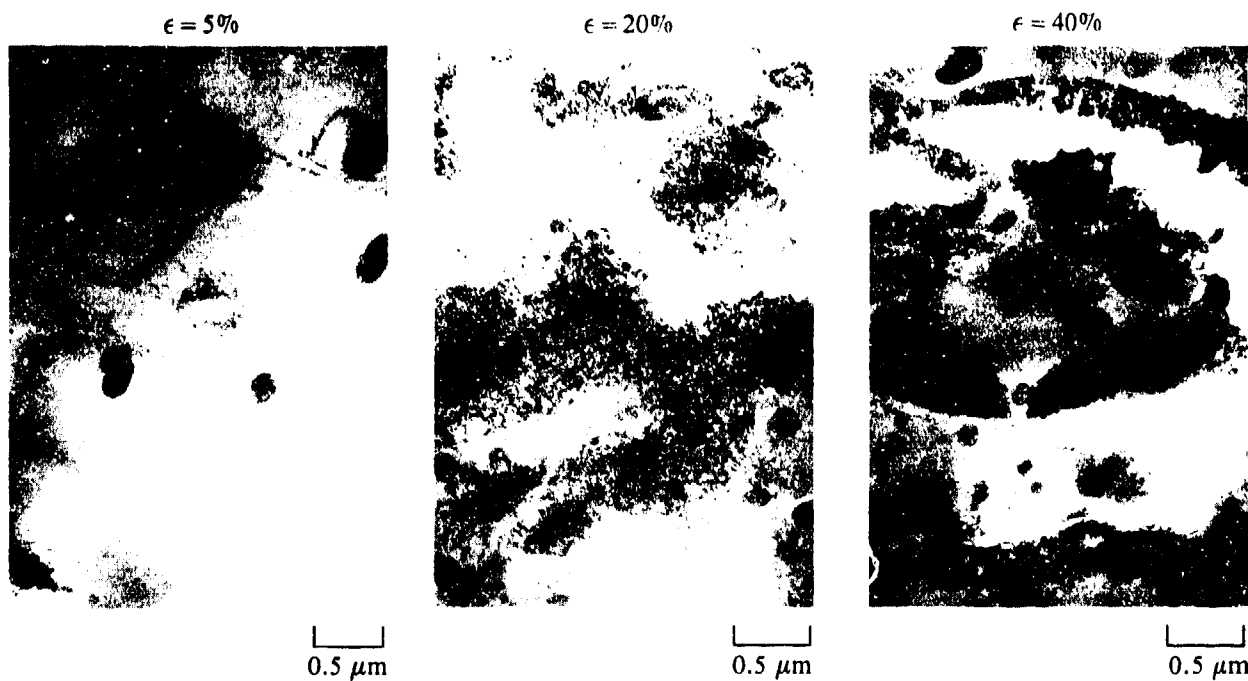


Figure 15. Deformation substructure at 25°C of (a) solution-treated and (b) solution-treated-and-aged Al-Li-Co alloy.



GP21-0766-42

Figure 16. Dislocation substructures in Al-3Li-0.6Co deformed in compression at 25°C.



GP21-0766-46

Figure 17. Deformation substructure at 75°C in solution-treated Al-Li-Zr alloy.

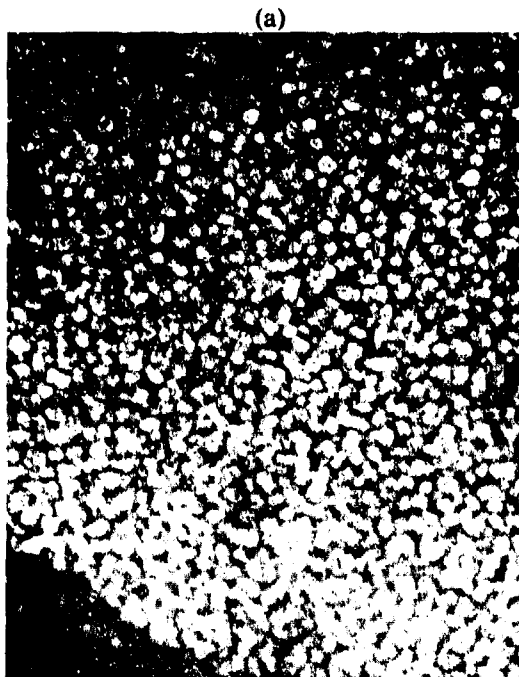


0.5 μm



0.5 μm
GP21-0766-40

Figure 18. Deformation substructure at 200°C in Al-Li-Co alloy.



0.5 μm



0.5 μm
GP21-0766-41

Figure 19. Al_3Li morphology in solution-treated-and-aged Al-3Li-0.2Zr alloy deformed in tension at (a) 75°C and (b) 200°C.

4.2 Microstructures of Multicomponent Al-Li Base Alloys

To obtain commercially attractive combinations of high specific-modulus and specific-strength in Al and Al alloys, a minimum addition of 2.5-3.0 wt% Li appears necessary. Although binary Al-Li alloys containing such levels of Li possess the desired low density and high stiffness, their strength levels are not sufficiently high. Furthermore, as shown in Figure 20, the decreasing solid solubility of the major alloying elements such as Cu (and similarly Mg and Zn) with increasing Li concentration limits the amount of Li that can be added without significant loss of strength to about 1.5% in Al-Cu and about 1% in Al-Zn-Mg-Cu alloys. Because the presence of Mg limits the solution-treatment temperature to less than 500°C in Al-Cu-Mg alloys such as 2024, additions of Li to such alloys will not result in high strength levels. Alloys with high levels of specific strength and specific modulus can be obtained in the Al-Cu-Li system by reducing the amount of Cu relative to that nominally present in 2xxx series alloys, and in the Al-Zn-Mg system by reducing the amount of Zn relative to that nominally present in the 7xxx series alloys.

An interesting and important aspect of the Al-Cu-Li system is the change in the types of strengthening phases that precipitate from the supersaturated Al solid-solution with changing Cu:Li ratios (Figure 21) (References 5, 37,

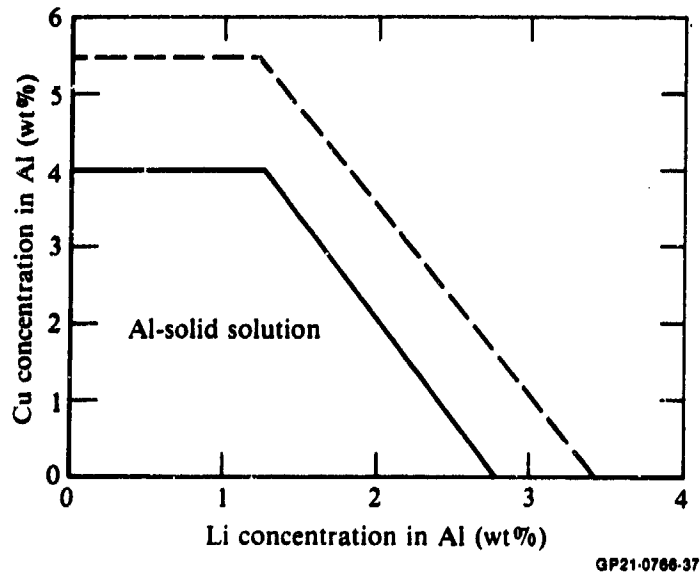


Figure 20. Solvus lines at 500°C (solid line) and 550°C (dashed line) for the Al-rich region of the Al-Li-Cu ternary system.

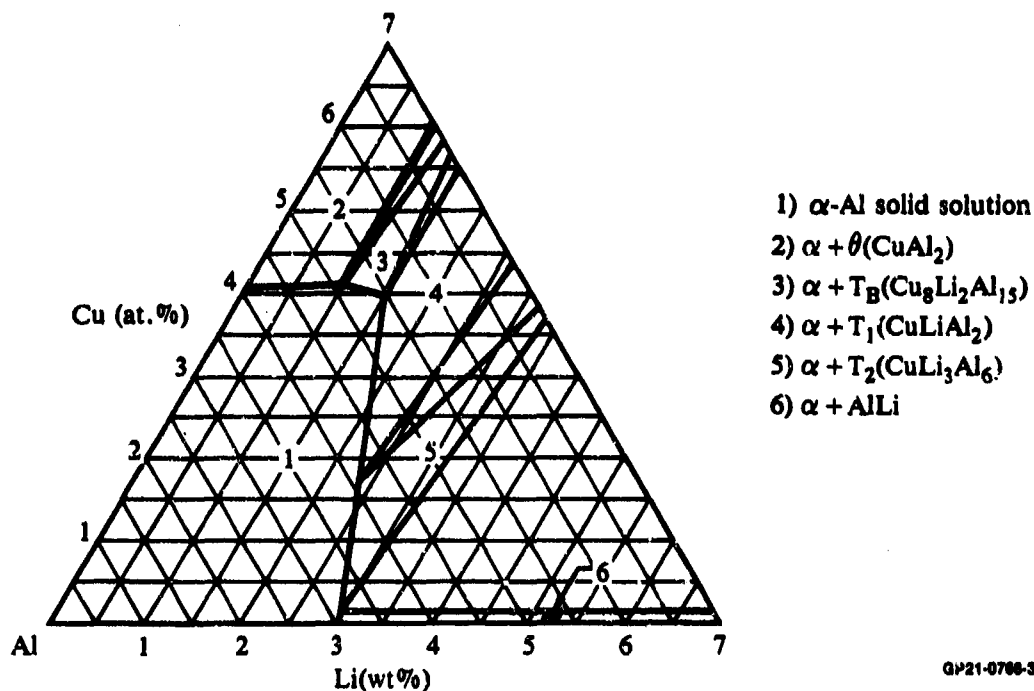
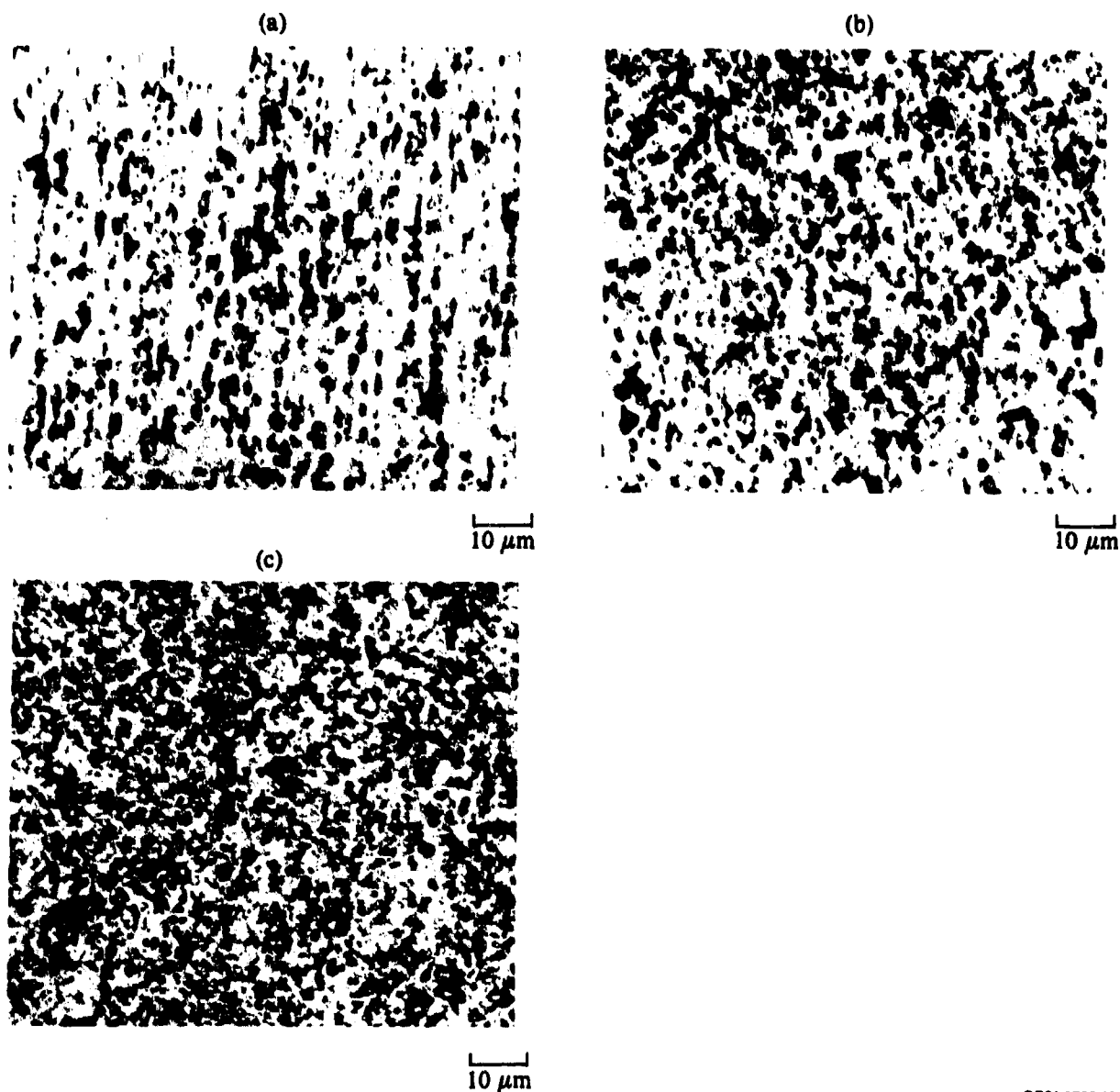


Figure 21. Phase relations at 500°C at the Al-corner of the Al-Cu-Li system.

and 38). In alloys with a high Cu:Li ratio (≈ 4), precipitation is similar to that in binary Al-Cu alloys with the precipitates being Guinier-Preston (G.P.) zones and θ'' . Guinier-Preston zones are layers of Cu atoms oriented parallel to the $\{100\}$ Al planes, and θ'' is a tetragonal, metastable, intermediate phase composed of disks of Cu and Al atoms coherent with the $\{100\}$ Al planes. Additional strengthening in high Cu:Li ratio alloys is provided by the Li dissolved in Al in underaged alloys or precipitated as δ' in peak-aged and overaged alloys. For intermediate Cu:Li ratios (≈ 3), formation of G.P. zones and θ' is accompanied by δ' precipitation. For lower Cu:Li ratios ($\approx 1.5-2.5$), θ'' is completely suppressed and δ' precipitation is accompanied by the equilibrium, hexagonal T_1 (Al_2CuLi) phase, which nucleates homogeneously from prior G.P. zones. As the Cu:Li ratio is lowered further to ≈ 1 , G.P. zones are completely suppressed, and δ' is accompanied by the heterogeneous precipitation of T_1 . The emphasis in this study was on alloys with nominally 3 wt% Li, a low (0.5-0.6) Cu:Li ratio, and dispersoid-forming additions of Mn, Ti, and Co. The effect of an 0.2Zr addition on the microstructure of rapidly solidified Al-Li-Cu alloys was also evaluated.

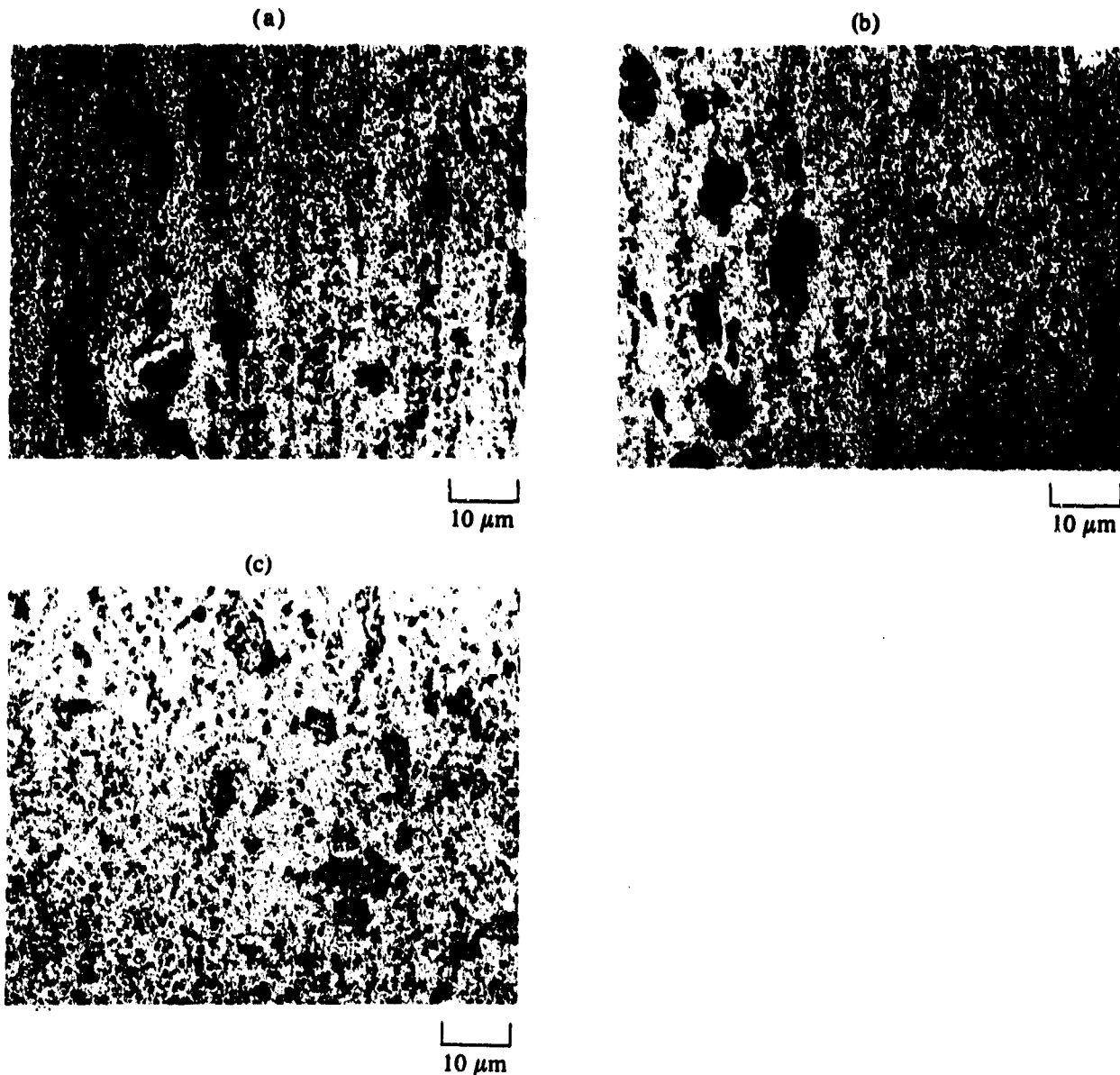
Microstructures of the extruded Al-Li-Cu-Mn, Al-Li-Cu-Ti, and Al-Li-Cu-Co-Zr alloys are shown in Figures 22-24. Considerable second-phase separation



GP21-0766-13

Figure 22. Microstructures of Al-3Li-1.7Cu-0.23Mn alloy in the extruded condition for (a) longitudinal, (b) long-transverse, and (c) short-transverse sections.

occurred during the consolidation process, but microstructural refinement was preserved in the two alloys (Figures 22 and 24) where composition was well-controlled. Second-phase particles, which are probably Al-Li-Cu ternary compounds such as T_1 or T_2 (Figure 21), had an average size of $\sim 2-3 \mu\text{m}$. Stringers of particles were observed in the extrusion direction. No major differences in sizes and shapes of second-phase particles were observed between the Al-Li-Cu-Mn alloy extruded from inert-gas-atomized powder (Figure



GP21-0766-14

Figure 23. Microstructures of Al-3.7Li-1.6Cu-0.98Ti alloy in the extruded condition for (a) longitudinal, (b) long-transverse, and (c) short-transverse directions.

22) and the Al-Li-Cu-Co-Zr alloy extruded from vacuum-atomized powder (Figure 24). The relatively high Mg, Zn, and Fe impurity levels in the Al-Li-Cu-Ti alloy led to formation of coarse (5-20 μm), second-phase particles upon extrusion (Figure 23).

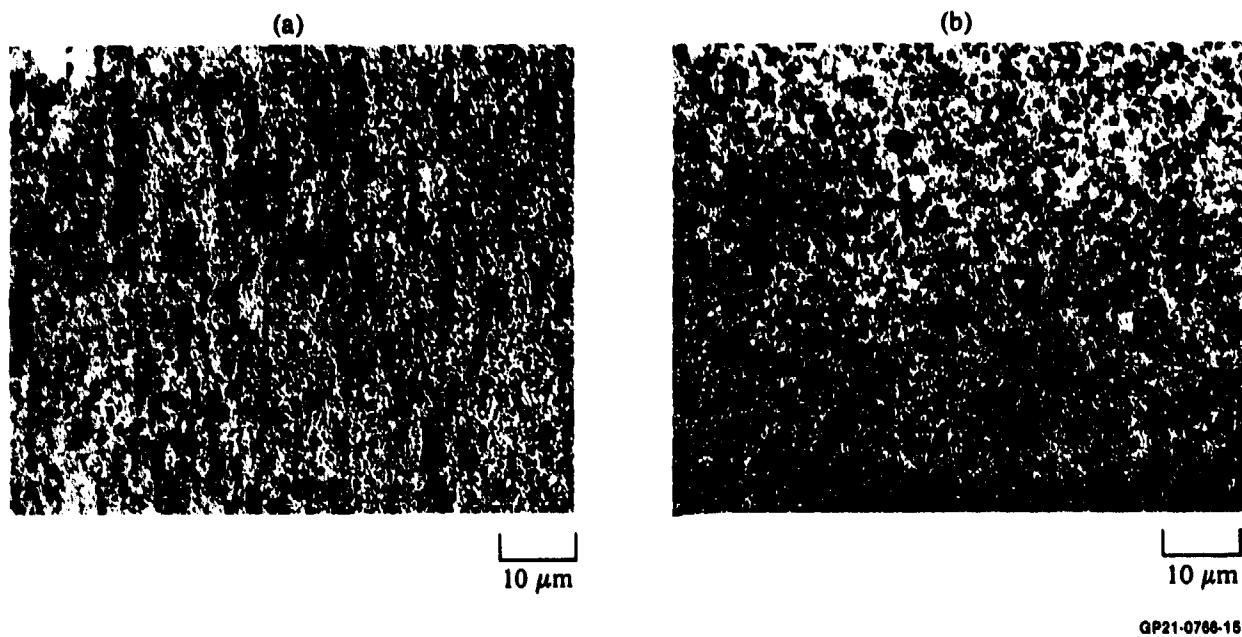
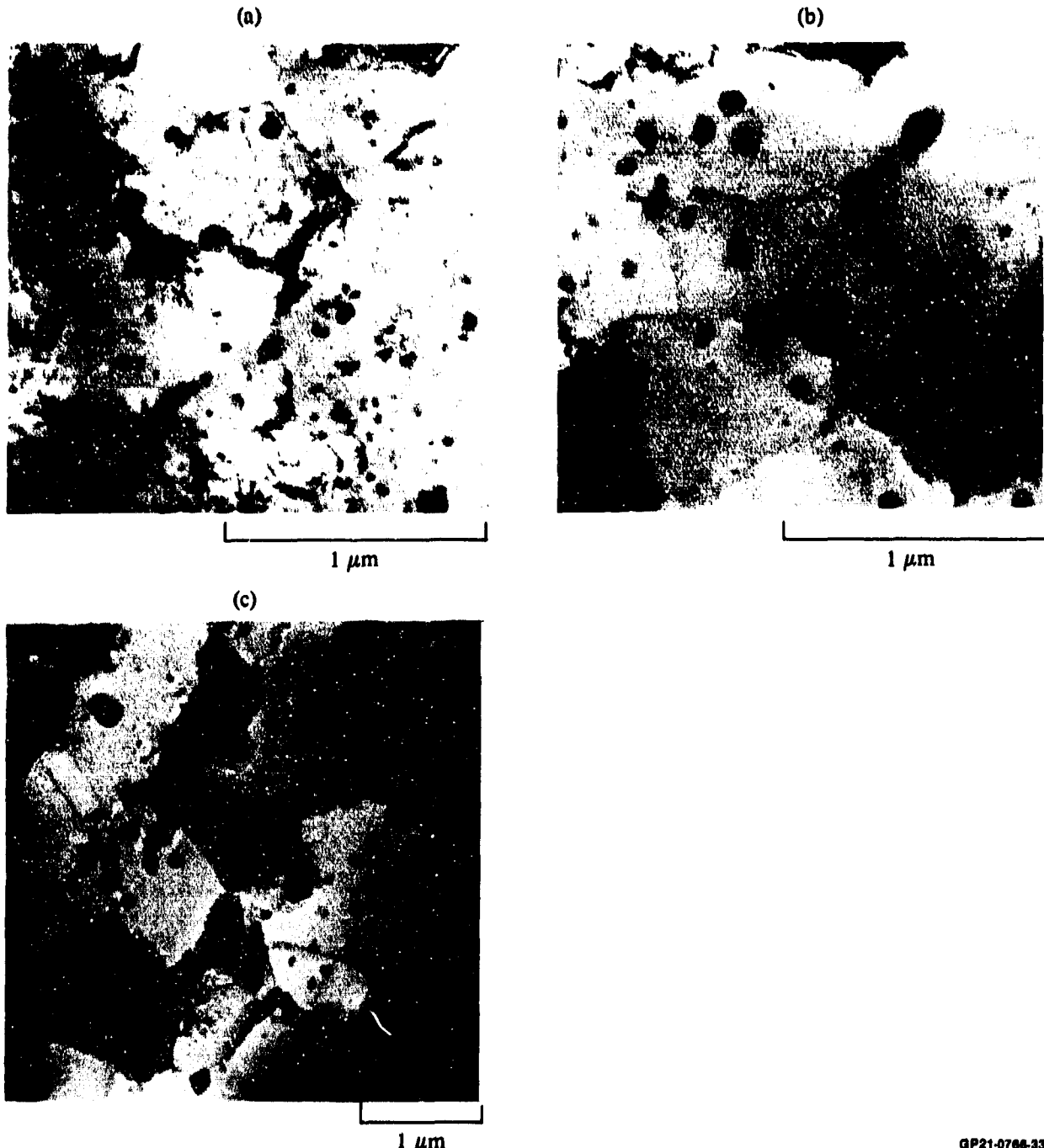


Figure 24. Microstructures of Al-3.1Li-1.7Cu-0.42Co-0.24Zr alloy in the extruded condition for (a) longitudinal and (b) transverse directions.

Microstructural refinement of subgrains and dispersoids is also evident in the as-extruded alloys (Figure 25a). Constituent particles and dispersoids are typically 0.05–0.2 μm in diameter. The sample shown in Figure 25a exhibits a fully recovered subgrain structure with 0.5–1 μm diam subgrains, in approximate agreement with the microstructure of the corresponding Al-3Li-0.23Co ternary alloy (Figure 6c).

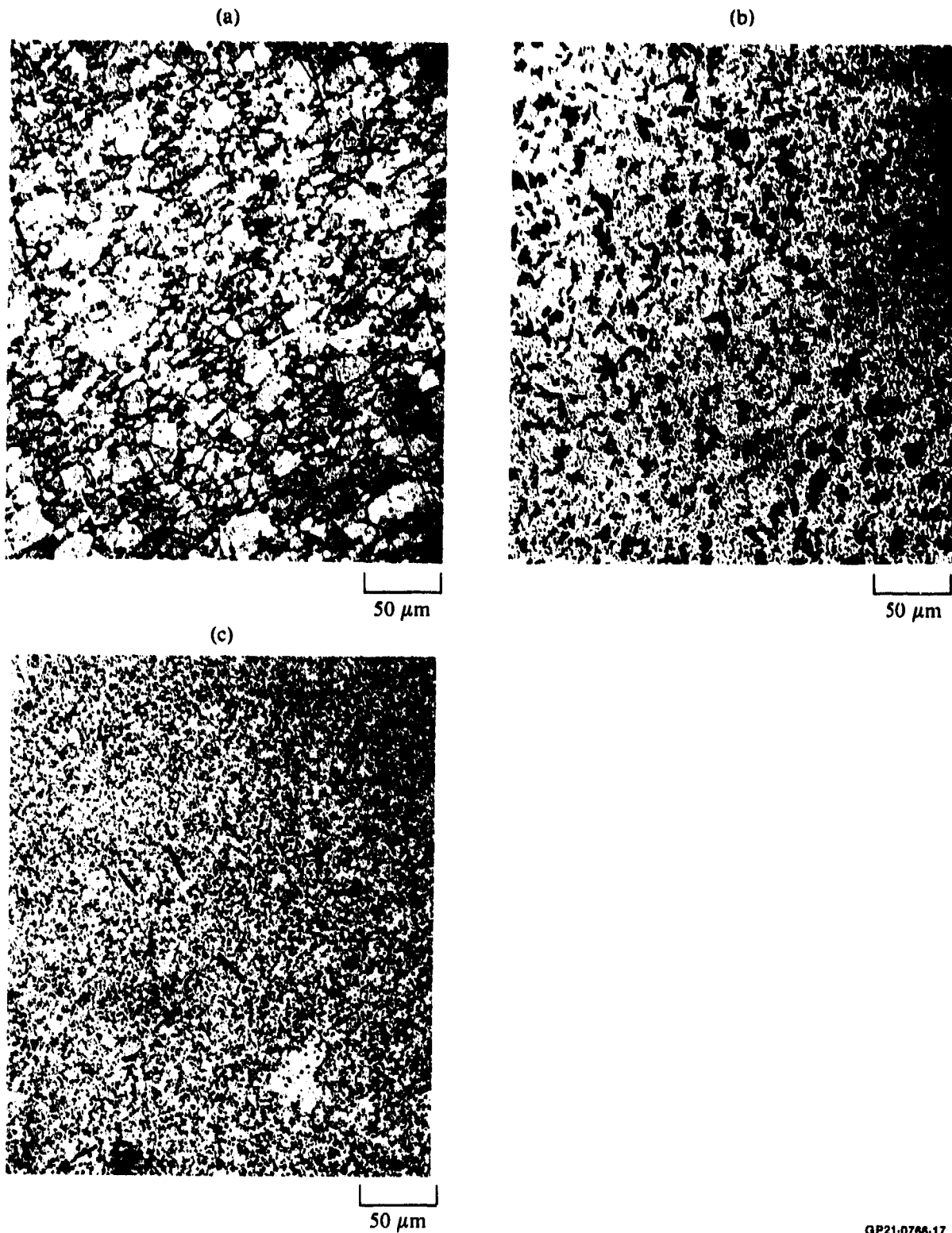
4.2.1 Microstructures of Solution-Treated Alloys

Microstructures of Al-Li-Cu alloys solution-annealed for 1 h at 530°C and water quenched are shown in Figures 25 and 26. The Al-Li-Cu-Mn alloy is recrystallized, with an average grain size of $\sim 20 \mu\text{m}$. The relatively low Mn level and relatively high solubility of Mn in the matrix led to a small volume fraction of Mn-containing dispersoids which did not present an effective barrier to recrystallization. The dispersoid-forming elements, particularly Zr, in the other two alloys allowed retention of the recovered but unrecrystallized subgrain structure typical of the as-extruded material (Figures 25b and 25c). The subgrains in the solution-annealed alloys are typically 1–3 μm in diameter and thus show little coarsening in comparison with the as-extruded subgrains.



GP21-0766-33

Figure 25. Transmission electron micrographs of (a) Al-Li-Cu-Co-Zr as-extruded, (b) Al-Li-Cu-Co-Zr solution-annealed 530°C/1 h, and (c) Al-Li-Cu-Ti solution-annealed 530°C/1 h.



GP21-0766-17

Figure 26. Microstructures of Al-Li-Cu alloys solution-annealed 530°C/1 h and water-quenched; (a) Al-Li-Cu-Mn, (b) Al-Li-Cu-Ti, and (c) Al-Li-Cu-Co-Zr.

The Al-Li-Cu-Mn and Al-Li-Cu-Co-Zr alloys show partial to complete dissolution of the second-phase particles formed during consolidation (Figures 26a and 26c). Little coarsening or further precipitation of second-phase particles is evident except for a few needle-like particles in the Al-Li-Cu-Co-Zr alloy (Figure 26c). The Al-Li-Cu-Ti alloy shows widespread precipitation of relatively large ($\sim 20 \mu\text{m}$) second-phase particles compared with the as-extruded condition. These particles, resulting from inadequate composition control in the original alloy, can act as sites for crack propagation and cause severe ductility limitations.

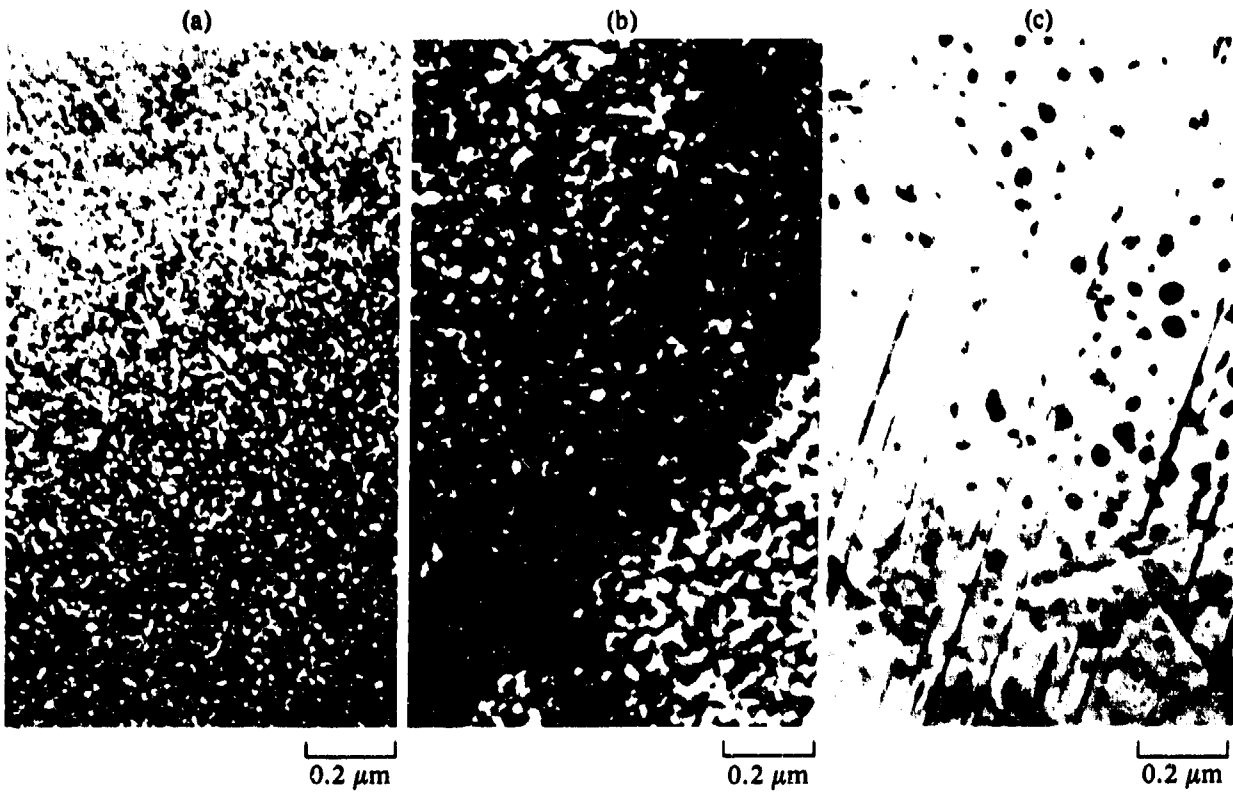
Dispersoids in the Al-Li-Cu-Co-Zr alloy are fine ($0.1\text{-}0.25 \mu\text{m}$ diam) and homogeneously distributed after solution annealing. The dispersoid size and distribution are comparable to those in the ternary Al-Li-Co alloy (Figure 7d), suggesting that the dispersoids in the multicomponent alloy contain primarily Al and Co and are not affected by the presence of multicomponent alloying conditions.

4.2.2 Microstructures of Solution-Treated-and-Aged Alloys

The solution-treated Al-Li-Cu alloys were aged at temperatures between 165 and 238°C for various lengths of times. These aging treatments cause the precipitation and subsequent overaging of δ' as illustrated for Al-3Li-1.7Cu-0.23Mn in Figure 27. As seen in Figure 27a, fine δ' precipitates ($\sim 10 \text{ nm}$) are observed in the underaged alloy. As aging proceeds, the size of δ' increases to about 10 nm in the peak-aged alloy (Figure 27b). The formation of T_1 is delayed until long aging times, and its formation is accompanied by the simultaneous coarsening and dissolution of δ' in the overaged alloy (Figure 27c). Thus, the precipitation in Al-Cu-Li alloys with a low Cu:Li ratio follows the sequence: Al solid-solution $\delta' \rightarrow T_1$.

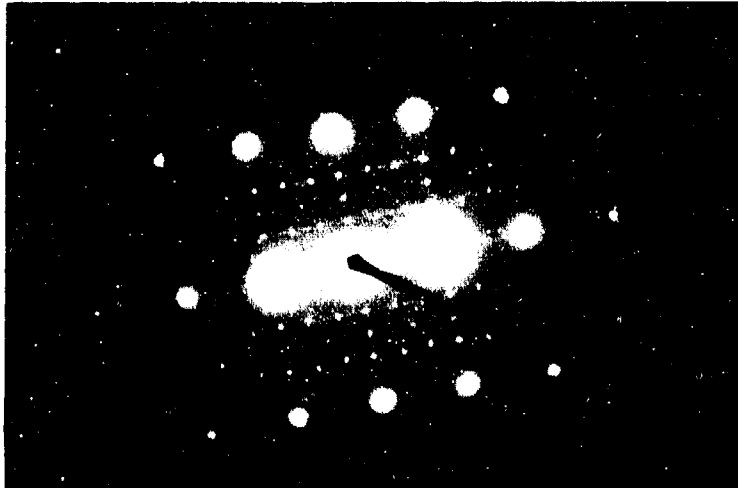
Analysis of the matrix and precipitate diffraction patterns (Figure 28-31) confirmed the hexagonal structure of T_1 and revealed the following orientation relations between the matrix and the T_1 and δ' precipitates:

$$(\bar{1}100)_{T_1} \parallel (\bar{2}20)_{Al} \text{ with } [11\bar{2}1]_{T_1} \parallel [001]_{Al} \text{ and } (100)_{\delta'} \parallel (100)_{Al} \text{ with } [110]_{\delta'} \parallel [110]_{Al}.$$



GP21-0766-18

Figure 27. Transmission-electron micrographs of Al-2Li-1.7Cu-0.23Mn alloy; (a) underaged (218°C/2 h), (b) peak-aged (218°C/8 h), and (c) overaged (238°C/12 h).



GP21-0766-50

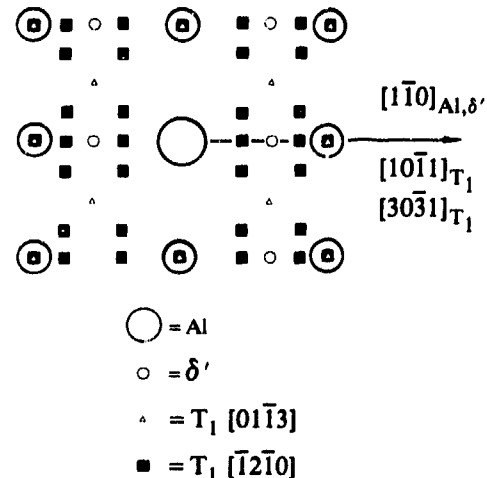
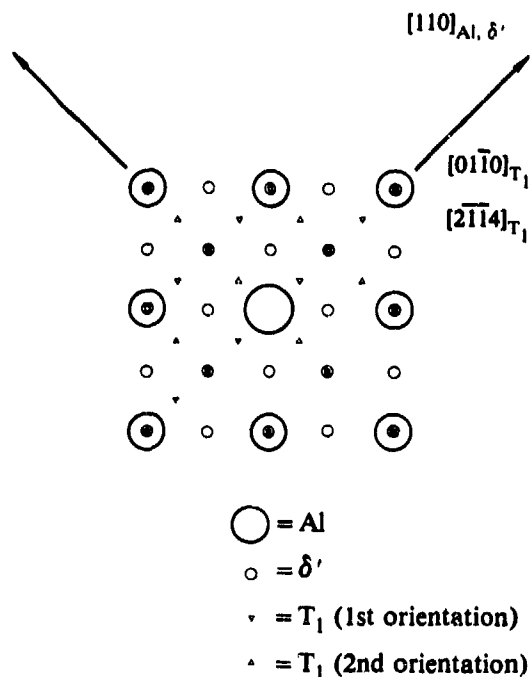
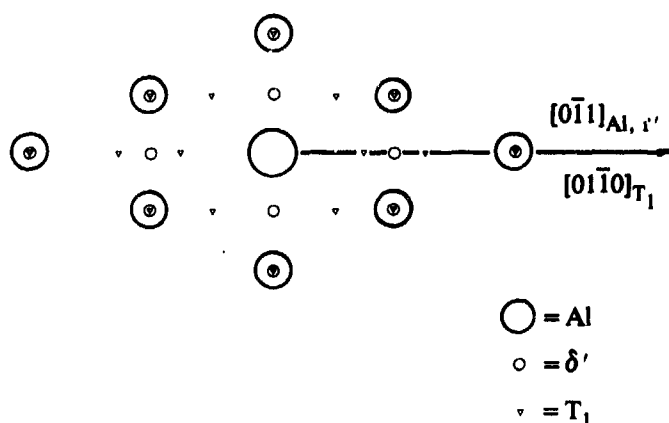
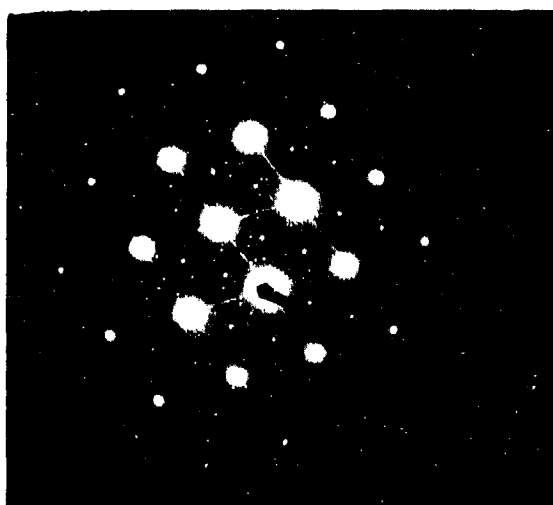


Figure 28. Selected area diffraction analysis of δ' and T_1 phases in Al-4Cu-2Li alloy solution-treated at 500°C for 0.5 h, water quenched to 25°C, and annealed at 100°C for 96 h. $[112]_{Al}$ zone axis, $[112]_{\delta'}$ zone axis, $[01\bar{1}3]_{T_1}$ zone axis, and $[\bar{1}2\bar{1}0]_{T_1}$ zone axis.



GP21-0766-47

Figure 29. Selected area diffraction analysis of δ' and T_1 phases in Al-4Cu-2Li alloy solution annealed at 500°C for 0.5 h, water quenched at 25°C, and annealed at 100°C for 96 h. $[001]_{\text{Al}}$ zone axis, $[001]_{\delta'}$ zone axis, and $[\bar{4}223]_{T_1}$ zone axis.



GP21-0766-48

Figure 30. Selected area diffraction analysis of δ' and T_1 phases in Al-4Cu-2Li alloy solution annealed at 500°C for 0.5 h, water quenched at 25°C, and annealed at 100°C for 96 h. $[011]_{\text{Al}}$ zone axis, $[011]_{\delta'}$ zone axis, and $[4223]_{T_1}$ zone axis.

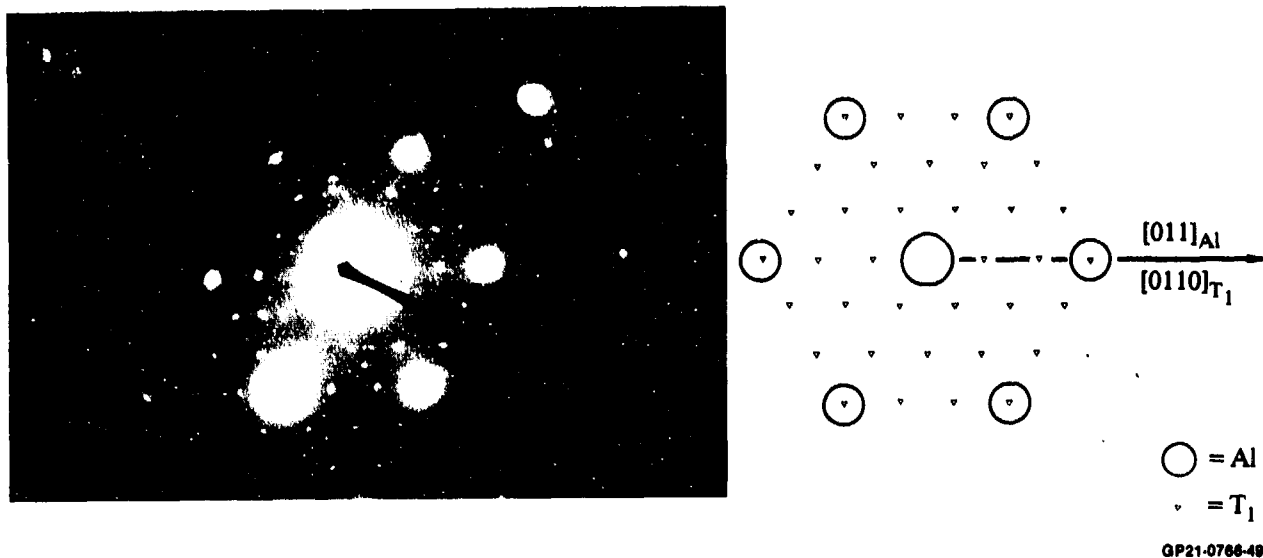


Figure 31. Selected area diffraction analysis of δ' and T_1 phases in Al-4C-2Li alloy solution annealed at 500°C for 0.5 h, water quenched to 25°C, and annealed at 225°C for 192 h. $[111]_{Al}$ zone axis and $[0001]_{T_1}$ zone axis.

The microstructures of the Al-Li-Cu-Co-Zr alloy, peak-aged at two different aging temperatures, are illustrated in Figures 32a-32d. The bimodal distribution of 20-40 nm diam δ' precipitates and 0.1-0.25 μm dispersoids is similar to that in the ternary Al-3Li-0.64 Co alloy (Figure 8c) and thus is little affected by Cu and Zr additions. Many of the favorable microstructural features of the ternary alloys and solution-treated Al-Li-Cu alloys are preserved in the aged Al-Li-Cu alloys.

4.2.3 Microstructures of Al-Li-Cu-Mg Alloy

Mg has a high solid solubility in Al, and the addition of Mg to Al-Cu alloys is known to increase strength through both solid-solution hardening and modification of the precipitation kinetics. The addition of Mg to Al-Li-Cu alloys was expected to result in increased strength without adversely affecting the toughness and secondary properties. Because of the possibility of coarse, heterogeneous precipitation of Al_2MgLi at high levels of Mg, the amount of this element was limited to 1.5 wt%. This alloy also contained the combined addition of 1 wt% each of Fe and Ni. In addition to determining the effects of Mg additions to Al-Li-Cu alloys, the Al-Li-Cu-Mg alloy was expected to provide data for comparison with the properties of the high-strength/high-temperature aluminum alloy 2618.

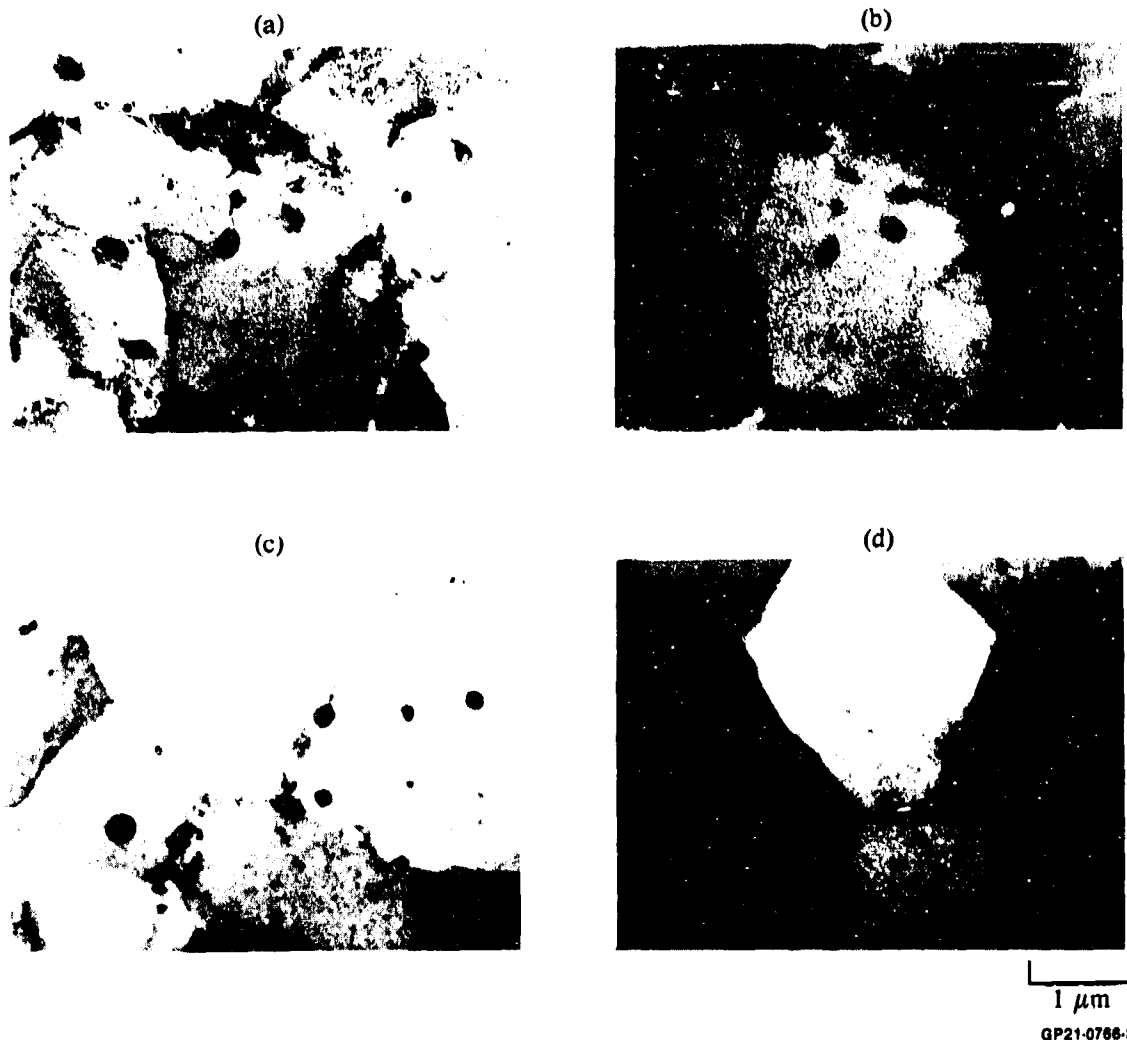


Figure 32. Transmission electron micrographs of Al-Li-Cr-Co-Zr alloy solution-treated 530°C/1 h and aged; (a) 190°C/8 h, bright field (b) 190°C/8 h, dark field, (c) 165°C/16 h, bright field, and (d) 165°C/16 h, dark field.

As in the case of the Al-Li-Cu-Ti alloy, the composition of the Al-Li-Cu-Mg-Fe-Ni alloy investigated here differed considerably from the nominal composition. Both Li and Cu contents were nearly 0.5 wt% too large, and 0.6 wt% Zn was present as an impurity (Table 3). This departure from the desired composition resulted in a large volume fraction of coarse (10-20 μm diam) second-phase particles in the as-extruded alloy which persisted in the solution-annealed and aged conditions (Figure 33). These particles adversely affect the ductility of the alloy.

Dispersoid formation, subgrain development, and the δ' precipitation sequence in the Al-Li-Cu-Mg-Fe-Ni alloy are similar to those in the Al-Li-Cu-

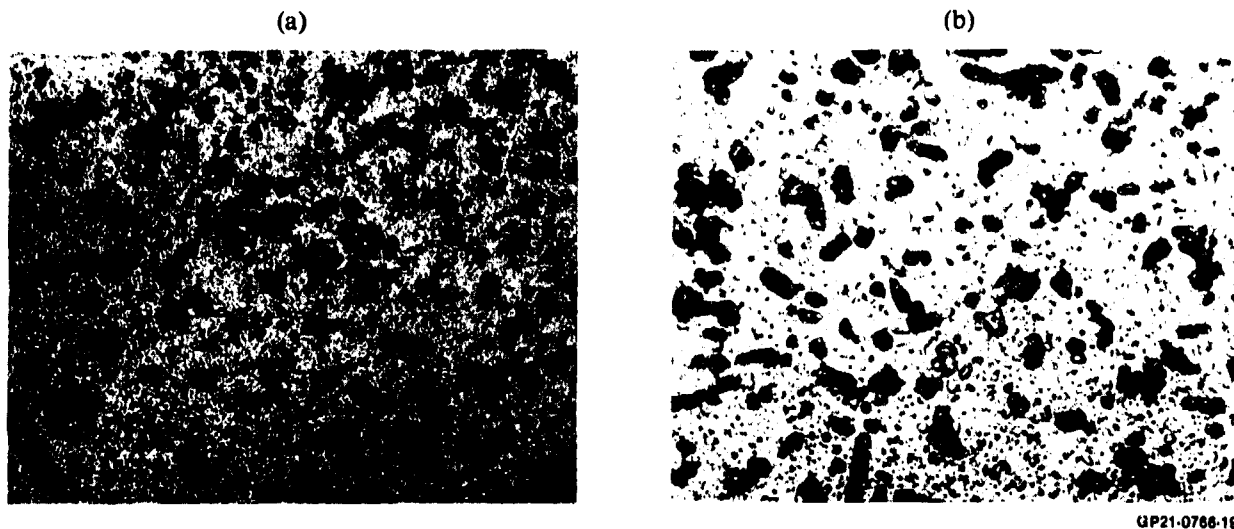


Figure 33. Microstructures of Al-Li-Cu-Mg-Fe-Ni alloy; (a) as-extruded and (b) as-solution-annealed 530°C/1 h.

Ti alloy. Typical dispersoid diameters of 0.25-1.0 μm and subgrain diameters of 1-3 μm as well as precipitate-free-zone formation in the peak-aged alloys were observed.

4.2.4 Microstructures of Al-Li-Mg-Zn Alloy

The effects of Li additions to alloys of the Al-Zn-Mg system (on which the 7xxx-series Al alloys are based) are not clearly known. However, with small amounts of Li (≈ 1 wt%), the phase relations in these alloys were not expected to be altered, and the effect of Li was expected to increase the specific strength and specific modulus. The Al-Zn-Mg-Li alloy was based on the composition of 7091Al and contained nominally 1.5 wt% Li and 0.5 wt% Co as ancillary additives.

On aging of an Al-Mg-Zn alloy such as 7091Al, the precipitation sequence, G.P. zones $\rightarrow \eta' \rightarrow \eta(\text{MgZn}_2)$, is followed. The peak strength (T6) temper corresponds to a mixture of G.P. zones and η' . The peak-aged alloy is susceptible to stress corrosion cracking (SCC), however, so that it is often overaged to the T73 condition to attain SCC resistance at the expense of strength. The addition of Li to the alloy is not expected to cause δ' formation at the relatively low temperature (typically 107°C) of peak-aging. The δ' phase does, however, precipitate at the temperatures (typically 177°C) of T73 heat

treatment. The precipitation of δ' is expected to produce an alloy with strength typical of the T6 condition and stress-corrosion-cracking resistance typical of the T73 heat treatment.

Samples of the extruded Al-Li-Mg-Zn-Co alloy were solution annealed at temperatures between 482 and 527°C. Typical micrographs of as-extruded and as-solution-annealed samples are shown in Figure 34. Second-phase particles are typically 1-3 μm in diameter in the as-extruded material, but coarsen to

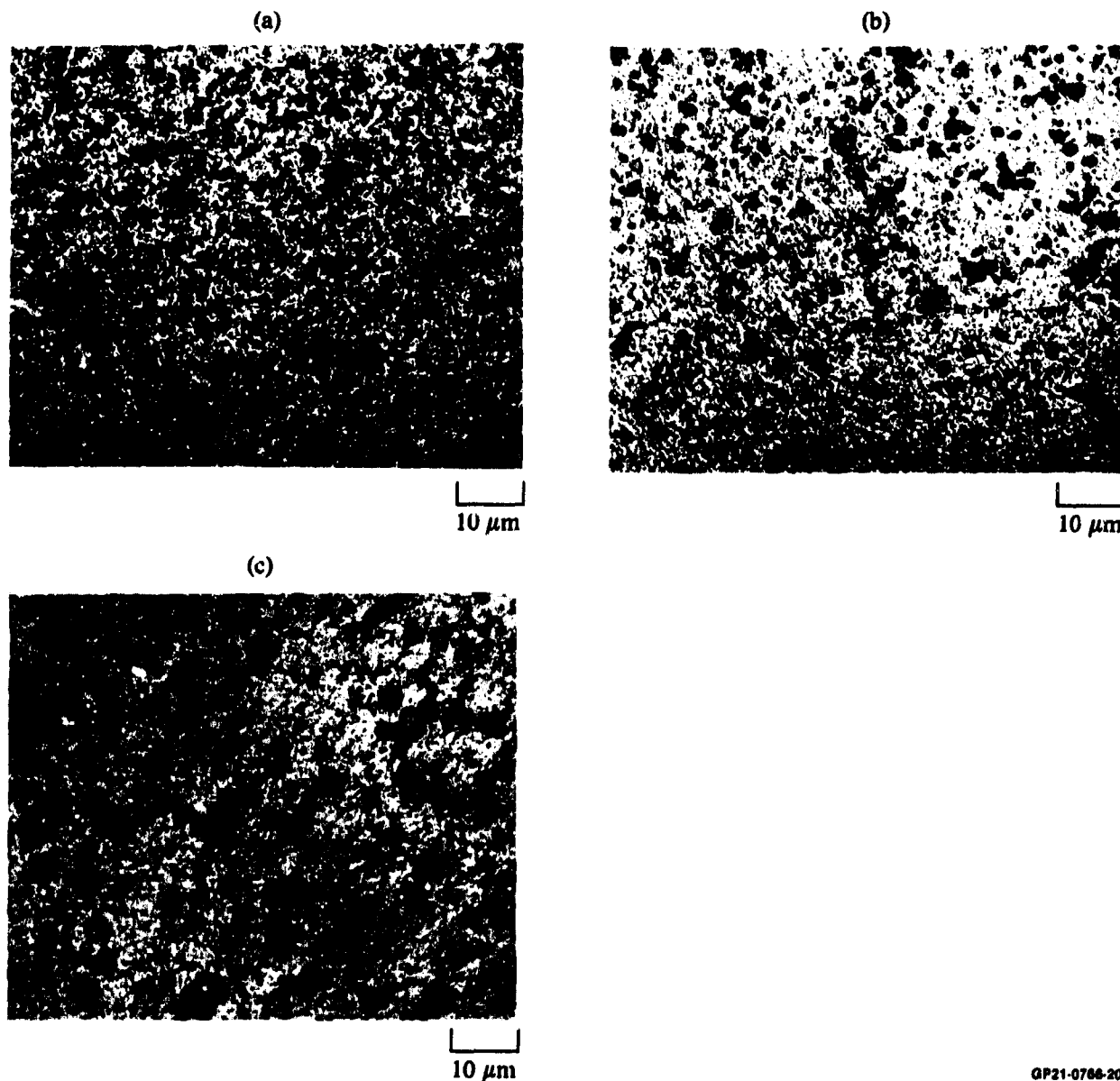


Figure 34. Microstructures of Al-Li-Mg-Zn-Cu-Co alloy; (a) as-extruded, (b) solution-annealed 482°C/1 h, and (c) solution-annealed 520°C/1 h.

2-5 μm diam after solution annealing for 1 h at 482°C and 2-10 μm diam after solution treatment at 520°C. Transmission electron micrographs of the solution-annealed alloy (Figure 35a) show relatively large (0.5-1 μm diam), presumably Co-containing dispersoids and relatively large (typically 5 μm) subgrain size.

Heat treatment of the Al-Li-Mg-Zn-Co alloy to T6 temper (Figure 35b) does not result in δ' precipitation, nor does it change the size or distribution of dispersoids. Upon subsequent aging at 177°C, it was found that δ' did not precipitate in samples previously solution-annealed at 482°C. However, aging of samples previously solution-annealed at 520°C results in a homogeneous distribution of δ' precipitates of ~ 20 nm average diameter (Figure 35c). Overaging of these precipitates causes coarsening to ~ 50 -60 nm average size after 64 h, formation of a precipitate-free zone at the subgrain boundaries, and precipitation of the phase T_1 (plates in Figure 35d). Thus the anticipated microstructural development of δ' upon overaging of this alloy occurs, provided the alloy is solution-annealed at a sufficiently high temperature to dissolve second-phase particles containing Li which formed during consolidation.

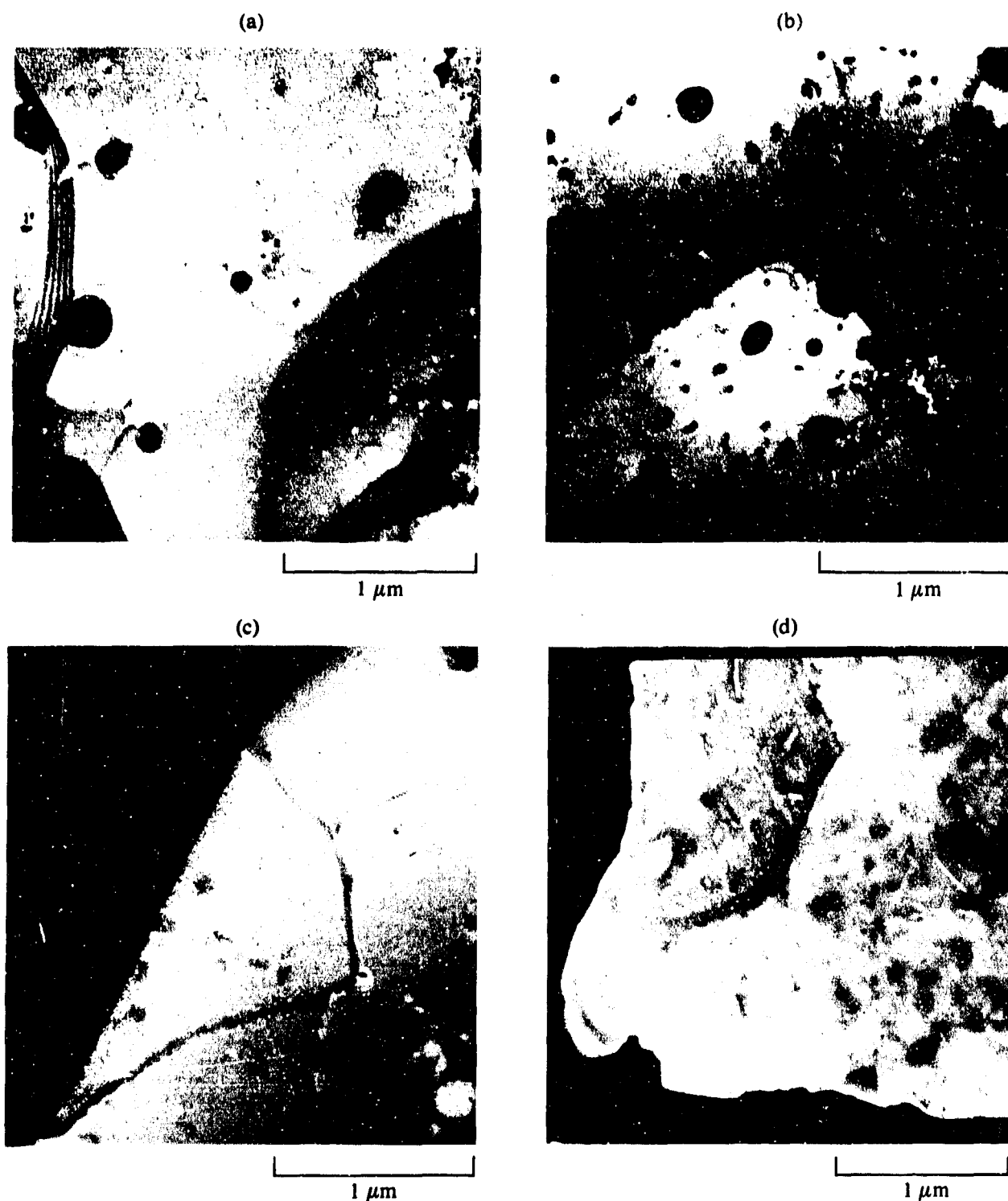
4.3 Deformation and Mechanical Properties of Al-Li-Cu and Al-Li-Mg Alloys

4.3.1 Mechanical Properties

Aging curves for the Al-Li-Cu-Ti, Al-Li-Cu-Co-Zr, and Al-Li-Cu-Mg-Fe-Ni alloys are shown in Figure 36. A temperature near 190°C was established as the optimum aging temperature for these alloys to achieve peak strength in 4-8 h. Precipitation of the strengthening phase δ' is rapid at this temperature; hardness values near the peak were found after only 0.5 h of aging. Reduction of aging temperature to 165°C for the Al-Li-Co-Zr alloy increased the time for peak aging to 16 h.

Tensile test results on underaged, peak-aged, and overaged Al-Li-Cu and Al-Li-Cu-Mg alloys are summarized in Table 10. Comparison of results for the rapidly solidified alloys with properties of commercial 2024-Al allows the following conclusions to be drawn:

- a) The rapidly solidified alloys in general have longitudinal yield and ultimate tensile strengths in the peak-aged condition equal to or greater than those of 2024-Al. Except for the Al-Li-Cu-Mg-Fe-Ni alloy, however,



GP21-0766-35

Figure 35. Transmission electron micrographs of Al-Li-Mg-Zn-Cu-Co alloy (a) solution-annealed 520°C/1 h, (b) 520°C/1 h + 107°C/8 h (T6), (c) 520°C/1 h + 107°C/8 h + 177°C/8 h (T73) (dark field), and (d) 520°C/1 h + 107°C/8 h + 177°C/64 h (overaged) (dark field).

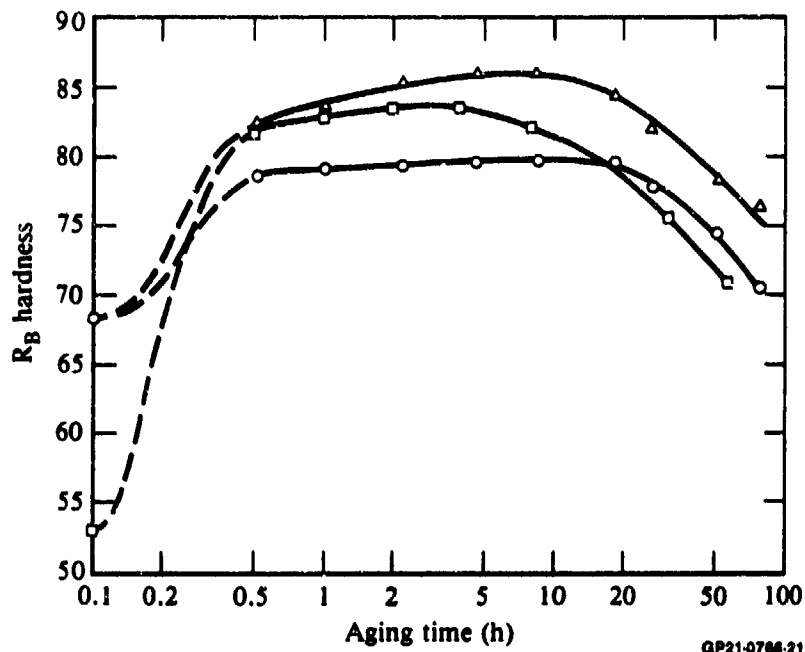


Figure 36. Aging curves for Al-Li-Cr and Al-Li-Cu-Mg alloys solution-annealed 530°C/1 h; (○) Al-Li-Cu-Ti, (◻) Al-Li-Cu-Co-Zr, and (△) Al-Li-Cu-Mg-Fe-Ni.

transverse yield and tensile strengths are well below the strength quoted for ingot 2024-Al.

b) As in the ternary alloys, addition of Zr to multicomponent Al-Li-Cu alloys results in significant (75-100 MPa) increases in yield strength because of substructure stabilization and direct strengthening by the Al_3Zr dispersoids.

c) Ductilities of the peak-aged alloys are lower than that of 2024-Al, and several of the alloys have poor (< 1%) ductility in the peak-aged condition. Even in the solution-treated condition, ductilities of Al-Li-Cu-Ti and Al-Li-Cu-Co-Zr are only 3.6-4.6%.

d) Increasing the solution-annealing temperature of the Al-Li-Cu-Co-Zr alloy from 530 to 560°C results in a noticeable decrease in yield strength. This decrease is associated with increased dissolution of constituent particles formed during consolidation as the solution-annealing temperature is increased. The mechanical properties of the alloy in the aged condition are not significantly affected by increasing the solution-annealing temperature, however.

e) Although the elastic moduli of the Al-Cu-Li alloys are larger than that of 2024-Al, only in the Al-Li-Cu-Mn alloy and in the Al-Li-Cu-Co-Zr alloy

TABLE 10. MECHANICAL PROPERTIES OF Al-Li-Cu AND Al-Li-Cu-Mg ALLOYS.

Alloy	Heat treatment	0.2% yield stress MPa (ksi)	Ultimate tensile stress MPa (ksi)	Elongation (%)	Young's modulus GPa (10 ⁶ psi)	
Al-3Li-1.7Cu-0.23 Mn	530°C/1 h } + 218°C/2 h }	L 448 (65.0)	496 (71.9)	2.1	86.2 (12.5)	
		T 296 (42.9)	336 (48.7)	2.0		
	530°C/1 h } + 218°C/8 h }	L 440 (63.8)	517 (75.0)	5.1		
T 310 (45.0)		376 (54.6)	1.4			
Al-3.7Li-1.6Cu-0.98Ti	530°C/1 h } + 238°C/12 h }	L 303 (43.9)	400 (58.0)	4.5		77.5 (11.24)
		T 200 (29.0)	310 (45.0)	0.6		
	530°C/1 h } + 190°C/8 h }	L 180 (26.1)	279 (40.5)	4.5		
T 183 (26.5)		226 (32.8)	1.5			
Al-3Li-1.6Cu-0.42Co-0.24Zr	530°C/1 h } + 190°C/4 h }	L 442 (64.0)	479 (69.5)	0.6	77.8 (11.28)	
		T — —	316 (45.8)	0.0		
	530°C/1 h } + 165°C/16 h }	L 270 (39.2)	391 (56.7)	3.6		
L 515 (74.6)		523 (75.9)	0.7			
Al-3Li-1.6Cu-0.42Co-0.24Zr	530°C/1 h } + 190°C/4 h }	L 544 (78.5)	549 (79.6)	0.5		83.8 (12.15)
		L 241 (35.0)	413 (59.9)	4.6		
	560°C/1h } + 190°C/4h }	L 225 (32.6)	392 (56.8)	4.0		
		L 529 (76.8)	535 (77.6)	0.1		
	Al-3.4Li-1.9Cu-1.5Mg-0.9Fe-0.8Ni	530°C/1 h } + 190°C/8 h }	L 417 (60.6)	455 (65.9)	0.8	
T 413 (59.9)			425 (61.6)	0.4		
Al-4.4Cu-1.5Mg-0.6Mn- (2024-Al)	500°C/1 h } + 190°C/8 h }	L 393 (57.0)	476 (69.0)	10	72.4 (10.5)	

GP21-0766-32

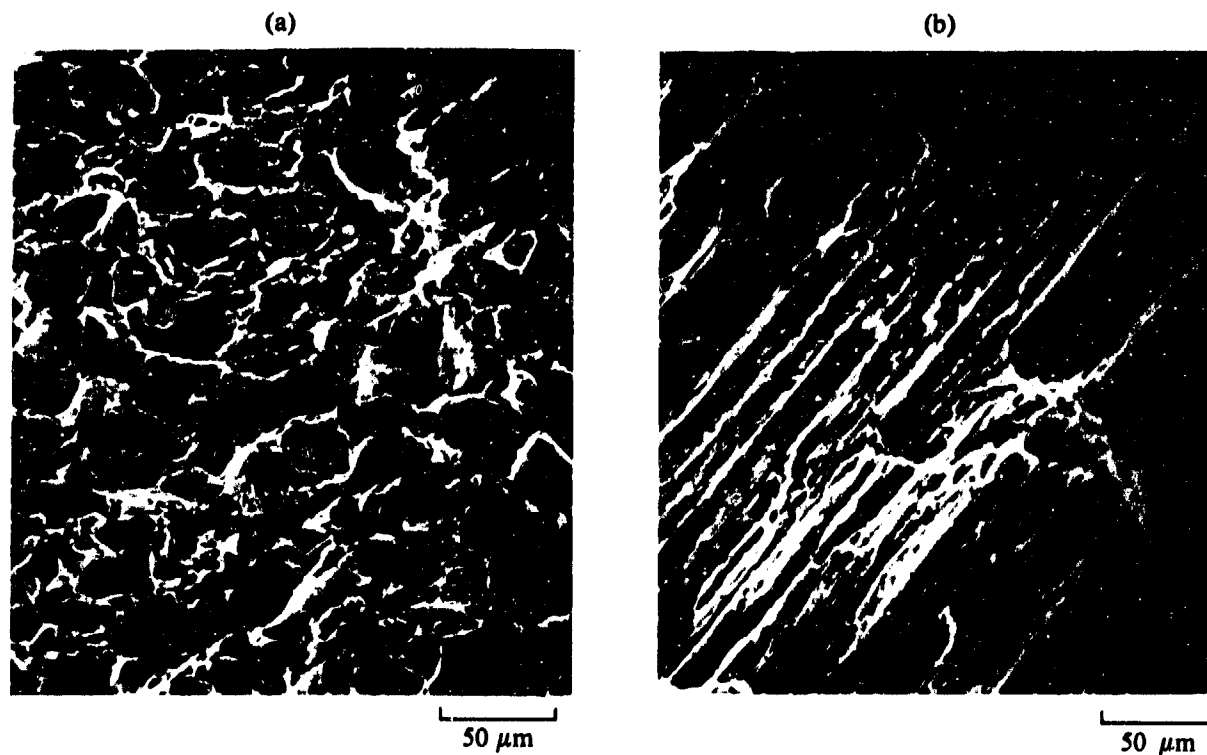
aged at 165°C does the measured modulus equal or exceed the value of 83.3 GPa measured in binary Al-Li alloys containing δ' . The absence of constituent particles in the Al-Li-Cu-Mn alloy (Figure 26a) and their presence in the alloys of lower modulus (Figure 26b, c) suggests that the presence of copper and other multicomponent alloying elements reduces the solubility of Li in the matrix and promotes the formation of ternary or complex constituent particles. The effect is not the result of copper additions alone, since there is a large difference in number of constituent particles between the Al-Cu-Li-Mn and Al-Li-Cu-Co-Zr alloys (Figures 26a and 26c), both of which have approximately the same Li and Cu concentrations.

f) Addition of 1.4 wt% Mg to an Al-Cu-Li alloy does not result in significant increases in strength. The microstructure of the Al-Cu-Li-Mg alloy contains numerous, relatively large, constituent particles (Figure 33), suggesting that Cu, Li, and Mg are removed from the matrix to these phases as the sum of their concentrations increases.

4.3.2 Fracture Morphology

To better understand the sources of low ductility in the Al-Li-Cu alloys, fracture surfaces of tensile specimens of aged Al-Li-Cu-Mn and Al-Li-Cu-Co-Zr alloys were examined by scanning electron microscopy (SEM). Fractographic results were correlated with the microstructures, and the mode of fracture and its microscopic nature were identified.

Micrographs of tensile fracture surfaces of the Al-Li-Cu-Mn alloy tested in the longitudinal and transverse directions are shown in Figure 37. As shown in Figure 37a, tensile fracture is intergranular, and the size of the



GP21-0788-22

Figure 37. Micrographs of tensile fracture surfaces of Al-3Li-1.7Cu-0.23Mn; (a) longitudinal and (b) transverse.

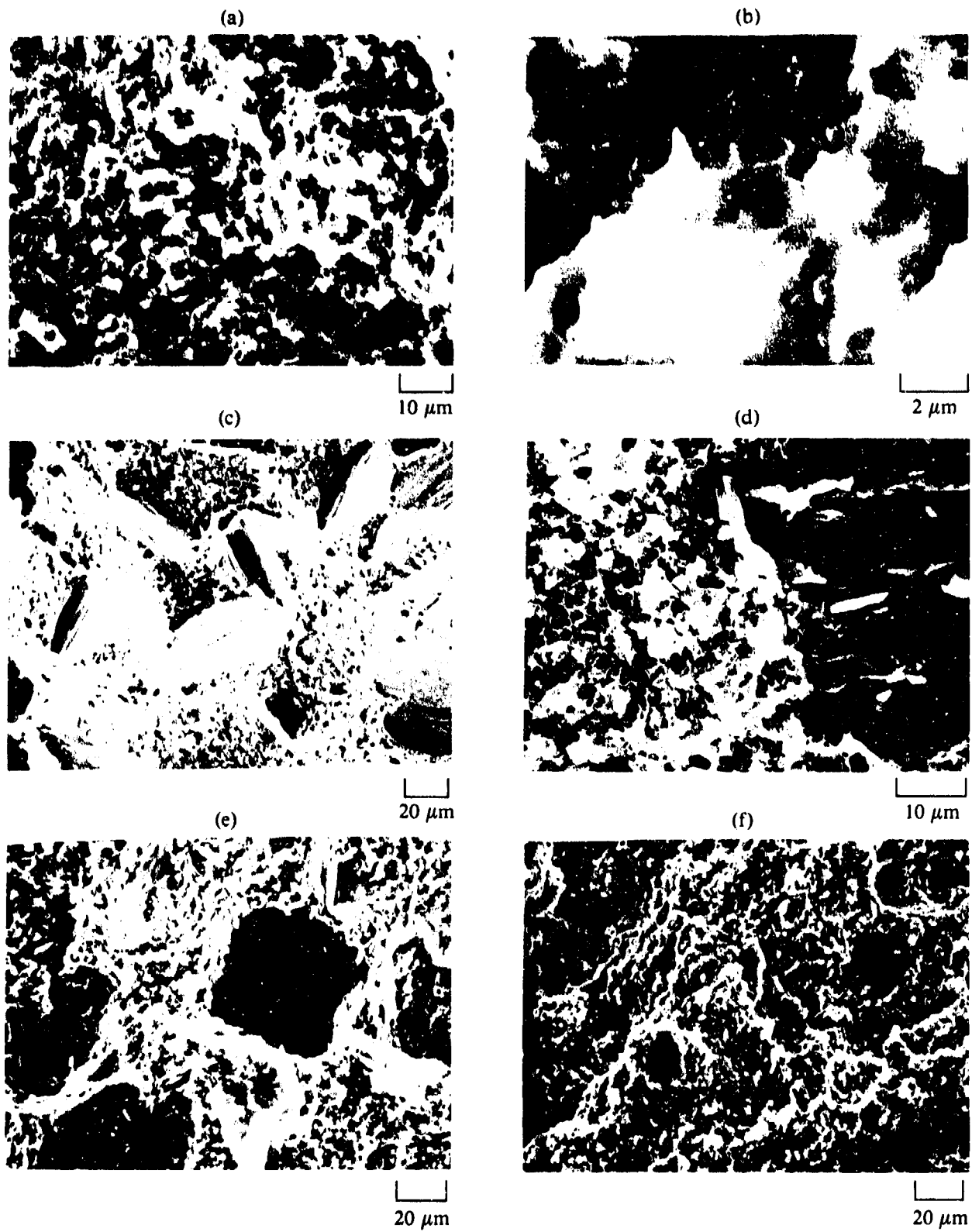
grain boundary facets closely corresponds to the grain size of the alloy (Figure 26a). Considerable delamination is observed in the fracture surfaces of the specimens tested in the transverse direction (Figure 37b), and this delamination results in lower transverse strength levels in the alloy.

Longitudinal tensile fracture surfaces of the Al-Li-Cu-Co-Zr alloy for various heat treatment conditions are shown in Figure 38. The fine dimples visible on the surface of the as-extruded sample (Figures 38a and 38b) correspond well in size to the subgrain diameter of the alloy (Figure 25a, 25b), and thus represent an essentially ductile inter-subgranular fracture mode. After solution-annealing, the subgranular fracture mode occupies about half of the fracture surface, with the other half being occupied by cleaved regions about 40-50 μm in diameter. This combination of subgrain and cleavage fracture persists on aging at 190°C, but aging at 165°C results in a predominantly inter-subgranular fracture surface containing only about 10% cleaved area.

The reason for partial cleavage fracture in solution-annealed and in aged alloys is not clear. These explanations are possible:

- a) cleavage occurs on favorably oriented planes which vary little in orientation across colonies of subgrains,
- b) the alloy is partially recrystallized in the solution-annealed condition and cleavage occurs across the recrystallized grains, or
- c) there are compositional inhomogeneities in the alloy which lead to variations in resistance to crack propagation across the fracture surface.

No evidence for partial recrystallization of the alloy is provided by optical or transmission electron micrographs of the solution-annealed alloy (Figures 25b and 26c). Energy-dispersive x-ray analysis of the cleavage fracture surfaces shows somewhat higher Cu concentrations than in the inter-subgranular fracture regions, but the difference is not large. Thus, explanation (a) appears most probable. It is also interesting that the percentage of cleaved area on the fracture surface does not correspond well to the ductility of the alloy.



GP21-0766-23

Figure 38. Tensile fracture surfaces of Al-Li-Cr-Co-Zr alloy; (a) and (b) as-extruded, (c) and (d) solution-annealed 530°C/1 h, (e) 530°C/1 h + 90°C/4 h, and (f) 530°C/1 h + 165°C/16 h.

4.3.3 Discussion of Structure-Properties Relations

Although the addition of dispersoid-forming elements to rapidly solidified, binary Al-Li alloys has been shown to increase ductility by dispersing planar slip, a similar effect of dispersoid-forming elements in multi-component alloys has not been demonstrated. Part of the problem lies in lack of compositional control in the Al-Li-Cu-Ti and Al-Li-Cu-Mg alloys, resulting in large concentrations of brittle second-phase particles which promote crack propagation and loss of ductility. Even in the Al-Li-Cu-Mn and Al-Li-Cu-Co-Zr alloys, where composition was well-controlled, ductilities were substantially lower than in the ternary Al-Li-X alloys. The reasons for this ductility decrease need to be understood to produce Al-Li alloys with a favorable combination of properties through changes in composition and/or processing.

In the Al-Li-Cu-Mn alloy, ductility in the longitudinal direction was relatively low because of the small volume-fraction of Mn-containing dispersoids and the large recrystallized grain size of 20-50 μm . These conditions allowed unhindered planar slip over relatively large distances, large stress concentrations at recrystallized grain boundaries, and consequent intergranular fracture as shown in Figure 37a. The delamination fracture mode in the transverse direction is not well understood, but it is a common phenomenon in nonaxisymmetric extrusions of this type.

In the Al-Li-Cu-Co-Zr alloy, the ductility should have been improved by the small subgrain size and presence of slip-dispersing Co-containing dispersoids. One possible cause of the poor observed ductility could be the large numbers of constituent particles observed in this alloy in the solution-treated condition (Figure 26c). Extrapolation of the solubility limits in the Al-Li-Cu system given by Mondolfo (Reference 23) to the annealing temperature of 530°C gives a solubility limit for Li in an Al-1.5% Cu alloy of 2.6% in contrast to 3.2% at the same temperature in the binary Al-Li system. The excess Li should be present as $\text{Al}_5\text{Li}_3\text{Cu}$ or δ (AlLi), which may correspond to the second-phase particles shown in Figure 26c. These particles are brittle and about the same size as the subgrains and thus may have promoted the observed sub-granular fracture in the solution-annealed-and-aged Al-Li-Cu-Co-Zr alloy. The volume fraction of constituent particles was decreased by solution annealing at 560 rather than 530°C, but the remaining volume fraction was large enough for the above explanation to possibly still be valid.

Another possible explanation for the low ductilities observed in aged Al-Li-Cu alloys is hydrogen embrittlement. Hydrogen concentrations in conventionally processed, commercial aluminum alloys are typically < 1 p.p.m. so that no effect of hydrogen on their properties should be observed. However, hydrogen concentrations in powder-processed Al alloys, and in particular in Li-containing alloys, may be much larger. The hydrogen can be picked up by the reaction of lithium in the alloy with moisture or by adsorption of water vapor on particulate surfaces, or it may be present as an impurity in the Al-Li master alloy.

Samples of the alloy powders and extrusions listed in Table 11 were analyzed for hydrogen by Leco, Inc., by a fusion method which measures total bulk hydrogen content. The lithium-containing powder and flake alloys were shown to have hydrogen contents larger by at least an order of magnitude than those of ingot or powder metallurgical commercial alloys. Hydrogen levels appear to remain high in flake materials, which have smaller surface-to-volume ratios than powders, and in extrusions. It has not been shown that these hydrogen levels are correlated with decreases in ductility, and indeed the Al-Li-Zr alloy with 30 p.p.m. has 7% elongation to fracture. Nonetheless, the combination of high hydrogen levels and low ductilities in rapidly solidified Al-Li alloys suggests that further exploration of possible hydrogen effects on properties is required.

TABLE 11. HYDROGEN CONTENTS OF ALUMINUM ALLOY POWDERS AND CONSOLIDATED FORMS.

Alloy composition	Form	Hydrogen content (p.p.m.)
Al-4.4Cu-1.5Mg-0.6Mn (2024-Al)	Plate (Ingot alloy)	0.05 ± 0.02
Al-6.5Zn-2.5Mg-1.5Cu-0.4Co (7091-Al)	Plate (P/M alloy)	0.49 ± 0.02
Al-3.7 Li-1.6Cu-0.98Ti	Vacuum-atomized powder	22.0 ± 0.5
Al-3.1Li-1.6Cu-0.4Co-0.2Zr	Extrusion (Vacuum-atomized powder)	10 ± 5
Al-2.95Li-0.27Zr	Extrusion (Roller-quenched flakes)	31.6 ± 0.5

GP21-0700-61

4.4 Deformation and Mechanical Properties of Al-Li-Mg-Zr Alloy

Microstructural evaluation of the aged Al-Li-Mg-Zr alloy showed that the T73 heat treatment ($107^{\circ}\text{C}/8\text{ h} + 177^{\circ}\text{C}/8\text{ h}$) resulted in δ' precipitation for a prior solution annealing temperature of 520°C but not for 482°C (Section 4.2.4). The hardness and strength of this alloy in the T73 condition were thus expected to increase as the solution annealing temperature increased and more Li was dissolved for later precipitation as δ' . To test this hypothesis, Al-Li-Mg-Zr alloy samples annealed for 1 h at temperatures between 482 and 527°C were directly aged at 190°C , and the age hardening curves were determined (Figure 39). The peak-aged hardness of the alloy increases with increasing temperature, in accord with the above hypothesis and the microstructural evidence.

Mechanical properties data for the Al-Li-Mg-Zr alloy solution-annealed at 520°C for 1 h and aged to the T6 ($107^{\circ}\text{C}/8\text{ h}$) and T73 ($107^{\circ}\text{C}/8\text{ h} + 177^{\circ}\text{C}/8\text{ h}$) conditions are shown in Table 12. Deviations from nominal composition in this

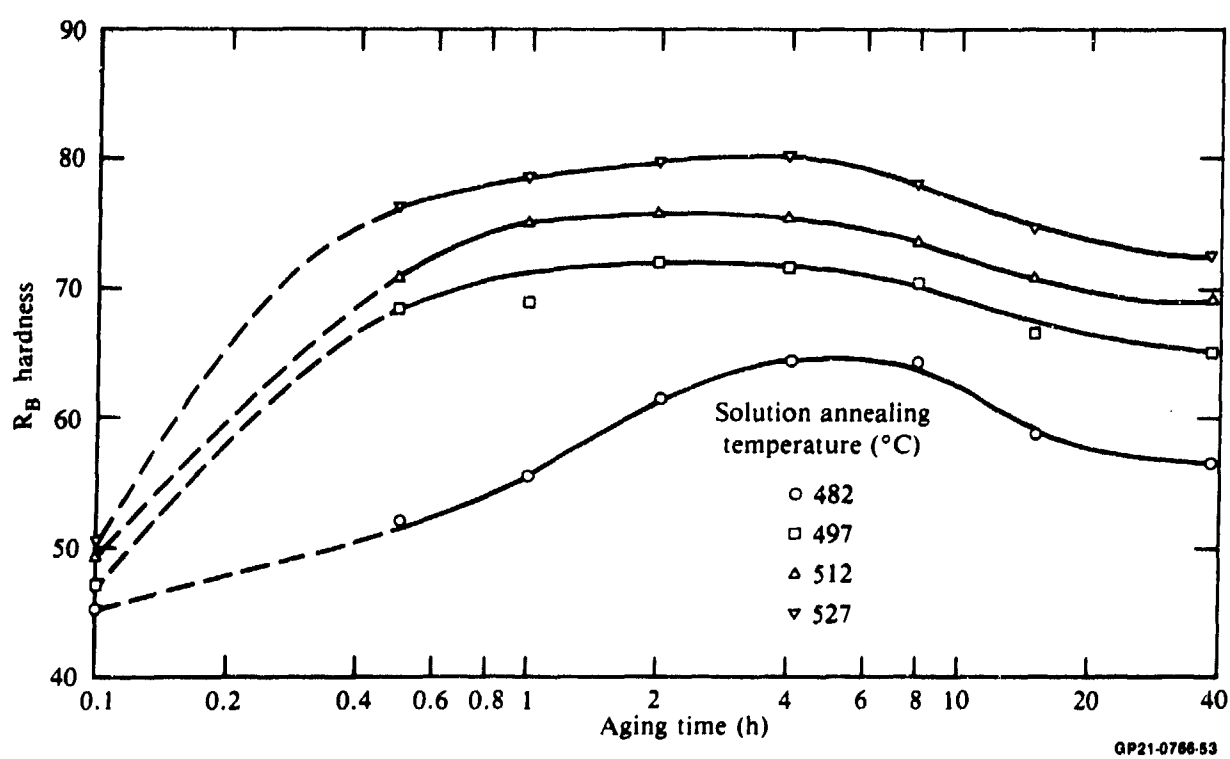


Figure 39. Aging curves for Al-Li-Mg-Zn alloy solution-annealed for 1 h at various temperatures and aged at 190°C .

TABLE 12. MECHANICAL PROPERTIES OF Al-Li-Mg-Zn ALLOY,
COMMERCIAL 7091 AND 7075.

Alloy	Heat treatment	0.2% yield stress, MPa (ksi)	Ultimate tensile stress, MPa (ksi)	Elongation (%)
Al-2.1Li-1.6Cu-1.8Mg-8.3Zn-0.4Co (T6)	520°C/1 h	L 322 (46.6)	6.6	
	+ 107°C/8 h	T 322 (46.7)	398 (57.8)	3.1
	520°C/1 h + 107°C/8 h + 177°C/8 h (T73)	L 373 (54.1) T 358 (51.8)	445 (64.5) 418 (60.7)	3.2 1.6
Al-1.5Cu-2.5Mg-6.5Zn-0.4Co (7091-Al)	T7	L 545 (78) T 510 (74)	593 (86) 552 (80)	12 8
	T6	L 503 (73)	572 (83)	11
Al-1.6Cu-2.5Mg-5.6Zn-0.23Cr (7075-Al)	T6	L 503 (73)	572 (83)	11
	T73	L 434 (63)	13	

GP21-0768-82

alloy caused it to have a lower Mg/Zr ratio and thus lower absolute strength than commercial 7091-Al. Precipitation of δ' during 177°C aging, however, prevented the yield and ultimate tensile strengths of the alloy from decreasing during this heat treatment step, and in fact increased the strength values by 15-50 MPa. The yield and ultimate tensile strengths of commercial 7075, by comparison, decrease by about 70 MPa on going from the T6 to the T73 condition. Thus, addition of Li to a 7xxx-series alloy increases its strength in the T73 condition to or above T6 levels provided that the preliminary solution anneal was at a temperature sufficient to take most or all of the Li into solid solution.

5. SUMMARY AND CONCLUSIONS

The effects of microstructural refinement resulting from rapid solidification, including the formation of fine, stable, incoherent dispersoids and grain refinement, on the microstructure and properties of Al-Li-X alloys have been determined. Flakes of high-purity and commercial-purity Al-3Li and Al-3Li with additions of Co, Cr, Fe, Mn, Ti, Y, and Zr were produced by twin roller quenching. Roller-quenched flakes have 1-2 μm grain sizes, in contrast to the $> 100 \mu\text{m}$ grain size in ingot-cast Al-Li alloys. All the alloys except Al-Li-Ti and Al-Li-Y have homogeneously distributed, $< 1 \mu\text{m}$ diam, incoherent dispersoids.

Flakes of Al-3Li and Al-3Li-X alloys were consolidated by extrusion at 300-400°C, solution annealed at 540°C, and aged for 16-24 h at 180-200°C. The extrusions show fully recovered subgrain structures with subgrain diameters $\sim 1-2 \mu\text{m}$ and preservation of a fine dispersoid distribution. The Al-3Li-Zr alloy resists recrystallization upon solution annealing because of formation of fine, coherent, metastable, cubic Al_3Zr dispersoids. The incoherent dispersoids are resistant to coarsening through solution annealing and aging steps. Upon aging, 40-nm diam δ' (Al_3Li) precipitates are formed, and a bimodal distribution of δ' and incoherent dispersoids is seen in aged Al-3Li-X alloys.

Tensile properties of peak-aged Al-3Li and Al-3Li-X extrusions were measured. Ductility of the rapidly solidified Al-3Li alloy is superior to that of the corresponding ingot alloy because of grain refinement and improved homogeneity. Addition of any ternary dispersoid-forming element except Ti results in a further 3-5% increase in ductility. The ductility improvement results from homogenization of planar slip resulting from the effect of incoherent dispersoids in forcing cross-slip and Orowan bypassing. The size and spacing of dispersoids, rather than their chemical nature, are important for increasing ductility.

Contributions to the yield stress of solution-annealed and solution-annealed-and-aged Al-3Li and Al-3Li-X alloys have been analyzed. Most of the strength ($\sim 300 \text{ MPa}$) of the aged alloys results from precipitation of δ' . Small (0.2-0.3 wt%) Zr additions cause a 180-200 MPa increment in yield strength of Al-3Li caused mainly by substructure strengthening. Direct dis-

persion strengthening by incoherent dispersoids has only a minor influence on the room-temperature strength of Al-3Li-X alloys.

The deformation behavior as a function of temperature for solution-annealed and solution-annealed-and-aged Al-3Li, Al-3Li-Co, and Al-3Li-Zr was studied. The flow stress of solution-annealed Al-3Li increases with increasing temperature because of in situ precipitation of δ' , and that of Al-3Li-Co changes little as a result of the presence of incoherent dispersoids. The flow stress of Al-3Li-Zr decreases sharply above 75°C because of the ineffectiveness of subgrains acting as slip barriers at high temperatures.

Powders of rapidly solidified multicomponent alloys in the Al-Li-Cu, Al-Li-Cu-Mg, and Al-Li-Mg-Zr systems were prepared by inert gas or vacuum atomization. The powders were consolidated by hot extrusion at 400°C, solution-annealed at 520-570°C, and aged for 4-64 h at 165-238°C. Microstructures and mechanical properties of the multicomponent alloys were determined as a function of heat treatment condition and time at temperature.

The microstructures of extruded Al-3Li-1.7Cu-0.23Mn and Al-3Li-1.7Cu-0.4Co-0.2Zr alloys show retention of microstructural refinement, with 0.05-0.2 μm diam constituent particles and 0.5-1 μm diam fully recovered subgrains, in agreement with results for Al-3Li-X alloys. Solution annealing at 520°C results in recrystallization of the Mn-containing alloy, but the Zr-containing alloy remains unrecrystallized. Aging of these two alloys leads to formation of fine δ' and retention of homogeneously distributed incoherent dispersoids, as in the ternary Al-3Li-X alloys. The aging sequence was shown to be Al solid-solution $\rightarrow \delta' \rightarrow T_1$ (Al_2CuLi).

Microstructures of Al-3.7Li-1.9Cu-1Ti and Al-3.4Li-1.9Cu-1.5Mg-0.9Fe-0.8Ni contained coarse (5-20 μm) constituent particles as a result of insufficient composition control. Dispersoid formation and subgrain and δ' development in the Al-Li-Cu-Mg alloy were similar to those in the Al-Li-Cu alloys.

It was determined that the δ' phase is formed in an Al-Li-Mg-Zr alloy upon aging at 177°C provided that prior solution annealing was carried out at 520°C rather than 482°C as specified for the base alloy, X7091. Cobalt-containing dispersoids and subgrain sizes were somewhat larger for the rapidly solidified Al-Li-Mg-Zr alloy than for the corresponding Al-Li-Cu or Al-Li-Cu-Mg alloys.

Room-temperature tensile mechanical properties of solution-annealed and solution-annealed-and-tempered Al-Li-Cu, Al-Li-Cu-Mg, and Al-Li-Mg-Zn alloys were measured. The rapidly solidified Al-Li-Cu and Al-Li-Cu-Mg alloys generally have longitudinal yield and ultimate tensile strengths equal to or greater than those of ingot 2024-Al, but transverse properties are noticeably poorer. Ductilities of the peak-aged alloys are well below that of 2024-Al. Most of the Al-Li-Cu alloys have elastic moduli below the value of 83.3 MPa measured for binary Al-Li alloys, suggesting that significant amounts of Li are tied up as insoluble constituent particles. Addition of 1.4 wt% Mg to an Al-Li-Cu alloy results primarily in division of alloying elements to the constituent particles, resulting in a decrease in ductility with no increase in strength. Fractography of Al-Li-Cu alloys showed primarily intergranular fracture in longitudinal specimens and delamination fracture in transverse specimens.

Addition of dispersoid-forming elements to multicomponent alloys did not result in the increased ductility observed in ternary Al-Li-X alloys. The absence of ductility improvement may be the result of retained constituent particles or increased hydrogen levels in rapidly solidified powders. Vacuum-atomized, Li-containing powders and powder extrusions contained 5-30 p.p.m. hydrogen compared with 0.05-0.5 p.p.m. hydrogen in commercial ingot and powder metallurgical alloys.

Tensile properties of the Al-Li-Mg-Zr alloy were measured in the T6 (107°C/8 h) and T73 (107°C/8 h + 177°C/8 h) tempers. Yield and ultimate tensile strengths of this alloy were slightly higher in the T73 than in the T6 condition as a result of δ' precipitation upon 177°C aging. This result suggests that addition of Li to 7xxx-series alloy may enable the alloys to be heat treated to obtain the stress-corrosion-cracking resistance normally associated with the T73 temper in combination with the strength levels of the T6 temper.

6. REFERENCES

1. C. Dresser. Air-to-Surface (ATS) Technology Evaluation and Integration Study. McDonnell Douglas Report MDC A4994, AFWAL-FD Contract No. F33615-76-C-3101 (January 1978).
2. R. E. Lewis. Development of Advanced Aluminum Alloys from Rapidly Solidified Powders for Aerospace Structural Applications. Lockheed Missiles and Space Co. Report LMSC-D674504, DARPA/AFML Contract No. F33615-78-C-5203 (March 1979).
3. J. W. Evancho. Development of an Al-Mg-Li Alloy. Final Report, Naval Air Development Center Contract No. N62269-73-C-0129 (June 1974).
4. T. H. Sanders, Jr. Development of an Al-Mg-Li Alloy. Final Report, Naval Air Development Center Contract No. N62269-74-C-0238 (June 1976).
5. T. H. Sanders. Factors Influencing Fracture Toughness and Other Properties of Aluminum-Lithium Alloys. Final Report, Naval Air Development Center Contract No. N62269-76-C-0271 (June 1979).
6. K. Dinsdale, S. J. Harris, and B. Noble. Relationship Between Microstructure and Mechanical Properties of Aluminum-Lithium-Magnesium Alloys. In Aluminum-Lithium Alloys, ed. by T. H. Sanders, Jr., and E. A. Starke, Jr. (The Metallurgical Society of AIME, Warrendale, PA, 1981), p. 101.
7. R. E. Lewis. Development of Advanced Aluminum Alloys from Rapidly Solidified Powders for Aerospace Structural Applications. Lockheed Missiles and Space Co. Report LMSC-D678772, DARPA/AFML Contract No. F33615-78-C-5203 (September 1979).
8. R. E. Lewis. Development of Advanced Aluminum Alloys from Rapidly Solidified Powders for Aerospace Structural Applications. Lockheed Missiles and Space Co. Report LMSC-D686125, DARPA/AFML Contract No. F33625-78-C-5203 (March 1980).
9. R. E. Lewis. Advanced Aluminum Alloys from Rapidly Solidified Powders. Lockheed Missiles and Space Co. Report LMSC-D770654, DARPA/AFML Contract No. F33615-78-C-5203 (June 1980).
10. R. E. Lewis. Advanced Aluminum Alloys from Rapidly Solidified Powders. Lockheed Missiles and Space Co. Report LMSC-D777825, DARPA/AFML Contract No. F33615-78-C-5203 (September 1980).

11. F. W. Gayle. Alloying Additions and Property Modification in Aluminum-Lithium-X Systems. In Aluminum-Lithium Alloys, ed. by T. H. Sanders, Jr. and E. A. Starke, Jr. (The Metallurgical Society of AIME, Warrendale, PA, 1981), p. 119.
12. N. J. Grant, S. Kang, and W. Wang. Structure and Properties of Rapidly Solidified 2000 Series Al-Li Alloys. In Aluminum-Lithium Alloys, ed. by T. H. Sanders, Jr. and E. A. Starge, Jr. (The Metallurgical Society of AIME, Warrendale, PA, 1981), p. 171.
13. D. Webster. Toughness and Ductility of Aluminum-Lithium Alloys Prepared by Powder Metallurgy and Ingot Metallurgy. In Aluminum-Lithium Alloys, ed. by T. H. Sanders, Jr. and E. A. Starke, Jr. (The Metallurgical Society of AIME, Warrendale, PA, 1981), p. 228.
14. P. S. Pao, K. K. Sankaran, and J. E. O'Neal. Microstructure, Deformation, and Corrosion-Fatigue Behavior of a Rapidly Solidified Al-Li-Cu-Mn Alloy. In Aluminum-Lithium Alloys, ed. by T. H. Sanders, Jr. and E. A. Starke, Jr. (The Metallurgical Society of AIME, Warrendale, PA, 1981), p. 307.
15. P. P. Pizzo. The Relative Stress-Corrosion-Cracking Susceptibility of Candidate Aluminum-Lithium Alloys for Aerospace Structural Applications. Advanced Research and Applications Corp. Report TR-45-1, NASA-Ames Contract No. NAS-10365 (September 1980).
16. D. Webster. Properties and Microstructure of Aluminum-Copper-Magnesium-Lithium Alloys. *Met. Trans.* 10A, 1913 (1979).
17. R. E. Lewis. Advanced Aluminum Alloys from Rapidly Solidified Powders. Lockheed Missiles and Space Co. Report LMSC-D802523, DARPA/AFML Contract No. F33615-78-C-5203 (January 1981).
18. K. K. Sankaran and N. J. Grant. The Structure and Properties of Splat-Quenched Aluminum Alloy 2024 Containing Lithium Additions. *Mat. Sci. Eng.* 44, 213 (1980).
19. B. Noble and G. E. Thompson. Precipitation Characteristics of Aluminum-Lithium Alloys. *Met. Sci. J.* 5, 114 (1971).
20. D. B. Williams and J. W. Edington. The Precipitation of δ' (Al_3Li) in Dilute Aluminum-Lithium Alloys. *Met. Sci.* 9, 529 (1975).
21. T. H. Sanders, Jr., E. A. Ludwiczak, and R. R. Sawtell. The Fracture Behavior of Recrystallized Al-2.8%Li-0.3%Mn Sheet. *Mat. Sci. Eng.* 43, 247 (1980).

22. Yu. M. Vaynblatt, B. A. Kopeliovich, and Yu. G. Gol'der. Subboundary Embrittlement of the Alloy Al-Mg-Li by Horophile Impurity Sodium. *Phys. Met. Metallogr.* 42, 105 (1976).
23. L. F. Mondolfo. Aluminum Alloys: Structure and Properties (Butterworths, Boston, 1976), p. 308.
24. W. L. Otto, Jr. Metallurgical Factors Controlling Structure in High Strength P/M Products. AFML-TR-76-60 (1976).
25. N. Ryum. Precipitation and Recrystallization in an Al-0.5 wt% Zr Alloy. *Acta Met.* 17, 269 (1969).
26. P. Haasen. Physical Metallurgy (Cambridge University Press, Cambridge, England, 1978), p. 338.
27. H. Gleiter and E. Hornbogen. Precipitation Hardening by Coherent Particles. *Mat. Sci. Eng.* 2, 285 (1967/68).
28. S. Ceresara, G. Cocco, G. Fagherazzi, and L. Schiffrini. Determination of the δ' Coherent Solvus in the Al-Li System by Small-Angle X-ray Scattering. *Phil. Mag.* 35, 373 (1977).
29. W. R. D. Jones and P. P. Das. The Mechanical Properties of Aluminum-Lithium Alloys. *J. Inst. Met.* 88, 435 (1959-1960).
30. L. M. Brown and R. K. Ham. Dislocation-Particle Interactions. In Strengthening Methods in Crystals, ed. by A. Kelly and R. B. Nicholson (Applied Science Publishers Ltd., London, 1971), p. 12.
31. M. F. Ashby. On the Orowan Stress. In Physics of Strength and Plasticity, ed. by A. S. Argon (Massachusetts Institute of Technology Press, Cambridge, MA, 1969), p. 113.
32. H. K. Hardy. Trace Element Effects in Some Precipitation-Hardening Aluminum Alloys. *J. Inst. Met.* [84], 429 (1955-1956).
33. R. G. Davis and T. L. Johnson. The Metallurgical Design of a Superalloy. In Ordered Alloys: Structural Application and Physical Metallurgy, ed. by B. H. Kear, C. T. Sims, N. S. Stoloff, and J. H. Westbrook (Claitor's Publishing Division, Baton Rouge, LA, 1970), p. 447.
34. A. Gysler and S. Weissman. Effect of Order in Ti_3Al Particles and of Temperature on the Deformation Behavior of Age-Hardened Ti-Al Alloys. *Mat. Sci. Eng.* 27, 181 (1977).
35. B. H. Kear. Dislocation Configurations and Work Hardening in Cu_3Au Crystals. *Acta Met.* 12, 555 (1964).

36. A. E. Vidoz and L. M. Brown. On Work Hardening in Ordered Alloys. *Phil. Mag.* 7, 1167 (1962).
37. J. M. Silcock. The Structural Aging Characteristics of Aluminum-Copper-Lithium Alloys. *J. Inst. Met.* 88, 357 (1959-60).
38. B. Noble and G. E. Thompson. T_1 (Al_2CuLi) Precipitation in Aluminum-Copper-Lithium Alloys. *Met. Sci.* 8, 167 (1972).

7. PUBLICATIONS RESULTING FROM THIS CONTRACT

1. S. M. L. Sastry and K. K. Sankaran. Microstructure and Properties of Powder-Processed Aluminum-Lithium Alloys. DARPA/AFML Advanced Aluminum Alloy Technology Review, Pittsburgh, PA, 13 September 1979.
2. S. M. L. Sastry and K. K. Sankaran. Microstructure and Properties of Powder-Processed Aluminum-Lithium Alloys. Review of Government Sponsored Work on P/M Aluminum, Dayton, OH, 13 February 1980 (Published in Proceedings).
3. K. K. Sankaran, S. M. L. Sastry, and J. E. O'Neal. Microstructure and Deformation of Rapidly Solidified Al-3Li Alloy Containing Incoherent Dispersoids. First International Conference on Al-Li Alloys, Stone Mountain, GA, May 1980; in Aluminum-Lithium Alloys, ed. by T. H. Sanders, Jr. and E. A. Starke, Jr. (The Metallurgical Society of AIME, Warrendale, PA, 1981), p. 189.
4. J. E. O'Neal, K. K. Sankaran, and S. M. L. Sastry. Transmission Electron Microscopic Observations of Al₃Li and Al₃Ti Precipitation in a Rapidly Solidified Al-3Li-0.2Ti Alloy. 38th Annual Meeting of the Electron Microscopy Society of America, Reno, NV, August 1980; in Proceedings of the Electron Microscopy Society of America, ed. by G. W. Bailey (Claitor's Publishing Division, Baton Rouge, LA, 1980), p. 336.
5. K. K. Sankaran, S. M. L. Sastry, and J. E. O'Neal. Microstructure and Deformation Behavior of Rapidly Solidified Al-3Li Alloys Containing Incoherent Dispersoids. TMS-AIME Fall Meeting, Pittsburg, PA, October 1980.
6. K. K. Sankaran, J. E. O'Neal, and S. M. L. Sastry. Effects of Second Phase Dispersoids on Deformation Behavior of Al-Li Alloys. Met. Trans. (submitted).
7. J. E. O'Neal, K. K. Sankaran, and S. M. L. Sastry. Effects of Temperature and Incoherent Dispersoids on Slip Dispersal in Al-3Li Alloys. In Proceedings 40th Electron Microscopy Society of America, ed. by G. W. Bailey (Claitor's Publishing Division, Baton Rouge, LA, 1982), p. 474.
8. K. K. Sankaran and J. E. O'Neal. Precipitation in Al-Li-Cu Alloys, In Proceedings 39th Electron Microscopy Society of America, ed. by G. W. Bailey (Claitor's Publishing Division, Baton Rouge, LA, 1981), p. 66.

9. P. J. Meschter, S. M. L. Sastry, and J. E. O'Neal. Dispersoid Forming Element Additions to Powder Processed Al-Cu-Li and Al-Zr-Mg-Cu-Li Alloys. TMS/AIME Fall Meeting, St. Louis, MO, 24-28 October 1982.
10. S. M. L. Sastry and J. E. O'Neal. High Temperature Deformation Behavior and Mechanical Properties of Rapidly Solidified Al-Li-Co and Al-Li-Zr Alloys. To be presented at the Second International Aluminum-Lithium Conference, Monterey, CA, 12-14 April 1983.

8. COUPLING ACTIVITIES WITH GROUPS DOING RELATED RESEARCH

1. Presentations on MDRL/AFOSR Al-Li alloy research were made to Mr. J. F. Collins of NASC, Dr. B. B. Rath of NRL, and Lt. Col. L. A. Jacobson of DARPA on 5 February 1981; to Dr. A. P. Divecha of NSWC/White Oak Laboratory on 6 February 1981; to Lt. Col. L. A. Jacobson of DARPA, Dr. Terry Ronald of AFWAL-ML, Capt. D. Voss of AFWAL-ML, and Dr. M. Greenfield of NASA (HQ) on 2 April 1981; to Mr. B. Lisagor of NASA-LaRC on 3 April 1981; and to Dr. J. J. DeLuccia and Dr. G. Longon of NADC on 22 April 1981.
2. Discussions on Al-Li alloy research were held with Dr. E. A. Starke and Dr. T. H. Sanders of Georgia Institute of Technology, Dr. H. Paris of Alcoa, Dr. G. Chanani of Northrop, and Dr. G. Hari Narayan and Mr. M. V. Hyatt of Boeing Commercial Airplane Co. during the TMS/AIME Fall Meeting, Chicago, 23-25 February 1981.
3. MDRL participated in AFOSR working Group Meeting on P/M Aluminum Alloys, Louisville, KY, 15 October 1981.
4. MDRL participated in Lockheed Contract Review for Aerospace and Government Agencies on Development of Advanced Aluminum Alloys from Rapidly Solidified Powders for Aerospace Structural Applications, Palo Alto, CA, 6 November 1981.
5. Discussion on Aluminum Powder Metallurgy Research was held with Dr. Barry Lisagor (NASA) on 17 November 1981.

DISTRIBUTION

	Copies		Copies
H. C. Graham Branch Chief AFWAL/MLLM W-PAFB, OH 45433	1	Alan Lawley Drexel University 32nd & Chestnut Street Philadelphia, PA 19104	1
G. E. Eichelman Branch Chief AFWAL/MLLS W-PAFB, OH 45433	1	Arthur J. McEvily University of Connecticut Department of Metallurgy, U-136 Storrs, CT 06268	1
L. R. Bidwell AFWAL/MLLS W-PAFB, OH 45433	1	T. Ronalds AFWAL/MLLS W-PAFB, OH 45433	1
R. E. Lewis Senior Staff Scientist M/S 52-31/204 Lockheed Missiles and Space Company 3251 Hanover Street Palo Alto, CA 94304	1	James T. Staley ALCOA Laboratories ALCOA Technical Center ALCOA Center, PA 15069	1
David L. Davidson Staff Scientist Southwest Research Institute P. O. Drawer 28510 San Antonio, TX 78284	1	Edgar A. Starke, Jr. Georgia Institute of Technology School of Chemistry & Metallurgy Atlanta, GA 30332	1
Morris E. Fine Northwestern University Evanston, IL 60201	1	Anthony W. Thompson Carnegie-Mellon University Department of Metallurgical and Materials Science Pittsburgh, PA 15213	1
H. Fraser Department of Metallurgy University of Illinois Urbana, IL 61801	1	Robert P. Wei Lehigh University 327 Sinclair Lab, Bldg. 7 Bethlehem, PA 18015	1